

The Pennsylvania State University
The Graduate School

**INFLUENTIAL SUBSPACES
IN SELF-ORGANIZING MULTI-AGENT SYSTEMS**

A Dissertation in
Mechanical Engineering
by
Kshitij Jerath

© 2014 Kshitij Jerath

Submitted in Partial Fulfillment
of the Requirements
for the Degree of

Doctor of Philosophy

December 2014

The dissertation of Kshitij Jerath was reviewed and approved* by the following:

Sean Brennan
Associate Professor of Mechanical Engineering
Dissertation Co-Advisor, Co-chair of Committee

Asok Ray
Distinguished Professor of Mechanical Engineering
Dissertation Co-Advisor, Co-chair of Committee

Vikash V. Gayah
Assistant Professor of Civil and Environmental Engineering

Hosam Fathy
Assistant Professor of Mechanical Engineering

Karen Thole
Professor of Mechanical Engineering
Department Head of Mechanical and Nuclear Engineering

*Signatures are on file in the Graduate School

ABSTRACT

This dissertation addresses the issue of influence in self-organizing multi-agent systems by using traffic jams as a prototypical example of self-organized behavior. Specifically, the problem of ascertaining the influence of a set of agents on the ensemble dynamics is addressed through two complementary approaches. In the first approach, discussed in [Part I](#) of the dissertation, the ability to influence ensemble dynamics is studied as a function of changing agent population demographics. Statistical mechanics-inspired methodologies, such as the master equation and the generalized Ising model, are used to study the effect of introduction of vehicles equipped with adaptive cruise control (ACC) algorithms on the self-organized dynamics of traffic jams. Results indicate mixed positive and negative effects of introduction of ACC-equipped vehicles at various traffic densities.

While this approach can help guide long-term intelligent vehicle deployment strategies on the time scale of years or decades, population demographic control is not a feasible solution for influencing large-scale multi-agent systems on the time scale of minutes or hours. Thus, the second approach, discussed in [Part II](#) of this dissertation, addresses the problem by identifying appropriate regions of the state space within which the control efforts exerted by a small set of agents can influence the self-organized dynamics of the ensemble. The methodologies adopted in this approach make use of the kinematic wave theory of traffic flow and the notion of controllability to present the novel concept of *influential subspaces*. Results indicate that there exists a strong spatial dependence that governs an agent's ability to influence the self-organized dynamics of large-scale multi-agent systems.

CONTENTS

List of Figures	vii
Acknowledgements	xiv
1 INTRODUCTION	1
1.1 Motivation: Complex systems, self-organization and macroscopic control	1
1.1.1 Motivating questions in complex systems research	2
1.2 Motivation: Controlling self-organized traffic jams	3
1.2.1 Motivating questions in intelligent transportation research	5
1.3 Goals of the study	5
1.4 Outline of remaining chapters	6
2 LITERATURE REVIEW	8
2.1 Macroscopic modeling and dynamics	8
2.1.1 Macrostate identification	9
2.1.2 Synchronization theory	10
2.1.3 Consensus dynamics	12
2.1.4 Statistical mechanics	13
2.2 Influence in multi-agent systems	14
2.2.1 The need for the concept of influence	14
2.2.2 The subspace selection problem in agent-centric control of large-scale systems	15
2.2.3 The agent selection problem	21
2.3 Traffic flow theory	28
2.3.1 Traffic modeling	28
2.3.2 Intelligent vehicle technologies	32
2.3.3 Self-organized traffic jams	36
2.3.4 Limitations of prior work	38
2.4 Summary	38
I INFLUENCE VIA POPULATION MODIFICATION	39
3 EFFECT OF ACC PENETRATION ON FORMATION OF SELF-ORGANIZED TRAFFIC JAMS	41
3.1 Introduction	41
3.2 Prior work	42
3.3 Master equation approach	43
3.3.1 Vehicular cluster (or traffic jam) dynamics	43
3.3.2 Transition probability rates	45
3.4 New transition probability rates	46
3.4.1 General Motors' car-following model	46
3.4.2 Derivation of new transition probability rates	48
3.5 Steady-state analysis	53

3.5.1	Steady-state analysis for single species environments	53
3.5.2	Introduction of ACC-enabled vehicles into traffic flow	54
3.5.3	Steady-state analysis for multi-species environment	56
3.6	Results and mesoscopic simulations	57
3.6.1	Results for single species traffic flow	57
3.6.2	Results for multi-species or mixed traffic flow	59
3.7	Conclusions, contributions and broader impacts	61
4	GENERALIZED ISING MODEL TO STUDY EFFECTS OF DRIVER ALGORITHMS ON VEHICLE CLUSTER DISTRIBUTION	63
4.1	Introduction	63
4.2	Prior work	64
4.2.1	Statistical mechanics-based techniques	65
4.2.2	Limitations of the Ising model	65
4.3	Problem setup	65
4.3.1	Traffic system description	66
4.3.2	Space partitioning and lattice structure of traffic system	66
4.4	Generalized Ising model formulation	67
4.4.1	External field	69
4.4.2	Interaction strength	70
4.4.3	Modeling driver behavior via interactions	71
4.4.4	Exchange dynamics	73
4.4.5	Transition probability rates	73
4.5	Monte Carlo simulations	75
4.5.1	Calibration of parameters	75
4.5.2	Simulation results	78
4.6	Results	80
4.6.1	Conclusions and broader impacts	82
II	INFLUENCE VIA SUBSPACE SELECTION	83
5	INFLUENTIAL SUBSPACES OF CONNECTED VEHICLES	85
5.1	Introduction	85
5.2	Prior work	86
5.3	Influential subspaces and event horizons	87
5.3.1	Notion of agents and macrostate in a traffic system	87
5.3.2	A thought experiment	88
5.4	Problem setup	91
5.5	Analytical solution of influential subspaces of connected vehicles	93
5.5.1	Interpretation of time-space diagrams	93
5.5.2	Analytical solution of influential subspaces	96
5.6	Results	102
5.6.1	Dependence on reduced speed v_s	103

5.6.2	Dependence on initial jam length x_q	104
5.6.3	Dependence on upstream traffic density k_A	105
5.7	Conclusions, contributions and broader impacts	107
6	SPATIAL DEPENDENCE OF AGENT INFLUENCE IN SELF-ORGANIZING SYSTEMS	108
6.1	Introduction	108
6.2	Prior work	109
6.2.1	Eising's measure of controllability	110
6.2.2	Hamdan's geometric measure of modal controllability	110
6.2.3	Degree of controllability	111
6.2.4	Limitations of prior work	111
6.3	A prototypical self-organizing system	112
6.3.1	Intelligent driver model	112
6.3.2	System dynamics	113
6.3.3	Studying agent influence	114
6.4	Minimum embedding dimension of low-dimensional manifold	116
6.4.1	Method of false neighbors	117
6.4.2	Minimum embedding dimension via Cao's methodology	118
6.5	Identification of influential agents	120
6.5.1	Model order reduction via Krylov subspaces	120
6.5.2	Influential agents in 3-vehicle system	122
6.6	Conclusions, contributions and broader impacts	122
7	FUTURE DIRECTIONS	124
7.1	Summary of work	124
7.1.1	Key insights	124
7.1.2	Unsuccessful avenues and some general advice to new researchers in this field	126
7.2	Potential future directions	127
7.2.1	Short-term future work	128
7.2.2	Long-term future work	129
A	THE ONE-DIMENSIONAL ISING MODEL WITH NEAREST-NEIGHBOR INTERACTIONS	131
A.1	Model description	131
A.2	Partition function	132
A.3	Transfer matrix	132
A.4	Solution of the partition function	133
B	INDEX	134
	BIBLIOGRAPHY	136

LIST OF FIGURES

Figure 1.1	Example of self-organizing behavior. Spatial patterns are evident to the human observer. . . .	2
Figure 1.2	Evidence of increasing cost of congestion. [1] .	4
Figure 2.1	Different types of synchronization that may potentially serve as models to describe the macroscopic dynamics of self-organizing systems . .	12
Figure 2.2	Schematic depicting controllable and reachable sets. A controllable set X_0 in forward time is identical to the reachable set (reachable from X_1) in backward time provided that the system mapping is invertible.	16
Figure 2.3	Undirected graph, associated graph Laplacian, and adjacency and degree matrices.	23
Figure 2.4	Directed graph (or <i>digraph</i>), associated graph Laplacian, and adjacency and degree matrices.	23
Figure 2.5	Depiction of different convergence rates to consensus, as a function of the network topology [2]. Note the difference in time scales for plots in parts (e) and (f), which represent the consensus dynamics for interaction topologies shown in parts (b) and (c), respectively. Part (a) represents a network with random topology.	24
Figure 2.6	Greenshields et al. postulated a linear relationship between vehicle speed and average traffic density using photographic measurements of traffic flow.	29
Figure 2.7	State evolution in the gas kinetic model of traffic flow as described by Prigogine and Andrews	31
Figure 2.8	Experimental study of self-organized traffic jams performed by Sugiyama et al. [5]. A self-organized vehicle cluster can be seen in the top-right section of the image	37
Figure 2.9	Position data for vehicles in experiments performed by Sugiyama et al. [5]. A vehicle cluster is formed and moves backward in space as time progresses.	38

Figure 3.1	Single-lane closed road system under consideration showing (a) vehicles in free flow, (b) vehicles transitioning from free flow to jammed state (joining a cluster), (c) vehicles stuck inside a traffic jam (cluster), and (d) vehicles transitioning from jammed state to free flow. . . .	44
Figure 3.2	Description of variables used in analysis. (a) Vehicles in free flow (h_{free} = free flow headway, v_{free} = free flow velocity; (b) Vehicles transitioning from free flow to jammed state (joining a cluster): $h(t)$ = headway as a function of time, $v(t)$ = velocity as a function of time; (c) Vehicles stuck inside a traffic jam (cluster): $h_{cluster}$ = headway inside a cluster, $v_{cluster}$ = velocity inside a cluster.	47
Figure 3.3	Acceleration profiles for a vehicle entering a cluster with the GM fourth model serving as the ACC algorithm with varying driver sensitivities. A driver model with low driver sensitivity ($\alpha = 0.3$) reacts later than a driver with high driver sensitivity ($\alpha = 0.7$).	48
Figure 3.4	Maximum observed deceleration during simulation of a vehicle joining a cluster in typical traffic conditions, with varying driver sensitivities. The range of admissible driver sensitivities is approximately $[0.4, 0.6]$	49
Figure 3.5	Time taken to join a cluster (t_{join}) using the expression derived from the GM fourth model nonlinear ODE. The truncated hypergeometric series quickly converges to the exact solution as more terms are included.	51
Figure 3.6	Range of admissible driver sensitivities limits the variation of the truncation ratio, $\zeta = t_{join}/t_1$. Based on the driver sensitivity α of the car-following algorithm, an appropriate value of $\zeta(\alpha)$ can be used to approximate the time taken to join a cluster.	52
Figure 3.7	Steady-state phase portrait of normalized cluster size versus dimensionless density consisting of a single driver species based on GM fourth model with $\alpha = 0.4$. The solid line indicates the stable cluster sizes or traffic jams. Clusters or traffic jams first begin to appear when the dimensionless density reaches a critical value of $k_c^* \approx 0.1$	54

Figure 3.8	Experimental data for traffic flow consisting solely of human drivers on German highways. Dots indicate experimental observations [6]. The observed dimensionless critical density is close to 0.1 [7].	55
Figure 3.9	Steady-state phase portrait describing analytical results for special cases of mixed traffic. Traffic consists of (i) human-driven vehicles only ($p = 0.0$), and (ii) ACC-enabled vehicles only ($p = 1.0$).	58
Figure 3.10	Monte Carlo simulation validates the analytical results obtained for the relationship between normalized cluster size and dimensionless density, for a single species environment. Thick dashed line denotes analytical solution. Solid dots indicate the mean steady-state cluster sizes obtained from the simulation.	58
Figure 3.11	Increased ACC penetration results in an increase in the critical density at which traffic jams first appear. Points A and B operate at the same threshold (Δk) away from the critical density line. Identical changes in vehicle proportion (Δp) produce different results at the operating points.	59
Figure 3.12	Sensitivity of critical density to ACC penetration. Traffic flows with high ACC penetration are up to 10 times more susceptible to the formation of self-organized traffic jams, as compared to traffic flows with low ACC penetration.	60
Figure 3.13	Results from the Monte Carlo simulation for mixed traffic flow appear to agree with the analytical results. Isolines indicate number of simulation (out of 1000 total iterations) that resulted in a vehicular cluster (self-organized traffic jam). Dashed line indicates normalized critical density from analytical results.	61
Figure 4.1	Discretized version of traffic system for statistical mechanics-based numerical analysis. Arrow indicates direction of travel. Vehicles travel in direction of reducing site number. Three states, $\sigma_i \in \Sigma = \{0, 1, 2\}$, are possible for each site in accordance with the generalized Ising model approach.	68

Figure 4.2	Interaction coefficients for vehicles determined using differences in local density. Dashed box denotes the neighborhood for the respective vehicles. (a) Difference in local density is negative for a vehicle (circled) entering a cluster. (b) Difference in local density is positive for a vehicle (circled) exiting a cluster.	72
Figure 4.3	Calibration of generalized Ising model parameters B and c_0 to match free flow speed on a highway ($v_f = 25$ m/s). Contours indicate free flow speeds (m/s) obtained with corresponding set of model parameters. The values are chosen to be $B = 125$ and $c_0 = 0.05$	76
Figure 4.4	(a) Backward wave speed (u_{out}) evaluated for vehicles exiting a cluster. (b) Backward wave speed (u_{in}) evaluated for vehicles entering a cluster. Parameters J_{in} and J_{out} are calibrated to match backward wave propagation speeds for both human-driven (H) and ACC-enabled (A) vehicles, evaluated using $B = 125$ and $c_0 = 0.05$. Contours indicate backward wave speeds (m/s) obtained with corresponding set of model parameters.	77
Figure 4.5	Queued traffic system is simulated with $k^* = 0.5, c_0 = 0.05, B = 125, J_{in}^H = -0.325 \times 10^4$, and $J_{out}^H = -1.395 \times 10^5$. Use of a queued traffic system helps ensure that calibrated model parameters lead to behavior that mimics real-life and agrees with existing theory (LWR model). .	79
Figure 4.6	Probability of a randomly selected vehicle lying in a cluster of size r^* for varying levels of ACC penetration and densities of interest. Lines of decreasing thickness indicate increasing levels of ACC penetration. Dotted line corresponds to a traffic system consisting entirely of ACC-enabled vehicles. Clusters of size $r^* = 1/M$ (or $r = 1$) not shown in the distribution.	81
Figure 5.1	Thought experiment for understanding the concept of influential subspaces of connected vehicles, and event horizons in highway traffic. White arrow indicates direction of travel. The letter M relates to the macrostate, whereas a relates to individual agents.	88

Figure 5.2	Fundamental diagram of traffic flow for single species traffic. State of traffic flow is defined using macroscopic variables such as flow (q) and density (k). Traffic states C and J are depicted as the critical and jammed states in the diagram, respectively. Slopes in the figure indicate speeds. Slope of segment OC is v_F , the free flow speed.	92
Figure 5.3	Fundamental diagram of traffic flow for slow and fast moving traffic. Traffic states A and S are depicted on the free flow and congested flow branches of the diagram, respectively. Slopes in the figure indicate speeds. Slope of segment OA is v_F , the free flow speed. Slope of segment OS is v_s , the reduced speed at which the connected vehicle drives to avoid the jam. v_{AS} denotes the interface speed between states A and S which may co-exist on neighboring regions of the highway.	92
Figure 5.4	Description of traffic states and interface speeds in the time-space diagram. Dashed line indicates jam evolution without connected vehicles. Dash-dotted lines are vehicle trajectories of connected vehicles.	94
Figure 5.5	Space-time diagram for connected vehicles separated by (a) 200 m, (b) 350 m, (c) 700 m, and (d) 5000 m, for $v_s = 10$ km/hr and $x_q = 500$ m. Figure(c) shows the time saved with this control policy.	95
Figure 5.6	Evaluation of dissipation time t_0 in a simple jam dissipation scenario.	96
Figure 5.7	Evaluation of t_f using time-space diagram. Only relevant quantities needed for deriving analytical solution are labeled. Note that the interface speeds between states are derived from the fundamental diagram of traffic flow.	97
Figure 5.8	Evaluation of t_s using time-space diagram. Only relevant quantities needed for deriving analytical solution are labeled.	100
Figure 5.9	Evaluating influential subspace of the second connected vehicle for $x_q = 500$ m and $v_s = 10$ km/hr, given the pre-determined macrostate $\psi_d = 0$ and a specified time t_{d_i} within which to reach it ($i = 1, 2, 3$). Solid line indicates time taken to reach the state $\psi_d = 0$ as a function of distance between connected vehicles.	102

Figure 5.10	<p>Influential subspace contracts as reduced speed v_s of connected vehicle is raised, and vanishes at the free flow speed $v_f = 90$ km/hr. Other system parameters are held constant: $x_q = 500$ m, and $k_A = 10$ veh/km. Contours represent the time t_d (s) taken to reach the pre-determined macrostate $\psi_d = 0$. The range of values enclosed by the contour reach the macrostate $\psi_d = 0$ in time $t < t_d$, and hence can be used to determine the influential subspace using the x-axis. 104</p>
Figure 5.11	<p>Influential subspace is pushed further upstream as initial jam length x_q increases. Other system parameters are held constant: $v_s = 30$ km/hr, and $k_A = 10$ veh/km. Contours represent the time t_d (s) taken to reach the pre-determined macrostate $\psi_d = 0$. The range of values enclosed by the contour reach the macrostate $\psi_d = 0$ in time $t < t_d$, and hence can be used to determine the influential subspace using the x-axis. 105</p>
Figure 5.12	<p>Influential subspace vanishes and the event horizon tends to infinity ($\zeta_e \rightarrow \infty$), as upstream free-flowing traffic state k_A nears critical density k_C. Other system parameters are held constant: $v_s = 10$ km/hr, and $x_q = 500$ m. Contours represent the time t_d (s) taken to reach the pre-determined macrostate $\psi_d = 0$. The range of values enclosed by the contour reach the macrostate $\psi_d = 0$ in time $t < t_d$, and hence can be used to determine the influential subspace using the x-axis. 106</p>
Figure 6.1	<p>The degree of controllability indicates how easy it is control the system. As ρ tends to zero, the system becomes less controllable. At $\rho = 0$ the system is uncontrollable. $\bar{\rho}$ represents the approximate degree of controllability based on a parallelopiped approximation of the recovery region [8]. 112</p>
Figure 6.2	<p>Three vehicle system on a ring road with dynamics manifesting as self-organized stop-and-go waves. 115</p>
Figure 6.3	<p>Behavior similar to a limit cycle observed in the \mathbb{R}^3 projection given by vehicle spacings $[s_1, s_2, s_3]^T$. Arrow indicates the direction of system evolution. The shaded region indicates the plane in which the limit cycle resides. 115</p>

Figure 6.4	Behavior similar to a limit cycle observed in the \mathbb{R}^3 projection given by vehicle velocities $[v_1, v_2, v_3]^T$. Arrow indicates the direction of system evolution.	116
Figure 6.5	False neighbors (e.g. point C) exist when the Hénon map is observed in 1-dimensional space. System was simulated with parameters $a = 1.4$ and $b = 0.3$	118
Figure 6.6	Minimum embedding dimension for the self-organized dynamics of the 3-vehicle system is found to be $d_0 = 2$. The minimum embedding dimension is determined via Cao's method as the dimension at which E_1 and E_2 approach unity.	120
Figure 6.7	State trajectories for the 3-vehicle system. For configurations where different vehicles are designated as controllers, the minimum singular values help identify influential agents. Shaded yellow regions indicate the spatial locations where a particular agent (or vehicle) has the most local influence on the self-organized dynamics of the system.	123

ACKNOWLEDGEMENTS

For a long time now, I have held firm the belief that our lives on this planet are meant to serve a purpose. Our journey from birth to death is governed, for some, by the need to understand the nature of this purpose, and for a few lucky ones, to act on it. I believe that this journey is currently taking me towards developing an understanding, both scientific and philosophical, of how this universe – the thoughts in our brains, the jams on our roadways, and life itself – ticks. This journey has been shaped by several forces, and I would like to acknowledge them here.

I would like to begin by acknowledging all my teachers to date, who have helped foster an attitude for questioning and inquiry, both scientific and philosophical. I would like to thank my advisor, *Dr. Sean Brennan*, for being patient and allowing me to freely roam the unexplored forests of scientific knowledge. His support through my years in graduate school has been crucial for my work. I would also like to thank my co-advisor, *Dr. Asok Ray*, for his support, especially during my interdisciplinary forays. I would like to acknowledge *Dr. Vikash V. Gayah* for his guidance when I encountered unfamiliar issues as I developed a new area of competency. I would like to thank *Dr. Hosam Fathy* for listening to my ideas and providing critical constructive feedback. I would also like to thank people on the administrative staff – *Jen Houser*, *Debbie Weaver*, and *Diana Lyons* – who have made my life at Penn State so much easier. I would also like to take this opportunity to thank the Larson Transportation Institute, Department of Mechanical and Nuclear Engineering, and The Pennsylvania State University, for providing me the opportunity and the platform to pursue my dreams.

To my lab mates, thank you for making graduate school such a fun experience. *Sittikorn* and *Pramod*, your friendship and guidance has been invaluable – your company is sorely missed. *Jesse* and *Alex*, thanks for listening to me when my endeavors seemed headed towards troubled waters. To my roommates (current and previous) and my friends, thanks for helping me on this journey.

And finally, I would like to acknowledge the greatest educators in my life – my parents, my sister, and her family. None of my achievements would have been possible without them. My life is testament to their divine powers of patience, perseverance, and caring. Thank you for making me laugh. Thank you for driving me further. Thank you for always being there for me.

δῶζ μοι πᾶ στῶ καὶ τὰν γᾶν κινάσω

Give me a place to stand and I will move the earth

— Archimedes (287 BC - 212 BC)

INTRODUCTION

The work presented in this dissertation has been undertaken to broadly address the question of how microscopic agents may be able to control the macroscopic dynamics of complex systems. Specifically, the presented work focuses on developing methods that may help control the self-organizing behavior observed in many complex systems, with emphasis on self-organized jams observed in highway traffic flow.

1.1 MOTIVATION: COMPLEX SYSTEMS, SELF-ORGANIZATION AND MACROSCOPIC CONTROL

The study of complex systems is easily motivated: these systems are ubiquitous in the natural and, increasingly, in the engineered world. Systems typically touted as being complex in character include stock markets [9], the human nervous system [10], communication networks [11] etc. While the definition of what constitutes a complex systems remains nebulous in nature, it is widely understood that any system consisting of a ‘large’ number of entities which interact with one another may be referred to as a *complex system*.

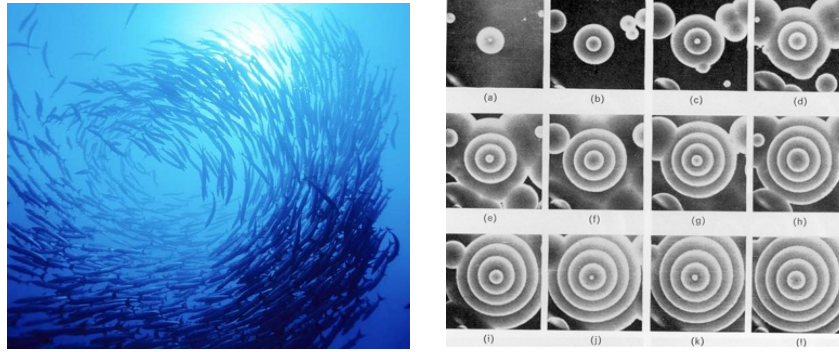
complex system

Complex systems are often said to exhibit *self-organization*, which is vaguely defined as the ‘spontaneous often seemingly purposeful formation of spatial, temporal, spatio-temporal structures or functions in systems composed of few or many components’ [12]. Humans have an innate ability for pattern recognition, so it is not surprising that we are able to ‘identify’ several systems that tend to self-organize. Examples of self-organization exhibited by complex systems include flocking of birds, ant colonies, chemical reactions, communication networks, and avalanches on snow-capped mountains, to name a few.

self-organization

In many situations, *macroscopic control* of the complex system may be required, i.e. it may be desirable to lead the system to a pre-determined spatio-temporally patterned global state (or *macrostate*). However, one of the characteristic features of self-organized systems is that they evolve to the spatio-temporally patterned state in the absence of any external control. For example, the seminal work by Per Bak and his colleagues indicates how sand piles self-organize to maintain a stable slope – the same underlying ability of complex systems also causes avalanches and earthquakes, and self-organization in several other complex systems. It then seems reasonable to assume that introduction of a small set of agents with some characteristics that differ from the existing agent population may cause a change in the macroscopic dynamics. For example, in a traffic jam, controlling a few

macrostate



(a) Schools of fish often exhibit self-organized behavior to avoid predators.
 (b) The Belusov-Zhabotinsky reaction exhibits spatio-temporal patterns characteristic of self-organized behavior.

Figure 1.1: Example of self-organizing behavior. Spatial patterns are evident to the human observer.

select agents (intelligent vehicles) may cause the traffic jam to dissipate faster – a desirable macroscopic outcome. Some of the central issues that motivate complex systems research are discussed next.

1.1.1 *Motivating questions in complex systems research*

For a complex multi-agent system whose macroscopic dynamics need to be controlled, the research community is actively investigating several key problems. Broadly speaking, these problems can be divided into the following categories:

- Which *macrostate* is best suited to describe ‘global’ behavior? (The model order reduction problem)
- Which *agent controller design* leads to the desired global behavior? (The top-down agent design problem)
- Which *global behavior* is expected to be observed, given specific agent controllers or dynamics? (The bottom-up complex system design problem)
- Which *agent* is best suited for controlling global behavior? (The agent selection problem)

To which one could add another equally important, but overlooked, problem:

- Given a set of pre-selected agents, *in which region* are they best suited to control the global behavior? (The subspace selection problem)

Researchers in the domain of complex systems are motivated by these broad questions in some form or the other, albeit in their respective fields of expertise. While the study of complex systems is well motivated, the motivation for studying systems in a specific field of expertise may vary. In this thesis, some of these motivating questions are answered with respect to self-organized traffic jams on highways. The next section discusses the motivation for studying the interplay between intelligent vehicles and self-organized traffic jams. As we will see, some of these motivations are common across all engineered systems, such as the desire to improve operational efficiency of a system, while reducing costs and meeting the customers' needs.

1.2 MOTIVATION: CONTROLLING SELF-ORGANIZED TRAFFIC JAMS

To make meaningful progress towards answering these questions, attention has been directed towards a specific instance of a complex system, viz. traffic flow on highways. Specifically, this dissertation focuses on the formation of self-organized vehicular clusters in medium-to-high density traffic, and analyzes the effects that microscopic agents (i.e. vehicles) have on the macroscopic dynamics (i.e. traffic jam dynamics) in this complex system.

Until recently, highway congestion was not considered to be a consequence of the complex nature of the traffic system. However, a slew of advances in traffic flow modeling in the 1990s [13], followed by some commendable experimental work in the 2000s [5], have resulted in a strong case for pursuing complex systems-based analyses for traffic systems, especially in the case of self-organized traffic jams. The choice to study traffic systems as a prototypical complex system is not accidental – it is motivated by the special nature of the traffic system. Specifically, traffic flow essentially generates a one-dimensional problem, significantly simplifying analysis of an otherwise complex problem. Additionally, traffic dynamics have been studied for a significant period of time and we possess a reasonable understanding of vehicular behavior.

More importantly though, the key motivator for pursuing research on self-organized traffic jams is the rising cost of congestion, accompanied by the limited avenues for infrastructure expansion required to alleviate congestion. The cost of congestion is experienced not only in terms of financial expenditure, but also as a loss of human productivity (travel delay) and damage to the environment (emissions and wasted fuel). Recent studies indicate that “between 1985 and 2006, vehicle miles traveled increased by nearly 100 percent, while highway lane miles only increased 5 percent during the same period” [14], and that “between 1982 and 2005, the percentage of the major road system that is congested grew from 29 percent to 48 percent” [15]. These

cost of congestion

data lead to the conclusion that directing infrastructure investments towards building new roads is quickly becoming an infeasible solution to the congestion problem.

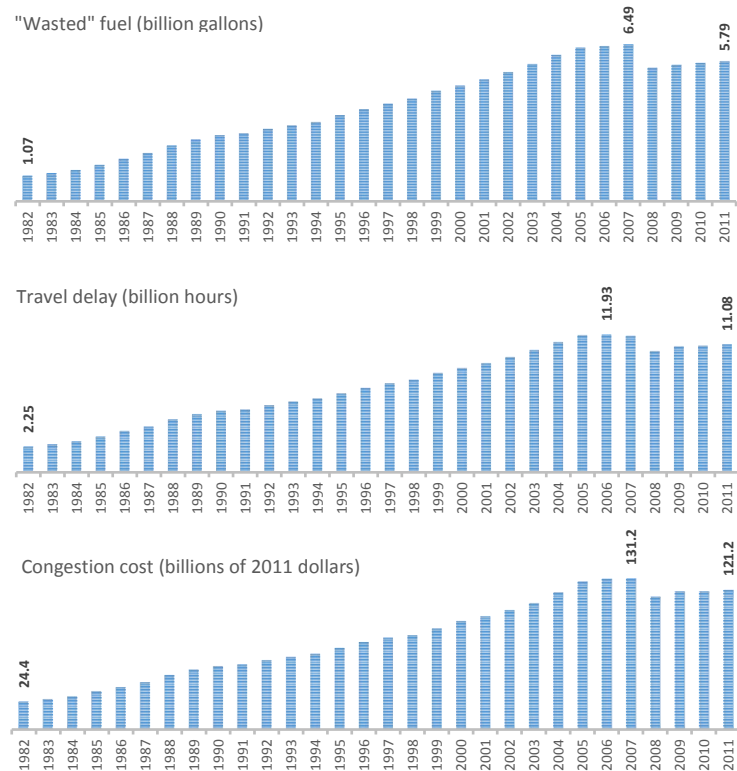


Figure 1.2: Evidence of increasing cost of congestion. [1]

An evolving traffic landscape, now comprising intelligent vehicles equipped with adaptive cruise control (ACC), and infrastructure-to-vehicle (I2V) and vehicle-to-vehicle (V2V) technologies, presents new avenues for directing infrastructure investment. Apart from making roads safer, reducing congestion is perhaps the key motivator for investing in intelligent transportation systems. In this scenario, the central theme naturally progresses towards addressing how introduction of intelligent vehicles could impact traffic jam dynamics. More importantly, the presented work considers critical issues pertaining to the spatial location of these microscopic agents (intelligent vehicles), and how varying these spatial locations can affect macroscopic traffic jam dynamics. This work lays the foundations of the novel concepts of influential subspaces and event horizons in multi-agent systems, discussed later in the text. The next section discusses some key problems in the domain of intelligent transportation systems pertinent to self-organized traffic jams.

1.2.1 *Motivating questions in intelligent transportation research*

Traffic systems and automobiles have been under development for over a century now, but the rate of change occurring today has not been observed in the past. That the present-day traffic system, dominated by human drivers, will transition to a future where most vehicles are driven by algorithms on intelligent highways, is almost a foregone conclusion. Technical progress along key areas, such as sensing, data fusion, database management etc., has continued at such an explosive rate, that today the primary hurdles to widespread adoption are seen to be legal in nature. However, while technical advances have been demonstrated in specific scenarios, certain questions remain unanswered. In the context of reducing congestion arising from self-organized traffic jams, these questions can be broadly classified into the following categories:

- *Which algorithm or technology is best suited to serve the transition period and long-term requirements of improving macroscopic traffic flow? (The technology selection and deployment problem, closely related to the top-down agent design problem)*
- *Given a specific technology, how widespread should its acceptance be in order to produce a meaningful improvement of the macroscopic traffic behavior? (The technology penetration rate problem, closely related to the bottom-up complex system design problem)*
- *Given a specific technology, what communication and messaging specifications need to be satisfied in order to benefit the macroscopic traffic behavior? (The communication protocol problem, closely related to the subspace selection problem)*

Researchers in the intelligent transportation community continue to tackle these questions using various approaches. The work presented in this dissertation addresses all three questions in varying degrees of detail. In the included analyses, the macroscopic traffic behavior corresponds to the formation of self-organized traffic jams.

1.3 GOALS OF THE STUDY

The primary goals of this study are:

- To understand and quantify of the impact of introduction of ACC-enabled vehicles on macroscopic traffic jam dynamics, via:
 - Analytical techniques that make use of known agent dynamics (i.e. car-following behavior), and
 - General numerical techniques that do not require explicit knowledge of microscopic agent dynamics.

- To formalize the notion of *influential subspaces*, loosely defined as regions within which the application of a limited local control input to a small set of agents has the potential to modify the macroscopic dynamics of a self-organizing multi-agent system, and
- To identify the influential subspaces of connected vehicles in a traffic system with self-organized jams.

1.4 OUTLINE OF REMAINING CHAPTERS

The remainder of this dissertation is organized into two parts which discuss two different types of influence inducing strategies. In [Part I](#), the influence of agents on ensemble dynamics is approached from the perspective of population modification. In this part, secondary agents that have different characteristics than the original population are gradually introduced into the system. As the population of the secondary agents increases as a ratio of the total population, their influence on the ensemble dynamics is observed. [Chapters 3 and 4](#) constitute [Part I](#). In [Part II](#), an alternative approach is attempted, where agent-specific subspaces of the state space are selected such that one agent has significant influence on the ensemble dynamics. [Chapters 5 and 6](#) constitute [Part II](#). The remainder of the thesis is organized as follows:

- **Chapter 2** discusses prior work performed in the fields of multi-agent systems with specific emphasis on agent selection, macroscopic dynamics, and influential subspaces, as well as relevant research pertaining to traffic flow theory.
- **Chapter 3** develops a master equation-based approach to analyze the evolution of self-organized traffic jams on a single-lane highway, as a function of a specific driver algorithm. The analysis is then extended to study the impact of increasing ACC penetration rates on reducing congestion.
- **Chapter 4** builds upon the analysis presented in chapter 3, by presenting a statistical mechanics-inspired numerical technique for analyzing the evolution of self-organized traffic jams for varied mixed traffic flows. The numerical analysis presented here is general enough to be applied to several complex systems, with minimal knowledge of the individual agent dynamics.
- **Chapter 5** presents a kinematic wave theory-based analysis of influential subspaces of connected vehicles present in highway traffic where self-organized traffic jams have formed.

- **Chapter 6** formalizes the concept of spatial dependence of agent influence in a rigorous control-theoretic framework for multi-agent systems.
- **Chapter 7** summarizes the major conclusions of this work, presents the major contributions, and lists potential future work.

LITERATURE REVIEW

By necessity, the study of complex systems borrows mathematical tools and elements from a wide range of existing fields of research. Some of these fields include synchronization theory, information theory, consensus dynamics, network science, multi-agent systems, and statistical mechanics, to name a few. In the following discussion, prior work relevant to the study of control of self-organized behavior in complex systems will be presented. Specifically, the discussion will include literature relevant to:

- Macroscopic modeling and dynamics,
- Influence in multi-agent systems, and
- Traffic flow theory

2.1 MACROSCOPIC MODELING AND DYNAMICS

A prerequisite for the study of control of complex systems is a model that describes the system's behavior. Specifically, an appropriate model of a complex system must mimic a key feature: self-organization, i.e. the presence of spatio-temporal patterns that evolve at a scale that is larger than the spatial and temporal scales of the individual agents. In order to accurately model the evolution of a complex system, including these spatio-temporal patterns, one must identify the system macrostate and its associated dynamics. While identification of the macrostate is a significant step in understanding the macroscopic dynamics in a complex system, we forego a detailed discussion on this topic to maintain focus on the stated goals of the study. Instead, the following subsections discuss research related to modeling the macroscopic dynamics of a multi-agent system when the macrostate is known to us. Specifically, the following discussion focuses on existing literature in the fields of:

- Macrostate identification,
- Synchronization theory,
- Consensus dynamics, and
- Statistical mechanics

A detailed discussion on the specifics of macroscopic dynamics of traffic flow is reserved for the section on traffic flow theory presented in [Section 2.3](#).

2.1.1 Macrostate identification

As already mentioned, a detailed discussion of the field of macrostate identification – and it does represent an entire field of study – is beyond the scope of this dissertation. Nevertheless, a very brief survey of techniques geared towards this purpose is presented in this subsection.

Macrostate identification may essentially be treated as a model order reduction (MOR) problem. Often large-scale or complex systems have dynamics that evolve over distinct spatial or temporal scales. As a result, model order reduction techniques may be used to obtain a simplified description of the system dynamics. The states that describe the reduced-order dynamics may be referred to as *macrostates*. Model order reduction techniques have a rich history, and traditionally can be classified into two main categories: (a) singular value decomposition (SVD) techniques, and (b) moment matching techniques. A brief review of some standard model order reduction techniques can be found in the works of Antoulas et al. [16]. Some modern model reduction techniques also approach the problem from an information-theoretic perspective, and are also briefly mentioned here.

macrostate

Singular value decomposition techniques

As the name suggests, SVD techniques for model order reduction rely on identifying a set of the largest singular values of a matrix and neglecting the smaller singular values, in the process obtaining a reduced order representation of the system. The largest singular values are assumed to encapsulate the most important dynamics of the system. Specifically, if a linear system (A, B) is given by $\dot{x} = Ax + Bu$, where $A \subseteq \mathbb{R}^{N \times N}$ and $B \subseteq \mathbb{R}^{N \times M}$, then by selecting the $k (< N)$ largest singular values of A , a reduced order representation of the system (\hat{A}, \hat{B}) can be obtained such that $\hat{A} \subseteq \mathbb{R}^{k \times k}$ and $\hat{B} \subseteq \mathbb{R}^{k \times M}$. More generally, for data-driven model order reduction, this process is also known as Karhunen-Loève decomposition, principal component analysis (PCA), and proper orthogonal decomposition (POD) [17]. One of the popular techniques for singular value decomposition is *balanced truncation* which preserves only those states that are simultaneously more controllable and observable than the others [17]. While this is a desirable property from the perspective of control, it is currently unknown if the underlying mechanisms governing self-organizing systems naturally prefer macrostates generated in this manner.

Moment matching techniques

Another approach to model order reduction, and eventual macrostate identification, makes use of the moments of the system's transfer

function $G(s) = C(sI - A)^{-1}B + D$, expanded about a point $s_0 \in \mathbb{C}$ as follows [16]:

$$G(s_0 + \sigma) = \eta_0 + \eta_1\sigma + \eta_2\sigma^2 + \dots \quad (2.1)$$

The goal of the moment matching approach to model order reduction is to obtain a reduced-order system where the expansion of the transfer function of the reduced-order system about $s_0 \in \mathbb{C}$ may be written as:

$$\hat{G}(s_0 + \sigma) = \hat{\eta}_0 + \hat{\eta}_1\sigma + \hat{\eta}_2\sigma^2 + \dots \quad (2.2)$$

such that the the first $k (\ll N)$ moments are identical, i.e. $\eta_i = \hat{\eta}_i (i = 1, 2, \dots, k)$. Popular moment matching approaches make use of Krylov subspaces and Padé approximations, and are implemented numerically using Lanczos or Arnoldi algorithms [16].

Information-theoretic techniques

Recently, several information-theoretic approaches have been proposed that may provide a better platform for approaching the problem of macrostate identification for self-organizing systems. These approaches are primarily applicable to discrete-state systems modeled by Markov chains. Model order reduction can be performed on such Markov chains either by *time aggregation* or *state aggregation*. The underlying premise in either case is that states that are ‘close’ to each other and indistinguishable during system evolution should be aggregated into a single state. Some of the earliest works on state aggregation of Markov chains was performed by Schweitzer in 1976 [18]. Recent works by Ren and Krogh [19], Cao et al. [20], Shalizi and Moore [21], and Adenis et al. [22] have proposed approaches to handle state aggregation or merging to obtain system macrostates.

In summary, model order reduction remains a rich and vibrant field of study and possesses significant untapped potential for application to macrostate identification in self-organizing systems. Further, the use of MOR techniques, especially those founded in information theory, may also help clarify the meaning of self-organization.

2.1.2 *Synchronization theory*

Synchronization theory refers to the study of self-sustained oscillating systems that interact with each other and have a tendency to achieve coherence in terms of frequency entrainment. This phenomenon is of interest when studying self-organizing multi-agent systems since it provides a natural model for ensemble dynamics. This is evident from the fact that an ensemble of agents (self-sustained oscillating systems with moderately disparate frequencies) whose trajectories reside in a high-dimensional state space can be described in a

low-dimensional (mesoscopic or macroscopic) space in terms of its ensemble dynamics that manifest as a common oscillating behavior. Thus, the dynamics of the oscillators over time, and their eventual synchronization, provides a reasonable starting point for the general study of self-organizing dynamics of complex systems. Examples of synchronization that motivated the development of this field include the collective behaviors observed in systems such as pendulum clocks, fireflies, circadian rhythm, neurons etc.

The first mathematical treatment of collective synchronization was offered by [Weiner](#) in 1958 [23]. However, the field of synchronization theory owes its origins to formal studies performed by [Winfree](#) in 1967 [24], who first used simplifying assumptions to obtain results pertaining to the onset of synchronization in weakly-coupled nearly identical oscillators. Specifically, [Winfree](#) assumed that each oscillator was coupled to the collective behavior of the entire ensemble of oscillators, analogous to a mean-field approximation, as follows [24] [25]:

$$\dot{\theta}_i = \omega_i + \left(\sum_{j=1}^N X(\theta_j) \right) Z(\theta_i), (i = 1, 2, \dots, N) \quad (2.3)$$

where θ_i denotes the phase of the oscillator i , ω_i denotes the oscillator's natural frequency, $X(\theta_j)$ is the phase-dependent influence of the j^{th} oscillator on all other oscillators and $Z(\theta_i)$ represents the i^{th} oscillator's sensitivity to the influence of the other oscillators. Later, [Kuramoto](#)'s work on identifying the evolution of a system of weakly interacting coupled oscillators provided a firm theoretical foundation for the study of phase transitions and synchronization [26]. He simplified Winfree's model as follows:

$$\dot{\theta}_i = \omega_i + \sum_{j=1}^N \Gamma_{ij}(\theta_j - \theta_i), (i = 1, 2, \dots, N) \quad (2.4)$$

where Γ_{ij} represents an interaction function relating the i^{th} and j^{th} oscillators.

As the field developed, several categories of synchronization were identified, such as *complete synchronization* (all oscillators possess identical states across time), *phase synchronization* (oscillator phases are identical across time) etc. Some of these categories are indicated in [Figure 2.1](#). However, the key element that distinguishes synchronized systems from self-organizing systems is the inability of individual entities in synchronized systems to acquire disparate states while still evolving on a low-dimensional subspace. In other words, synchronization forces the states of individual entities to be identical in some respect at a given instant of time, unlike self-organized systems that allow individual agents to have arbitrary states as long as the system evolution proceeds along a low-dimensional subspace.

*complete
synchronization
phase
synchronization*

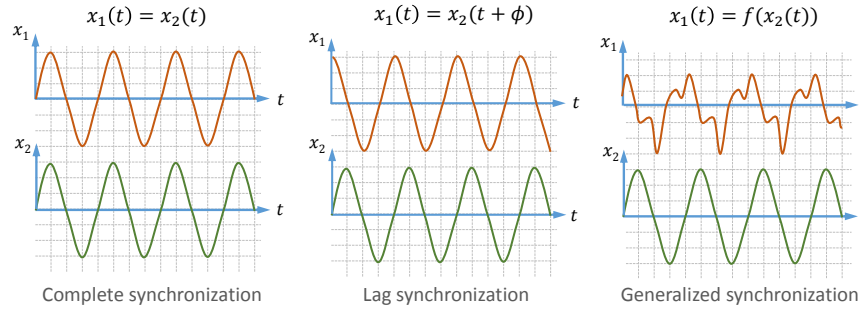


Figure 2.1: Different types of synchronization that may potentially serve as models to describe the macroscopic dynamics of self-organizing systems

Recent work by [Rosenblum et al.](#) introduces the concept of *lag synchronization*, wherein individual entities may be synchronized but with an included time lag [27]. In other words, lag synchronized systems allow individual oscillators to possess different states at the same instant of time, by ensuring that the oscillators follow identical time-shifted trajectories. While the concept of lag synchronization brings the theory closer towards explaining the phenomenon of self-organization in multi-agent systems, it still does not allow agents to possess arbitrary states while evolving on a low-dimensional subspace. A more general approach, proposed by [Rulkov et al.](#), introduces the concept of *generalized synchronization*, wherein the states of a driven system only need to be functionally related to those of the driving system, without requiring an identity relationship in space or time [28][29]. In the realm of synchronization theory, such behavior most closely resembles that of self-organizing multi-agent systems. Unfortunately, these works are limited in their analysis to systems with unidirectional coupling between driving and driven oscillators and hence do not accurately represent the interactions or topology that lead to self-organized behavior in multi-agent systems. However, it may be possible to use generalized synchronization to develop concepts of influential subspaces and control of self-organizing systems in the future. In this regard, the work of [Kiss et al.](#) is perhaps the closest to the study of control of self-organizing systems that can be found in the literature [30].

lag synchronization

generalized synchronization

2.1.3 Consensus dynamics

Consensus dynamics are closely related to the study of synchronization, but are studied in the more general context of multi-agent systems using the framework provided by network theory. Recent research has looked into consensus-type problems in multi-agent systems in several applications areas such as synchronization of coupled oscillators, flocking, distributed sensor fusion, and distributed forma-

tion control [2]. A more detailed discussion of consensus-type problems and related literature will be provided in [Section 2.2](#), when some aspects of control of networked systems are discussed.

2.1.4 *Statistical mechanics*

Statistical mechanics deals with the evolution of states of a large number of entities or agents in terms of their probability distributions and statistics. Developments in the field of statistical mechanics are of interest because they deal directly with the ensemble dynamics of a large number of entities that interact with one another. The knowledge of these ensemble or macroscopic dynamics is necessary to achieve the stated goals of this study.

The field of statistical mechanics owes its origins to the works of Boltzmann in 1872, who first presented the idea of statistical analysis of positions and momenta of gas particles, i.e. the study of their probability distributions rather than the individual gas molecules themselves [31]. Over the years, this fundamentally novel approach towards handling the evolution of large scale systems has been applied to systems as diverse as protein folding [32], neural systems [33], financial markets [34], and traffic flow [4], to name a few. Later in 1925, Ising along with his advisor Lenz, developed a prototypical model of ferromagnetism that has since been used to model a wide variety of systems [35]. In 1944, Onsager was able to obtain an analytical solution of the 2-dimensional Ising model. Potts who later became active in the field of traffic flow analysis, also provided extensions to the Ising model which will be discussed in [Chapter 4](#). Gradually, interest in the application of statistical mechanics-based techniques to traffic flow analysis arose, with Prigogine and his colleagues providing a framework for the traffic flow problem in the 1960s [4]. However, while the field of statistical mechanics continued to prosper, with seminal works by the likes of Glauber (solution of the time-dependent dynamics of the Ising model) [36] and Wilson (renormalization group theory) [37], interest in its application to the problem of traffic flow analysis diminished. Recent works by Mahnke [38] and Sopasakis [39] that study statistical mechanics-based models of traffic flow hope to revive this interest. Some additional details about the general statistical mechanics approach to traffic flow analysis as presented by Prigogine will be provided in [Section 2.3](#). Later, this dissertation will build on this interest in macroscopic modeling of traffic flow dynamics in [Chapter 3](#) and [Chapter 4](#), where the influence of a population of a particular class of drivers on the self-organizing behavior in traffic jams will be studied.

Ising model

2.2 INFLUENCE IN MULTI-AGENT SYSTEMS

Armed with the knowledge of the system macrostate, one can proceed forward with the goal of developing the notion of influence and influential subspaces in self-organizing multi-agent systems. Over the past few decades, the study of multi-agent systems has been gaining traction as systems become more complex and decentralized. As a natural consequence, interest in identifying specific agents that are most influential in their group has also increased. Before outlining some of these research efforts, a case for developing the concept of influence in multi-agent systems must be made.

2.2.1 *The need for the concept of influence*

Before embarking on a quest to measure agent influence and define novel ideas such as influential subspaces, one must ask the broader question: Does there exist a need for such concepts? In recent years, the engineered and the natural world have begun to coalesce. Pacesetters have been installed to control the cardiac cycle, intelligent vehicles will intermingle with and may affect the natural driving behavior of humans, strategies are being sought to improve human control over the Earth's climate, computer algorithms are performing stock trades in a traditionally human-centric arena, and experimental research is on the verge of providing techniques to control epileptic seizures in the human brain. This trend of interaction between natural and engineered worlds is expected to continue into the foreseeable future. In this scenario, certain entities in the system – the natural agents – are beyond our direct control, whereas other entities – the engineered agents – can easily be programmed to do our bidding. As a result, the solution to the macroscopic control of such self-organizing multi-agent systems hinges on answers to two questions already mentioned in [Chapter 1](#), and repeated here in a slightly modified form:

- Given a set of pre-selected engineered agents, *in which region* are they best suited to control the self-organized behavior of a natural-engineered complex system? (The subspace selection problem) *subspace selection*
- *Which engineered agent* is best suited for controlling self-organizing behavior of a natural-engineered complex system? (The agent selection problem) *agent selection*

The answer to the first question pertains to the problem of identifying the influential subspaces of engineered agents, within which action of these agents can help govern global dynamics. The answer to the second question helps identify which agents in a complex system are the most influential and hence have the greatest ability to govern

global dynamics. For a natural-engineered system, the first question is often more important than the second, since the selection of arbitrary agents based on their ability to influence global dynamics is not always an option. As we will see in [Chapter 5](#), engineered agents (connected or intelligent vehicles) have influence over the global dynamics (traffic jams) only in specific regions of the state space (highway). Agent selection is not a feasible option in this scenario, since a ‘dumb’ vehicle driven by a human cannot be arbitrarily controlled to influence the traffic jam dynamics.

2.2.2 *The subspace selection problem in agent-centric control of large-scale systems*

Large-scale systems often lend themselves easily to description in a multi-agent system framework. While the control of large scale systems has been a topic of research for a few decades, its formulation in a multi-agent systems framework is a recent phenomenon, taking the shape in the form of cooperative control and control of networked systems [2] [40]. While research in the domain of subspace selection has been limited, several important foundational elements, such as the identification of controllable and reachable sets, as well as application-specific research has been performed in the past. In the following discussion, research pertinent to the identification of influential subspaces will be discussed.

Controllable and reachable sets

While the concept of influential subspaces has not been studied previously in the context of multi-agent systems, related problems on identification of controllable and reachable sets have been studied for a few decades. The concept of controllability of a system was first formalized by [Kalman](#) in his seminal work presented in 1960 [41]. Over the years, these ideas have served the control systems research community quite well. Controllability and observability concepts have been heavily studied for linear systems, and to a somewhat lesser extent for nonlinear systems [42][43].

A natural extension of the idea of controllability is the notion of controllable and reachable sets. Simply put, a *controllable set* denotes the region of the state space from where admissible control policies can be applied to take the system to a pre-specified arbitrarily chosen final state. Quite often this final state is assumed to be the origin of the state space coordinate system. Similarly, the reachable set is defined as the region of the state space that can be reached from a pre-specified arbitrarily chosen initial state, which is often chosen to be the origin of the state space coordinate system, using the admissible control policies. It is evident that the controllable set for a system being controlled to the origin (determined by moving forward in time)

controllable set

is identical to the reachable set for a system beginning from the origin (determined by moving backward in time).

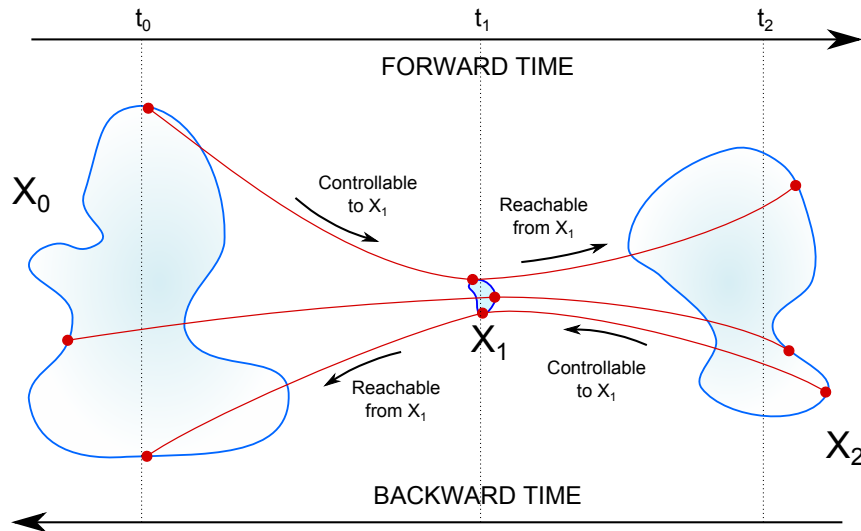


Figure 2.2: Schematic depicting controllable and reachable sets. A controllable set X_0 in forward time is identical to the reachable set (reachable from X_1) in backward time provided that the system mapping is invertible.

While controllability is well-defined and easily evaluated, the evaluation of controllable and reachable sets is a more difficult ordeal. Moreover, the research community has shown only limited interest in tackling this problem [44], despite the potentially appealing applications of input constrained controllability to self-organization in complex systems. Early work in controllable set evaluation was driven by specific applications, such as collision avoidance on roadways [45] and target capture [46]. Recent works aimed at determining controllable and/or reachable sets of a given system can be broadly classified into three categories based on their approach – they may make use of optimal control theory, Lyapunov-like functions, or polyhedron geometry. Some prior work in each of these categories is discussed below.

OPTIMAL CONTROL-BASED APPROACH Early attempts at evaluating controllable sets date back to the 1970s and relied on the relatively well-developed optimal control literature of the time [47]. One of the earliest works used Pontryagin’s minimum principle to identify the optimal control strategy, so that the resulting optimal solution $x^*(t)$ to the system equations resided on the boundary of the controllable set [48]. In later work, Vincent and Wu proposed a technique to decouple systems and subsequently identify over- and under-estimates of the controllable set [49][50]. Interestingly, Vincent and Wu also discuss projecting the controllable sets to a lower dimension to enhance

visualization of high-dimensional systems, but do not discuss projection in the context of identifying influential subspaces.

LYAPUNOV-LIKE FUNCTION-BASED APPROACH The Lyapunov-like function-based approach provides an alternative technique for identifying controllable sets and was developed almost simultaneously with the optimal control-based approach [51][52][53]. While applicable for both linear and nonlinear systems, the approach is presented here for the simpler case of linear systems, following Summers' analysis [54]. Considering a linear system given by:

$$\dot{x} = Ax + Bu \quad (2.5)$$

where $x \in \mathbb{R}^N$, A is stable and the scalar control $|u| \leq U$. If a Lyapunov-like function is given by:

$$V(x) = x^T Px \quad (2.6)$$

where P is the symmetric positive definite solution to the Lyapunov equation $A^T P + PA = -Q$, where $Q \in \mathbb{R}^{N \times N}$ is a positive definite symmetric matrix, then the time derivative of $V(x)$ is given by:

$$\dot{V}(x, u) = \frac{dV(x, u)}{dt} = -x^T Qx + 2x^T P Bu \quad (2.7)$$

In order to evaluate the reachable set, the condition $\dot{V}(x, u) \geq 0$ is used to obtain the inequality:

$$x^T Qx - 2x^T P Bu \leq 0 \quad (2.8)$$

which, considering the actuation constraints $|u| \leq U$, yields:

$$x^T Qx \pm 2x^T P BU \leq 0 \quad (2.9)$$

It is evident from Equation 2.6 and Equation 2.9 that the problem of identifying the reachable set reduces to the following:

$$\text{Maximize: } V(x) = x^T Px \quad (2.10)$$

$$\text{subject to the conditions: } x^T Qx \pm 2x^T P BU \leq 0 \quad (2.11)$$

where the maximum value of the objective function $V(x) \triangleq V^*$, so that the over-approximation $\hat{\mathcal{S}}$ of the reachable set \mathcal{S} from the equilibrium point $x = \mathbf{0}$ can be defined as follows:

$$\mathcal{S} \subseteq \hat{\mathcal{S}} \triangleq \{x \in \mathbb{R}^N | V(x) \leq V^*\} \quad (2.12)$$

If the positive definite matrix Q is set to be the identity matrix, then the over-approximation of the reachable set yields hyper-spheres; in all other cases the over-approximation results in hyper-ellipsoids in the state space. While extremely useful in identifying conservative approximations of the controllable set, especially for

nonlinear systems, this approach only yields conservative estimates of the controllable sets. The polyhedron-based approaches discussed next have the potential to determine a more accurate estimate of the controllable or reachable set, because they do not rely on any additional constructs (such as the Lyapunov-like function) other than the system equations themselves.

POLYHEDRON-BASED APPROACH Another approach to evaluate the controllable/reachable sets makes use of polyhedron geometry. Specifically, [Lasserre's](#) work uses concepts related to linear programming and polyhedron geometry to describe the controllable/reachable sets in terms of a set of linear inequalities [55]. One of the advantages of [Lasserre's](#) work is that it offers an algorithm to evaluate a closed-form solution of the controllable set in polynomial time. The works of [d'Alessandro and De Santis](#) and more recently, of [Hu et al.](#), extend this idea to higher dimensions in a more formal control-theoretic sense while retaining the insights gained by approaching the problem from the perspective of polyhedron geometry [44].

Actuator and sensor placement

Some of the earliest research similar to the concept of influential subspaces can be traced back to work on actuator and sensor placement in large-scale space structures by [Lim](#) [57] and [Gawronski](#) [58]. Whereas Lim attempted to identify locations on a flexible space structure where actuators (or sensors) must be placed so that a certain degree of controllability (or observability) is achieved, Gawronski's work focused on placing actuators and sensors in locations where they are able to replicate disturbance action and performance measurements, respectively.

Lim's work is sufficiently close to the central tenet of this dissertation to warrant a more detailed explanation. Taking a closer look, one observes an underlying theme that resonates with the idea behind the control of self-organizing behavior in complex systems. As a first step in [57], the large-scale linear system denoted by a second-order system:

$$M\ddot{\zeta}(t) + Q\dot{\zeta}(t) + K\zeta(t) = Eu(t) \quad (2.13)$$

where M , Q , and $K \in \mathbb{R}^{N \times N}$, is reduced in order using a linear transformation:

$$\zeta(t) = T\eta(t) \quad (2.14)$$

where $T \in \mathbb{R}^{N \times k}$ represents the structural mode shape vector corresponding to the k 'significant' modes that describe the vibration of

the flexible large-scale system [57]. The reduced-order system can be written in the state space form by defining the macrostate as:

$$\psi(t) = \begin{bmatrix} \eta(t) \\ \dot{\eta}(t) \end{bmatrix} \quad (2.15)$$

so that the reduced-order system may be expressed as follows:

$$\dot{\psi}(t) = \hat{A}\psi(t) + \hat{B}u(t) \quad (2.16)$$

$$y(t) = \hat{C}\psi(t) + \hat{D}u(t) \quad (2.17)$$

Next, Lim identifies the controllable (or observable) subspace as the range space of the controllability (or observability) grammian, W_c (or W_o). The key insight presented here is that all states which lie within the controllable subspace (or the range space of the controllability Grammian) can be reached by an arbitrary actuation effort $u(\tau)$, $\tau \in [t_0, \infty]$. Another construct, the *intersection subspace* is defined as the ‘subspace of system states that can be both observed and controlled by the i^{th} actuator and j^{th} sensor’ and is expressed as [57]:

$$S_{ij} \triangleq \mathcal{R}(W_c) \cap \mathcal{R}(W_o) \quad (2.18)$$

where $\mathcal{R}(W_c^i)$ denotes the range space of the controllability grammian corresponding to the i^{th} actuator, and $\mathcal{R}(W_o^j)$ denotes the range space of the observability grammian corresponding to the j^{th} sensor. Now, for the ij^{th} intersection subspace S_{ij} , the projection of the r^{th} ‘significant’ mode ϕ_r onto this subspace is given by:

$$\phi_r^{ij} = S_{ij} S_{ij}^T \phi_r \quad (2.19)$$

By evaluating a combined index α_r^{ij} , defined as:

$$\alpha_r^{ij} \triangleq \left(\phi_r^{ijT} W_c^i \phi_r^{ij} \right) \left(\phi_r^{ijT} W_o^j \phi_r^{ij} \right) \quad (2.20)$$

that takes into account the controllability and observability grammians for different actuator and sensor location pairs, the optimal actuator/sensor locations that maximize the index can be found. Thus, given a list of potential actuator/sensor pair locations, the location that optimizes the controllability and observability of the large-scale system can be found.

Limitations of prior work on subspace selection

While Lim’s work holds significant value and, at a first glance, may perhaps appear to be conceptually similar to ideas presented later in the dissertation, there are a few distinguishing features that make the concept of an subspace selection novel. These will become evident when the concept is formally defined in [Chapter 6](#), but at this point it suffices to discuss some potential issues that were not addressed in Lim’s original work and other works discussed in this subsection:

- **Analytical solutions:** The original work presented by Lim was in essence a numerical exercise, where the controllability/observability of a large-scale system was evaluated for a fixed number of locations in the state space. An analytical solution that related system controllability to agent location was not presented.
- **Actuation constraints:** As with any other measure of controllability, actuation constraints have not been considered while assessing a system's ability to reach a pre-specified state. However, in the author's experience, when dealing with self-organizing multi-agent systems, constraints on the control effort play a significant role on the potential effect an agent may have on macroscopic dynamics. In some special cases, as in self-organized traffic jams, the actuation constraints may be state-dependent.
- **Controllable sets and temporal limits:** In the discussion provided in [57], controllable and reachable sets were mentioned but not discussed in relation to the time it took to reach certain states. Introduction of actuation constraints automatically introduces temporal limits into the analysis, as will be seen in [Chapter 6](#). While some works on controllable sets do provide analytical solutions, they do not extend the concept to the notion of subspace selection.

Influential subspaces of Isner and Noton

The work of [Isner and Noton](#) [59] deserves an honorable mention in this literature review because they were perhaps the first to use the term *influential subspace* in a control theoretic setting, even though it was in a slightly different context. Their work was focused on identifying strategies to approximate the optimal control policy for a given system and cost function. Specifically, Isner and Noton approximated a control policy subspace (which they refer to as an *influential subspace*) to determine optimal control given a constrained set of initial conditions. In other words, the research attempts to identify a control policy subspace that is approximately optimal, from a wide range of potential control policies, for a constrained region of the state space that contains pre-specified initial conditions. As will be seen in later chapters, in the current work, a similar problem is addressed. Specifically, this study attempts to identify a state subspace (influential subspace) from the entire state space for a constrained region of the control policy space that contains pre-specified control policies. In other words, given the set of pre-specified control policies, the proposed work seeks to identify regions of the state space where the use of these policies produces the greatest effect on the ensemble dynamics. As mentioned earlier, the notion of using a constrained set of con-

control policies makes sense in several cases, especially when physical or other limitations of the agents disallow additional control policies.

2.2.3 *The agent selection problem*

The subspace selection problem discussed in the previous subsection is one that has not been addressed comprehensively by the multi-agent systems research community, yet one cannot overstate its importance in the context of natural-engineered systems, i.e. systems that contain both natural entities that cannot not be controlled directly and engineered entities that can be. However, the multi-agent systems and network control research community *has* been deeply involved with the concept of influential agents, i.e. agents that may have a significant impact on ensemble or global dynamics. In this regard, the research community has focused on two related areas:

- control of networked systems, and
- measures of agent influence

Control of networked systems

Systems where the agents can be represented as nodes or vertices in a graph, and the interactions between agents can be represented as edges of the graph, are referred to as *networked systems*. Several control problems can be framed in such a network-theoretic framework, and similarities between different systems can be leveraged to generate a common analysis scheme. In the literature, techniques related to the dynamics of consensus and cooperation provide the foundation for a control strategy known as *pinning control*, which can be used to analyze the influence of agents. Both consensus dynamics and pinning control will be discussed in the following subsections. Recent works, such as those by [Olfati-Saber et al.](#), [Porfiri and di Bernardo](#), [Wang and Chen](#), and [Lu](#) will be discussed.

CONSENSUS DYNAMICS The general idea behind consensus dynamics is the same as has been discussed before in [Section 2.1.2](#) and [Section 2.1.3](#). Specifically, the interactions between the agents and the agents' own dynamics cause the ensemble to converge to a single state (or *consensus*) over a period of time. However, the consensus is achieved only if all agents cooperate towards the common objective. The presence of the so-called stubborn agents that refuse to work towards the common goal results in the consensus not being achieved. The seminal paper by [Olfati-Saber et al.](#) provides an excellent description of the basics of consensus dynamics and outlines its applications in a wide range of systems such as synchronization of coupled oscillators, flocking theory, consensus in small-world networks, distributed sensor fusion, and distributed formation control.

One of the key elements in evaluation of consensus among the agents of networked systems is the graph or network topology, which determines the interactions between agents. In its simplest form, the interaction topology of agents in a networked multi-agent system can be represented as the graph $G = (V, E)$, where V is the set of vertices or nodes of the graph, which represent the individual agents, and E is the set of the edges of the graph, which represent the agent interactions. All nodes (agents) that share an edge with a given node (agent), form the neighborhood of that node (agent). The neighborhood of the i^{th} agent is denoted as $\mathcal{N}(i) = \{j \in V : (i, j) \in E\}$. The mathematical framework for addressing problems on consensus between agents in a networked multi-agent system is an n^{th} -order linear system on a graph, expressed as:

$$\dot{x}_i = \sum_{j \in \mathcal{N}(i)} (x_j(t) - x_i(t)) + b_i \quad (2.21)$$

with given initial conditions $x_i(0)$ and agent bias b_i . Readers may note the similarity between the above equation and Equation 2.4 which models the synchronization of coupled oscillators. Comparing the two equations, the oscillator's frequency ω_i represents its bias. In its simplest form, setting $b_i = 0$ for all i , Equation 2.21 can also be represented as follows:

$$\dot{x} = -\mathcal{L}x \quad (2.22)$$

where \mathcal{L} is referred to as the *graph Laplacian*, and its elements are given by:

graph Laplacian

$$l_{ij} = \begin{cases} -1, & j \in \mathcal{N}_i \\ |\mathcal{N}_i|, & j = i \end{cases} \quad (2.23)$$

where $|\mathcal{N}_i|$ represents the number of neighbors of node i . This description works for undirected graphs, i.e. graphs where edges (and by extension, agent interactions) do not have a specific direction.

If the network is represented by a directed graph, also referred to as a *digraph* (i.e. where the edges or interactions have a specific direction), then the graph Laplacian is defined more generally, as follows:

directed graph

$$\mathcal{L} = \mathcal{D} - \mathcal{A} \quad (2.24)$$

where \mathcal{D} denotes the *degree matrix*, and \mathcal{A} denotes the adjacency matrix. The elements of the degree matrix \mathcal{D} are defined as:

degree matrix

$$d_{ij} = \begin{cases} \text{deg}(v_i), & \text{if } i = j \\ 0, & \text{otherwise} \end{cases} \quad (2.25)$$

where $\text{deg}(v_i)$ denotes the out-degree, i.e. the number of outgoing edges from node i . A similar matrix may be constructed for the in-degree of a node, i.e. the number of incoming edges to a node, but

will not be considered here due to convention. The elements of the *adjacency matrix* \mathcal{A} are defined as:

adjacency matrix

$$a_{ij} = \begin{cases} -1, & \text{if } (i, j) \in E \\ 0, & \text{otherwise} \end{cases} \quad (2.26)$$

Here the notation (i, j) or $(i \rightarrow j)$ denotes an edge in the direction from node i to node j . The adjacency and degree matrices, as well as the graph Laplacian, can be determined for undirected graphs as well. Figure 2.3 describes a sample undirected graph along with its adjacency matrix, degree matrix, and the graph Laplacian. Note that in an undirected graph, the edges do not have an associated direction, so that an edge (i, j) may equivalently be written as edge (j, i) . Also note that the graph Laplacian is symmetric, and each of its row sums equals zero. Figure 2.4 shows the same graph but with directed edges, i.e. where the edges (i, j) and (j, i) represent different interactions. Note that graph Laplacian of the digraph is generally not symmetric, and its row sums don't always equal zero.

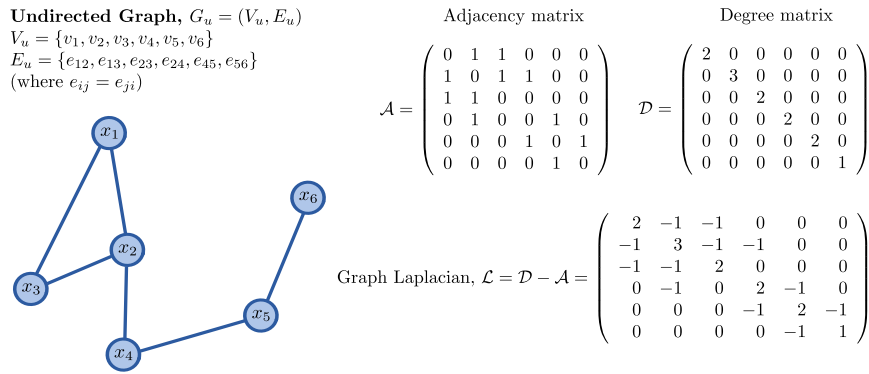


Figure 2.3: Undirected graph, associated graph Laplacian, and adjacency and degree matrices.

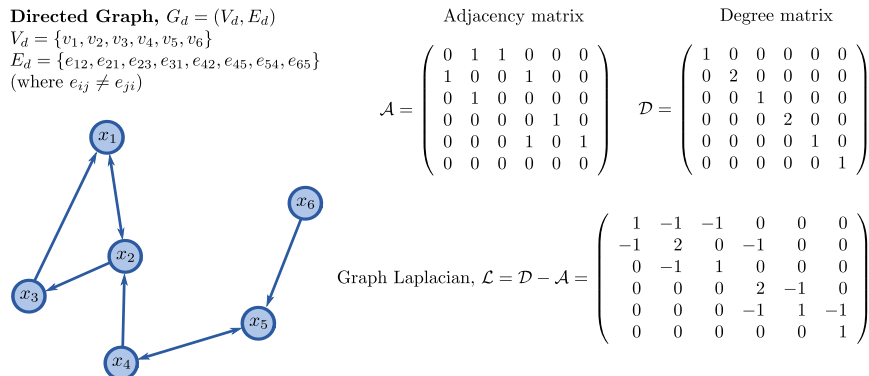


Figure 2.4: Directed graph (or *digraph*), associated graph Laplacian, and adjacency and degree matrices.

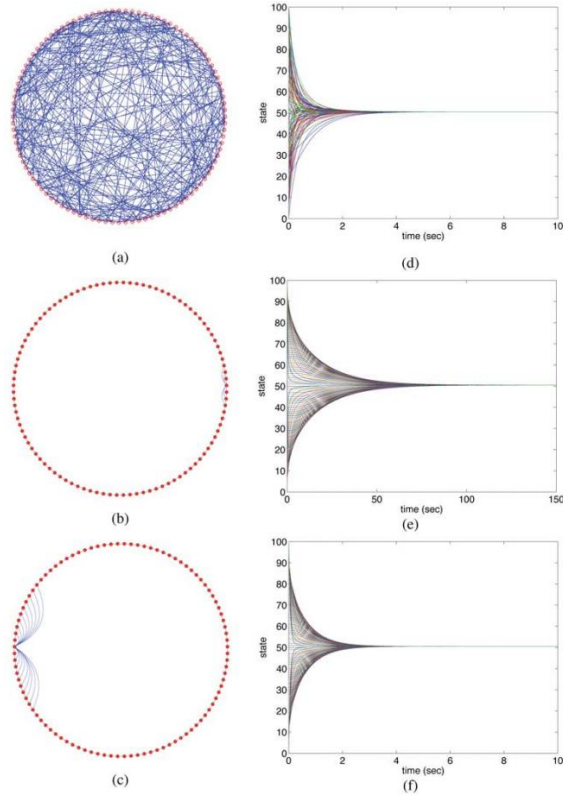


Figure 2.5: Depiction of different convergence rates to consensus, as a function of the network topology [2]. Note the difference in time scales for plots in parts (e) and (f), which represent the consensus dynamics for interaction topologies shown in parts (b) and (c), respectively. Part (a) represents a network with random topology.

The emphasis on the graph Laplacian is not unmotivated. The spectral properties of the graph Laplacian yield important information related to network connectivity and consensus dynamics of the networked multi-agent system. For example, if the eigenvalues of the graph Laplacian are given by $\lambda_1 < \lambda_2 \leq \dots \leq \lambda_N$, then λ_2 dictates the rate of convergence to consensus. Figure 2.5 offers an insight into how convergence rates to consensus depend on different graph topologies. Next, we consider how such consensus dynamics in networked multi-agent systems may be controlled via specific ‘influential’ agents.

PINNING CONTROL The foundations created by the study of consensus dynamics provide an excellent launchpad to dive into a discussion on pinning control and the determination of influential agents based on pinning control analysis. *Pinning control* may be defined as the control of a network of agents by forcing a small subset of network nodes to follow a predefined trajectory, i.e. ‘pinning’ them to the predefined trajectory. The result of pinning control is that all

agents that reside on the network nodes eventually end up following the predefined trajectory, i.e. attaining consensus.

The idea of pinning control perhaps took shape in 2002, when the earliest notions were presented by Wang and Chen in [61], which described the the control of a large networked system via local feedback applied to a fraction of the nodes of the network, thus ‘pinning’ them to a desired reference trajectory. Specifically, Wang and Chen compared the number of pinned nodes required to drive the network to consensus using specifically or randomly selected nodes. In recent years, there has been significant activity in this research area [63] [60] [64], and among these Porfiri and di Bernardo’s work provides an excellent strategy for the optimal selection of pinned nodes. In their work, Porfiri and di Bernardo model the dynamics of an i^{th} oscillator ($i = 1, 2, \dots, n$) as follows:

$$\dot{x}_i(t) = f(x_i(t)) - \sigma B \sum_{j=1}^n l_{ij} x_j(t) + u_i(t) \quad (2.27)$$

with known initial conditions $x_i(t_0) = x_{i0} \in \mathbb{R}^N$ and $t \geq t_0$. Here $f : \mathbb{R}^N \rightarrow \mathbb{R}^N$ denotes the i^{th} oscillator’s dynamics, σ denotes the coupling strength, $B \in \mathbb{R}^{N \times N}$ denotes the state variable interactions between the coupled oscillators, l_{ij} denotes the elements of the graph Laplacian \mathcal{L} , and $u_i(t)$ denotes the control input to the i^{th} oscillator.

In pinning control, the feedback control $u_i(t)$ is applied to a select subset of nodes in order to track a reference trajectory $s(t)$ which satisfies the oscillator dynamics $\dot{s}(t) = f(s(t))$. The feedback control input may be defined as:

$$u_i(t) = p_i K e_i(t) \quad (2.28)$$

$$\text{where } p_i = \begin{cases} 1, & \text{if node } i \text{ is pinned} \\ 0, & \text{otherwise} \end{cases}$$

K = feedback gain matrix, and

$$e_i(t) = s(t) - x_i(t)$$

which essentially means that the proportional control law is only applied to pinned nodes. The states of all the n oscillators can be combined into a single nN dimensional state vector, so that the system equations may be expressed as:

$$\dot{x}(t) = [1_n \otimes f]x(t) - \sigma \mathcal{L} \otimes Bx(t) + P \otimes K(1_n \otimes s(t) - x(t)) \quad (2.29)$$

where $P = \text{Diag}[p_1, \dots, p_n]$ and \otimes represents the Kronecker product. As a result of this reformulation, the error dynamics can be expressed as:

$$\dot{e}(t) = [1_n \otimes f]s(t) - [1_n \otimes f]x(t) - \sigma \mathcal{L} \otimes B e(t) + P \otimes K e(t) \quad (2.30)$$

Without going into lengthy details, the next step involves Lyapunov stability analysis to prove the asymptotic stability of the error dynamics. As a result, a measure of synchronization strength can be determined as a function of the exponential decay rate of the Lyapunov candidate function. Iterating over $\binom{n}{r}$ different combinations of r pinned nodes, the configuration of pinned nodes that maximizes the synchronization strength can be chosen to denote the set of r most influential pinned nodes. Thus, this combinatorial search strategy can be used to identify the influential agents in a networked multi-agent system.

Some other noteworthy works have focused on adaptive laws that govern interactions between network nodes so as to achieve pinning control [62], the use of structural controllability to define controllability of complex networks [65], and generation of sequential patterns and de-synchronization of weakly coupled oscillators via carefully designed interaction functions [30]. Next, we discuss some other attempts at generating measures of agent influence that also rely on controllability-like metrics, but not on the notion of pinning control.

Influential agents and measures of agent influence

Alternative approaches to the study of agent influence are primarily taken up from the viewpoint of leader selection in leader-follower multi-agent systems. Measures of agent influence in these approaches typically take the form of controllability metrics of the system [65] [66] [67] [68], or optimization of a performance metric [69] [70], though other measures of influence take inspiration from diverse applications, such as sensitivity-like measures inspired by studies of robotic arms [71].

CONTROLLABILITY-BASED MEASURES Initial studies on controllability of networked multi-agent systems have focused on determining the controllability of a network, and rightly so. With a well-developed understanding of controllability, it is not a far leap to generate a reliable controllability-based measure of agent influence. In the early 2000s, Tanner derived conditions for controllability of a connected graph for a single leader scenario. In this work, it was shown that increased controllability does not necessarily lead to increased network controllability [72]. Ji et al. derived a sufficient condition for controllability that depended on both number of leaders as well as the network topology, though the network was considered to be static [66]. Specifically, the controllability condition was obtained for a connected graph by comparing the null spaces of the incidence matrices of the set of leaders and followers, though a rigorous measure of leader influence was not evaluated.

Recent works have placed a greater emphasis in the identification of influential agents via controllability-like metrics. Specifically, Chap-

man and Mesbahi propose the calculation of the cost of anchor influence, which is the cost of introducing an external (possibly malicious) agent to influence the consensus dynamics of a networked multi-agent system [73]. They also discuss the use of the spectrum of a modified graph Laplacian, as well as the controllability Grammian, to determine the ability of the external agent to influence the consensus dynamics. Other works, such as by Pasqualetti et al. have also considered controllability-based metrics to determine the influence of a set of leaders on the networked systems. Often these controllability-based metrics take the form of the determinant $\det(\mathcal{C})$ or minimum eigenvalue $\lambda_{\min}(\mathcal{C})$ of the controllability Grammian \mathcal{C} , or the trace of the inverse of the controllability Grammian, $\text{Tr}(\mathcal{C}^{-1})$. Most works that utilize controllability-based metrics require some form of combinatorial search to find the optimal set of leaders, and this can be quite a challenging task for even moderately large networked multi-agent systems.

*controllability
Grammian*

OPTIMIZATION-BASED APPROACHES Optimization-based approaches, like their controllability-based counterparts, also rely on performing a combinatorial search, but the optimization is performed with respect to some performance characteristic of the multi-agent system such as network coherence [69] [70]. More recently, Clark et al. have pointed out some drawbacks to the optimization-based measures, viz., that while they may optimize leader selection for maximizing performance, they do not take into account the agent’s ability to control the network [67]. In their work, Clark et al. have combined both types of metrics using matroid theory to devise influence measures that take into account both performance and network controllability.

SENSITIVITY-BASED APPROACHES While the study of agent influence is a nascent field and only now beginning to gain traction, the use of sensitivity-like measures of influence is conspicuous by the fact that the literature contains even fewer instances of these measures. At least one sensitivity-like influence measure used for leader selection that deserves mention is referred to as the ‘manipulability’ measure and is derived from earlier research on the sensitivity of robotic arm manipulators. The *manipulability* of the ensemble in relation to a particular agent is defined as the ratio of the rate of change of the ensemble mean to the rate of change of the agent state [71].

manipulability

Limitations of prior work on agent selection

While several works presented in this section discuss consensus dynamics, pinning control, and the role of controllability-based metrics for agent selection, they surprisingly do not do so in the context of self-organizing systems. It is known that the dynamics of self-

organizing systems tend to evolve on a low-dimensional manifold as compared to the dimension of the networked multi-agent system itself. Specifically, agent selection for self-organizing multi-agent systems should be performed keeping in mind the low-dimensional nature of the dynamics that one desires to control or influence. Part of the work in this dissertation aims at remedying these deficiencies. Some of the early work on measuring controllability is also discussed in greater detail in [Chapter 6](#).

2.3 TRAFFIC FLOW THEORY

The dominant theme in this dissertation is to study the influence of individual agent behaviors on ensemble dynamics. As mentioned earlier, the choice to study traffic systems as a prototypical complex system is not accidental. Traffic flow essentially generates a one-dimensional problem, significantly simplifying analysis of an otherwise complex problem. Additionally, traffic flow dynamics have been studied for a significant period of time and we possess a reasonable understanding of vehicular behavior. This section¹ describes various research efforts in the past that have been directed towards the study of traffic flow. Its contents range from early works from the 1930's to model highway traffic – to attempts at modeling driver behavior in the 1960s – to recent advances in driver assist technologies and their effects on traffic flow. In addition, recent interest in treating traffic flow as a complex system and analyzing self-organizing traffic jams is also presented in this section. The aim of this section is to provide an overview of past attempts at explaining how driver behavior influences macroscopic traffic flow. Eventually, in [Parts I](#) and [II](#) that follow, different influence schemes that form the crux of this dissertation are explained.

2.3.1 *Traffic modeling*

In the early years of the growth of the automobile industry, an increase in vehicle population was counterbalanced by a corresponding increase in new highway construction. However, it was soon realized that highway construction could not keep pace with the growing societal demand for automotive transportation. In order to better understand methods for highway design, it was necessary to establish a relationship between traffic demand and highway capacity. One of the earliest recorded instances of traffic flow modeling can be traced back to 1934, when [Greenshields et al.](#) used photographic measure-

¹ AUTHOR'S NOTE This section borrows some content from the author's M.S. thesis titled 'Impact of Adaptive Cruise Control on formation of self-organized traffic jams on highways' published in 2010 [74].

ments to postulate a linear relationship between vehicle speed and average traffic density [3].

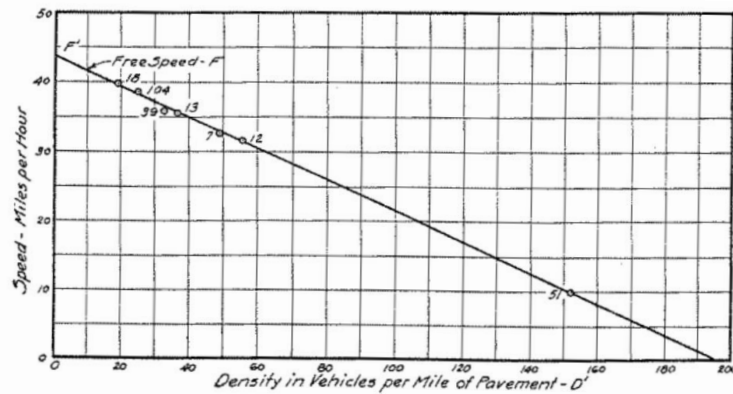


Figure 2.6: Greenshields et al. postulated a linear relationship between vehicle speed and average traffic density using photographic measurements of traffic flow.

The next major thrust in the field of traffic flow modeling came in the 1950s and 1960s, when on the one hand, researchers such as Lighthill and Whitham, and Richards began modeling traffic flow using macroscopic variables such as flow and density [75][76], whereas on the other, researchers such as Chandler et al. at General Motors began to investigate the car-following behavior of drivers. Over the years, several different modeling approaches developed. At this stage in the development of traffic flow theory, a few distinct categories have emerged into which these approaches can be classified. These categories are discussed in the following subsections.

Macroscopic modeling

Macroscopic models treat traffic flow as a one-dimensional compressible fluid and utilize bulk properties such as flow (q) and density (k) to model the system. Specifically, the model uses the continuity equation to describe the system evolution as time progresses. Assuming that the number of vehicles on a roadway is conserved, i.e. there are no on- or off-ramps, the simplest version of the model [75][78] yields:

$$\frac{\partial k(x, t)}{\partial x} + \frac{\partial q(x, t)}{\partial t} = 0 \quad (2.31)$$

where $q = kv$ represents the traffic flow, and v is referred to as the space mean speed [79]. The continuity equation has been used across the decades by relaxing the assumptions and making several modifications to model shock waves, nonlinear propagation and diffusion in traffic flow [80][81]. While macroscopic models are well suited to study the bulk behavior of traffic flow, they are typically not suited for a study how driver algorithms influence such behavior. However,

in certain simplistic scenarios, such as those presented in [Chapter 5](#), these models can be used to obtain some interesting results relevant to agent influence on ensemble dynamics.

Mesoscopic modeling

Mesoscopic models originated in the kinetic theory of gases due to work done by [Prigogine and Andrews](#) [4]. Mesoscopic models are referred to as such because they address traffic flow at a scale that lies in between macroscopic and microscopic modeling approaches ('mésos' is Greek for 'middle'). Recently, interest in modeling traffic flow has revived due to the works of [Mahnke and Kaupužs](#) [38]. Their work is discussed in the context of influencing traffic flow dynamics in [Chapter 3](#).

Mesoscopic models track the evolution of the probability distribution of a relevant traffic quantity. For example, [Prigogine and Andrews](#), and later [Prigogine and Herman](#), modeled the traffic system in a state space described by position and velocity. In the resulting gas kinetic model, the evolution of the probability distribution of a vehicle being in a particular state was studied. Specifically, the model included:

- a 'relaxation' term, which modeled a vehicle accelerating to achieve a desired velocity, and
- a 'collision' term, which modeled the deceleration of a vehicle to avoid a collision.

Mathematically, the gas kinetic model can be represented as:

$$\frac{df(x, v, t)}{dt} = - \left(\frac{\partial f(x, v, t)}{\partial t} \right)_{rel} + \left(\frac{\partial f(x, v, t)}{\partial t} \right)_{col} \quad (2.32)$$

In [Equation 2.32](#), the relaxation and collision terms are defined as follows:

$$\left(\frac{\partial f(x, v, t)}{\partial t} \right)_{rel} = \frac{1}{\tau_{rel}} (f(x, v, t) - k(x, t)F_{des}(v)) \quad (2.33)$$

$$\left(\frac{\partial f(x, v, t)}{\partial t} \right)_{col} = (\Gamma^+ - \Gamma^-)(1 - P) \quad (2.34)$$

where,

- $f(x, v, t)$ = velocity distribution function for each vehicle
- $k(x, t)F_{des}(v)$ = desired velocity distribution function
- τ_{rel} = relaxation time
- Γ^+ = collision term adding vehicles to element $dx dv$
- Γ^- = collision term removing vehicles from element $dx dv$
- P = probability of being unable to pass a vehicle

The term $f(x, v, t)dx dv$ represents the probability of a vehicle being present in the element $dx dv$. The mesoscopic model as described by Prigogine and Andrews can be better understood with the help of a visual aid, as shown in Figure 2.7. As explained in the figure, the relaxation term evolves via two processes, viz. the acceleration of a vehicle in the element $dx dv$ to leave the element, and the acceleration of a vehicle initially outside $dx dv$ to enter the element. In both these processes a vehicle is attempting to reach the desired velocity distribution. Similarly, the collision term also evolves via two processes, viz. the deceleration of a vehicle outside $dx dv$ to enter the element, and the deceleration of a vehicle inside $dx dv$ to leave the element. In both these processes, the vehicle is trying to avoid a collision with a preceding vehicle. The aggregation-based approach that uses the master equation to model the evolution of vehicle clusters is also built on the same fundamental principles [38], and is discussed in greater detail in Chapter 3.

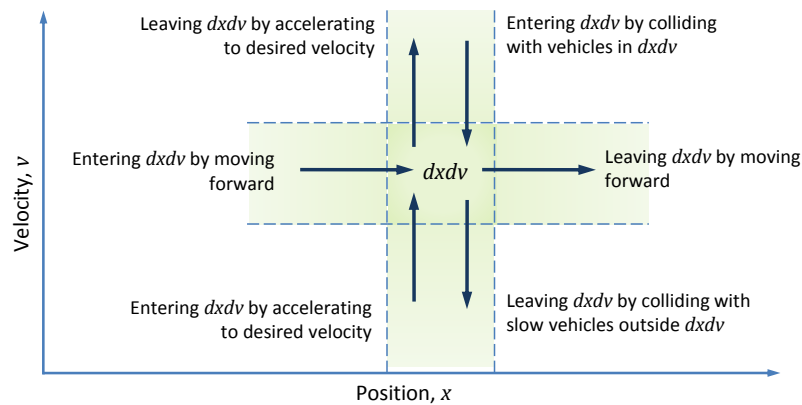


Figure 2.7: State evolution in the gas kinetic model of traffic flow as described by Prigogine and Andrews.

Microscopic modeling

Microscopic models of traffic flow track the evolution of the traffic system at the scale of individual vehicles. These models can be grouped into two categories, viz. car-following models and cellular automata models and are discussed below.

CAR-FOLLOWING MODELS Car-following models describe the evolution of a specific vehicle by using the states of the vehicle, such as position and velocity, as well as the states of neighboring vehicles to evaluate trajectory information. These models typically use ordinary differential equation, perhaps with time delays to model human reac-

tion times, to model vehicle trajectories. A prototypical version of a car-following model would take the following form:

$$\frac{d}{dt}x_j(t + \tau) = v(x_{j-1}(t) - x_j(t)) \quad (2.35)$$

where $x_j(t)$ denotes the position of the j^{th} vehicle at time t , τ denotes a response delay, and $v(\cdot)$ represents a desired velocity function that is dependent on the states of the vehicle and its neighbors.

Early versions of car-following models were developed by [Pipes](#), [Gazis et al.](#), and [Newell](#). While car-following models may describe the trajectories of individual vehicles very well, extending such knowledge to the macroscopic scale in order to evaluate the effects of individual driver behavior on traffic flow dynamics remains an extremely difficult enterprise. In this regard, analytical results are hard to come by, and the limited success that has been had is due to comprehensive numerical solutions [86]. However, car-following models are especially useful when designing cruise control algorithms and are discussed in more detail in [Section 2.3.2](#).

CELLULAR AUTOMATA MODELS Cellular automata (CA) and totally asymmetric simple exclusion process (TASEP) models significantly simplify the car-following dynamics. Cellular automata are essentially a class of ‘spatially and temporally discrete, deterministic mathematical systems characterized by local interaction and an inherently parallel form of evolution’ [87]. In these models, the roadway is discretized into sites which usually are modeled to exist in one of two states – they are either vacant or occupied by a vehicle. A discrete time evolution rule governs the probability with which a vehicle jumps or ‘hops’ from one site to another. The lineage of CA models can be traced back to the works of [Cremer and Ludwig](#) [88], and [Nagel and Schreckenberg](#) [13]. The simplicity and minimal computational expense of these models make them well suited for numerical simulations. Unfortunately, their simplicity masks the relationship between physical parameters and site transition probabilities resulting in a less than useful experience for studying the influence that drivers have on macroscopic traffic flow. Additional details about CA models of traffic flow can be found in [74][78].

While traffic flow modeling is a vibrant field of research, the effect that intelligent vehicles have on traffic flow dynamics is perhaps not as well studied. The next subsection discusses previous works that have attempted to establish the relationship between intelligent vehicles and their effects on traffic flow.

2.3.2 *Intelligent vehicle technologies*

Recent advances in sensing and data fusion have allowed the automotive research community to devise new technologies that make our

vehicles ‘smarter’. For example, vehicles can now respond to their immediate environments, as is the case with technologies such as adaptive cruise control and lane departure warning systems. New technologies can also enable vehicles to respond to environments not in their immediate vicinity, as is the case with connected vehicles that can take into account congested traffic conditions to suggest alternative routes. While these technologies benefit the individual by reducing driver effort and increasing passenger safety, their effects on the larger scale traffic flow dynamics remain unknown. This subsection discusses some relevant work in the field of intelligent vehicles technology and recent studies that have attempted to analyze their impact on traffic flow.

Adaptive cruise control algorithms

The concept of controlling the speed of a vehicle dates back to 1788, when James Watt and Matthew Boulton built the first centrifugal governor to control the speed of a steam engine. One of the earliest cruise control systems for automobiles was invented by Ralph Teetor in 1945. These early automotive cruise control technologies required the driver to manually bring the vehicle to a desired speed, after which the cruise control system would maintain the desired speed for the driver.

Recent advances in technology have enabled the use of lidar- and radar-based systems to gauge the distance between vehicles and use these measurements to maintain a safe distance. Modern systems are geared towards reducing driver effort and increasing passenger safety by controlling vehicle acceleration using measurements such as relative velocity and spacing between vehicles. These control algorithms are modern versions of the car-following algorithms of the 1960s, where the human controller has been replaced by computer algorithms.

The prototypical adaptive cruise control algorithm takes the following form:

$$\ddot{x} = f(\lambda, \Delta x, v, \Delta v) \quad (2.36)$$

- where,
- \ddot{x} = vehicle acceleration (or cruise control response)
 - λ = control gain(s)
 - Δx = spacing between vehicles
 - v = velocity of the following vehicle
 - Δv = relative velocity between vehicles

Several control schemes can be designed to fit the prototypical model for adaptive cruise control algorithm. Some of these schemes are discussed next.

CONSTANT TIME HEADWAY POLICY This policy is suggested as a common safe practice for human drivers and hence is a viable candidate for designing an adaptive cruise control algorithm [89]. The policy simply states that a following vehicle must always maintain a safe time headway (approximately 2 seconds) from the preceding vehicle. The desired safe spacing between vehicles can then be calculated as:

$$s = d_0 + Tv \quad (2.37)$$

where s denotes the safe spacing, d_0 denotes the minimum distance between stationary vehicles, T denotes the constant time headway, and v denotes the velocity of the following vehicle. An appropriate acceleration (cruise control response) can be evaluated as a function of the error in the headway.

GENERAL MOTORS' CAR-FOLLOWING MODELS These models are the result of extensive experimental work performed by researchers at General Motors in the 1960s [90]. The underlying principle of these models is that the response of a driver (or a cruise control algorithm) is a function of the driver sensitivity and an exciting stimulus. The most general form of these models is expressed as follows:

$$\ddot{x}_n(t + \tau) = \alpha \frac{[\dot{x}_n(t + \tau)]^l}{[x_n(t) - x_{n-1}(t)]^m} (\dot{x}_n(t) - \dot{x}_{n-1}(t)) \quad (2.38)$$

where x_n denotes the position of the following vehicle, x_{n-1} denotes the position of the leading vehicle, α denotes the dimensionless sensitivity coefficient of the driver of the following vehicle, and l and m are constants. In Equation 2.38, α represents the sensitivity, while the remaining terms correspond to the stimulus. For example, the vehicle will decelerate for a large stimulus which could be provided by any combination of large relative velocity, large velocity of following vehicle, and small spacing between vehicles. The sensitivity α controls the magnitude of the response in relation to the stimulus provided.

INTELLIGENT DRIVER MODEL The intelligent driver model (IDM) provides a more complicated car-following algorithm that guarantees crash-free driving [91]. The cruise control effort generated by the model is expressed as:

$$\ddot{x}_n = \alpha \left\{ 1 - \left(\frac{v_n}{v_0} \right)^4 - \left(\frac{s^*(v_n, \Delta v_n)}{s_n} \right)^2 \right\} \quad (2.39)$$

where v_n denotes the velocity of n^{th} vehicle, v_0 denotes the desired velocity of the n^{th} vehicle, s_n denotes the spacing to the preceding vehicle, and $s^*(v_n, \Delta v_n)$ denotes the desired minimum headway. The control law for the IDM can be thought of as comprising a 'relaxation'

term given by $(1 - (v_n/v_0)^4)$, which is dominant at large vehicle spacings (i.e. low density). As the vehicle speed approaches the desired speed v_0 , the acceleration effort tends to zero. The control law also consists of an interaction term given by $(s^*(v_n, \Delta v_n)/s_n)^2$, where the desired minimum spacing is given by:

$$s^*(v_n, \Delta v_n) = s_0 + vT + \frac{v\Delta v}{2\sqrt{ab}} \quad (2.40)$$

where s_0 denotes the minimum spacing in jammed traffic conditions, T denotes the safe time headway, a represents a constant acceleration term, and b denotes the comfortable braking deceleration. The interaction term is dominant and leads to large deceleration if the vehicle's velocity or relative velocity is large, or if the actual headway s_n is very small.

Connected vehicles

The advent of connected vehicles technologies is a relatively recent phenomenon and the research and automotive community has only begun to scratch the surface of potential applications that such technologies could offer. As the research field is in its nascency, most research capital has been expended towards implementation details such as communication protocols and network topologies, rather than towards the effect such technologies will have on traffic flow [92][93]. The work presented in this dissertation, especially in [Chapter 5](#), seeks to remedy this imbalance. Next, we discuss some studies that have attempted to assess the impact of adaptive cruise control algorithms on traffic flow. No such corresponding study could be found for connected vehicles technology, though a few researchers have begun to investigate related concepts [94][95].

Effect of intelligent vehicle behavior on traffic flow

Since the introduction of adaptive cruise control, numerous studies have been conducted to ascertain its influence on traffic flow. These studies can be considered to have been conducted in three different stages, which progressed as automated vehicle guidance technologies evolved [96]. The three stages are:

- Stage 1: Introduction of automated vehicles with ACC in mixed traffic
- Stage 2: Introduction of dedicated lanes for automated vehicles
- Stage 3: Introduction of intelligent infrastructure and communication networks

Each of these stages attempted to introduce technologies that would help improve traffic flow. Analyses for each of the stages comprised a

mixed approach of both simulation studies and real traffic data analysis. It may be observed that the infrastructure requirement for each stage was higher than that for the previous one.

Results from the **first stage** were mixed, with some studies indicating that addition of vehicles with adaptive cruise control resulted in decreased flow [97], whereas others indicated an increase in traffic flow [74]. One of the most prominent studies in this stage was the PROMETHEUS program, which suggested that addition of ACC would not degrade highway efficiency, while simultaneously improving driver comfort [74].

Results from the **second and third stages**, which involved additional infrastructure deployments such as dedicated lanes for automated vehicles, and vehicle-to-vehicle and vehicle-to-infrastructure communications, indicated a marked improvement in capacity. Many of the studies conducted during these stages were initiated by the National Automated Highway Systems Consortium (NAHSC) in the United States. Research indicated that formation of platoons of strings of cars could greatly increase highway capacity [98]. The California PATH program demonstrated the usage of such platoons. Other studies also indicated similarly impressive results of increased highway capacities [99][100].

While recent studies on automated highway systems indicate remarkable improvements in highway capacities, it remains a reality that these systems require a massive infrastructure overhaul and investment. Bringing such systems into practice would require a paradigm shift by both the industry and the average consumer. In the present financial climate, this approach doesn't seem feasible. Quite the contrary, the adaptive cruise control technologies already being introduced into the market today indicate a shift to an approach similar to the one that defined Stage 1. In other words, it is a more realistic goal to expect that highways in the near future will be populated with a mix of intelligent and human-driven vehicles. Further, as previously mentioned, there is no clear mandate on how highway capacity is impacted when human-driven and computer algorithm-driven vehicles are randomly interspersed on a highway. Thus an urgent need exists to evaluate the effects of such mixed traffic flow on highway capacities to design better algorithms that may help improve highway capacity in mixed traffic and also help avoid highway capacity reduction resulting from self-organizing traffic jams.

2.3.3 *Self-organized traffic jams*

The ensemble dynamics of interest in the current context are those related to the formation of self-organized vehicular clusters in highway traffic. It is apparent that each vehicle on a highway is driven by a driver who operates according to his or her own will. In other words,

each vehicle on a highway may be considered an independent agent, which operates without any influence of other vehicles. However, in medium-to-high density traffic conditions, these vehicles are closely spaced and can no longer operate without the influence of neighboring agents. Under such circumstances, the interactions between the vehicles (or agents) result in a collective behavior that cannot be derived from observing the behavior of a single agent. This behavior usually takes the form of what is known as *slinky waves* or *phantom traffic jams* or *stop-and-go* traffic. In other words, the interactions between individual vehicles results in a behavior that emerges when a group of vehicles comes together.

Nagel and Schreckenberg were perhaps the first to reproduce the phenomenon using a cellular automata model of traffic flow [13]. Later, Kerner and Konhäuser showed that given an 'initially homogeneous traffic flow, regions of high density and low average velocity can spontaneously appear, if the density of cars in the flow exceeds some critical value' [101]. Experimental verification of the spontaneous formation of jams is provided by Sugiyama et al. [5]. As has been previously mentioned, self-organization of vehicles in traffic flow into traffic jams can be described as an aggregation or cluster formation process. Mahnke and Kaupužs have studied the emergence of traffic jams from a nucleation or aggregation perspective [38]. In their paper, Mahnke and Kaupužs develop a deterministic analysis technique for the stochastic process of cluster formation to determine the time evolution of the average cluster size in a traffic jam.



Figure 2.8: Experimental study of self-organized traffic jams performed by Sugiyama et al. [5]. A self-organized vehicle cluster can be seen in the top-right section of the image

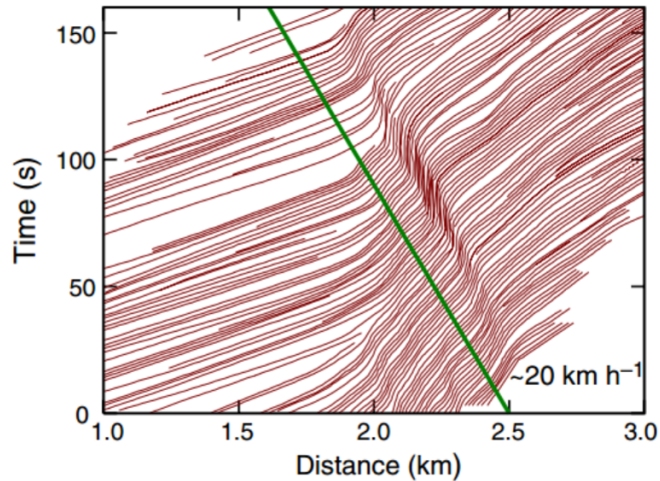


Figure 2.9: Position data for vehicles in experiments performed by Sugiyama et al. [5]. A vehicle cluster is formed and moves backward in space as time progresses.

2.3.4 Limitations of prior work

While the prior work described in this section has provided significant insight into the world of traffic flow modeling, several avenues remain to be explored. The most significant amongst these unexplored avenues is the role of individual computer algorithm-driven vehicles, either ACC-enabled or connected, in influencing ensemble dynamics, i.e. the traffic flow dynamics. In the following work, this problem has been addressed from both analytical and numerical approaches, as well as two significantly different methodologies of influence as discussed in [Parts I](#) and [II](#).

2.4 SUMMARY

This chapter covered a wide range of literature spanning several fields of study that are relevant to study the ability to influence ensemble dynamics in large-scale multi-agent systems such as traffic flow. These fields of study include consensus dynamics, control theory, statistical mechanics, and traffic flow modeling. Each of these will be used in the following chapters to assess the influence of individual drivers on traffic flow dynamics, as well as for the development of the general notion of influential subspaces. At this point, the author would like to re-emphasize that the choice of traffic flow as a prototypical system for studying influence and self-organization is primarily motivated due to its one-dimensional nature that greatly simplifies analysis.

Part I

INFLUENCE VIA POPULATION
MODIFICATION

INFLUENCE VIA POPULATION MODIFICATION

Part I of the dissertation deals with the ability to influence ensemble dynamics by modifying the nature of the ensemble's population. Specifically, in this part, the changes in steady state ensemble behavior are evaluated as a function of the changes in the population demographics of a two-species system. In [Chapter 3](#), an analytical relationship between the two-species population demographics and steady state behavior of the ensemble is developed, where the two species are human drivers and computer algorithms. The approach presented in this chapter uses some approximations specific to a two-species environment and cannot, in general, be extended to a multi-species environment. On the other hand, in [Chapter 4](#), a statistical mechanics-based numerical analysis is performed as the population demographics vary for a two-species environment, and this approach can be extended to a multi-species population. Despite these different approaches, the underlying principle in both chapters is the same – **ensemble dynamics are sought to be influenced by modifying the population demographics.**

EFFECT OF ACC PENETRATION ON FORMATION OF SELF-ORGANIZED TRAFFIC JAMS

AUTHOR'S NOTE This chapter borrows significant content from the author's publication titled "Analytical prediction of self-organized traffic jams as a function of increasing ACC penetration" published in *IEEE Transactions on Intelligent Transportation Systems* in December 2012.

Traffic flow represents an excellent example of a system whose ensemble dynamics, such as the dynamics of self-organized traffic jams, can be influenced by driver behavior. Self-organizing traffic jams are known to occur in medium-to-high density traffic flows, and it is suspected that a change in the population demographics by means of increased adaptive cruise control (ACC) penetration may affect their onset in mixed human-ACC traffic.

Unfortunately, closed-form solutions that predict the occurrence of these jams in mixed human-ACC traffic do not exist. In this chapter, both human and ACC driving behaviors are modeled using the General Motors fourth car-following model and are distinguished by using different model parameter values. A key insight of this chapter is the derivation of a closed-form solution that explains the influence of ACC penetration on congestion due to the formation of self-organized traffic jams (or *phantom jams*) is presented. The solution approach presented in this chapter utilizes the master equation for modeling the self-organizing behavior of traffic flow at a mesoscopic scale and the General Motors fourth car-following model for describing the driver behavior at the microscopic scale. It is found that, although the introduction of ACC-enabled vehicles into the traffic stream may produce higher traffic flows, it also results in disproportionately higher susceptibility of the traffic flow to congestion.

3.1 INTRODUCTION

The recent advent of Adaptive Cruise Control (ACC) technologies in mainstream vehicles holds the potential to significantly influence traffic flow dynamics and affect the formation of traffic jams. This chapter addresses the question of how an increase in penetration of ACC-enabled vehicles in highway traffic alters the dynamics of self-organizing traffic jams. Specifically, the effect of ACC penetration rate on critical vehicle density is examined for traffic flow on a closed ring road. The investigation of traffic flow on a closed ring road makes the anal-

ysis amenable to the derivation of a closed-form analytical solution by avoiding unwieldy open boundary conditions, such as on- and off-ramps, encountered on typical roads. A closed-form analytical solution helps simplify the study of the impact of increased ACC penetration on traffic flow and provides a much-needed analysis tool that is well supplemented by existing approaches which utilize numerical simulations or experimental data. The following sections discuss:

- the use of the master equation approach for modeling self-organized traffic jams developed by [Mahnke et al. \[7\]](#),
- the incorporation of adaptive cruise control algorithms into the master equation-based analysis framework,
- the analytical results indicating the influence of different penetration levels of ACC-enabled vehicles on steady state traffic flow, and
- the findings from numerical simulations which are used to validate the analytical results.

3.2 PRIOR WORK

As mentioned earlier in [Chapter 2](#), the study of adaptive cruise control and car-following algorithms has been a field of active research over the years [\[89\]\[91\]\[102\]\[103\]\[104\]](#) [\[105\]\[106\]](#). While some of these works present analytical results, they are predominantly restricted to single-species environments so the influence of changes in population demographics cannot be ascertained. Others that do deal with multi-species environments, such as the works of [Ioannou and Chien](#), are restricted to a limited number of scenarios, e.g. effect of lead vehicle maneuvers on platoon stability dynamics. Moreover, these analyses cannot be easily extended to situations where the different populations are randomly mixed in the ensemble, e.g. human-driven and ACC-enabled vehicles being randomly interspersed on the highway [\[84\]\[103\]\[106\]](#). Studies that do analyze effects of introduction of ACC-enabled vehicles in the traffic flow that are representative of real-life situations are unfortunately restricted to numerical simulations [\[86\]](#). Such studies do not yield analytical results that can provide a deeper insight and understanding of the problem.

In [Chapter 2](#), it was also mentioned that significant research effort has been directed towards understanding traffic flow dynamics [\[78\]\[79\]](#), and more specifically, towards modeling and simulation of self-organized traffic jams [\[101\]\[7\]\[107\]](#). These approaches primarily use either macroscopic models, which are not conducive for modeling variations in population demographics, or microscopic models, which rely on numerical simulations to obtain useful results. Further, self-organized traffic jams form at a scale between the macroscopic

and microscopic scales, so a mesoscopic approach is required for their analysis. The following sections discuss the mesoscopic approach proposed by [Mahnke et al.](#) that yields analytical results, and build upon it to study how changes in vehicular population (i.e. varying ACC penetration levels) influence the dynamics of self-organized traffic jams.

3.3 MASTER EQUATION APPROACH

Real-life traffic flows in the near future include ACC-enabled and human-driven vehicles. One would not wish to discover, after such mixed vehicle environments emerge, that the interaction between human and automated driver behavior induces or magnifies congestion effects. The fact that ACC-enabled and human-driven vehicles will most probably be randomly distributed in the traffic stream necessitates a probabilistic approach for analyzing the impact of ACC penetration on traffic flow. The master equation, which describes the time evolution of the probability distribution of system states, is a helpful tool for performing such an analysis. This approach for analyzing the dynamics of the size a vehicle cluster (or traffic jam) is described in the following subsections.

3.3.1 *Vehicular cluster (or traffic jam) dynamics*

To simplify the study of highway traffic, the system is often idealized as a single lane road forming a closed ring of length L with N vehicles on it [108] [7] as shown in [Figure 3.1](#). The primary reason in support of this idealization is that it helps avoid dealing with an open system representation of a highway which may include on- and off-ramps. The presence of ramps would require additional boundary conditions and could potentially complicate the system analysis. When the closed-road system is observed at the microscopic level, each vehicle in the traffic flow can be in one of two states:

- the vehicle is in free flow, i.e. it moves independently of any other vehicles on the road, or
- the vehicle is stuck in a cluster or traffic jam.

A consequence of this definition of the state is that at the microscopic level, the total number of possible states is 2^N . However, when studying the system at a mesoscopic scale, the state of choice is the cluster size ($r(t)$), which denotes the aggregate number of vehicles stuck in a cluster at time t . At the mesoscopic scale, the total number of states is N , which is a more manageable number to deal with during the modeling process.

[Mahnke et al.](#) model the formation of clusters, or self-organized traffic jams, using the mesoscopic definition of the system state. Specifically, the dynamics of the system in [7] are modeled as a stochastic

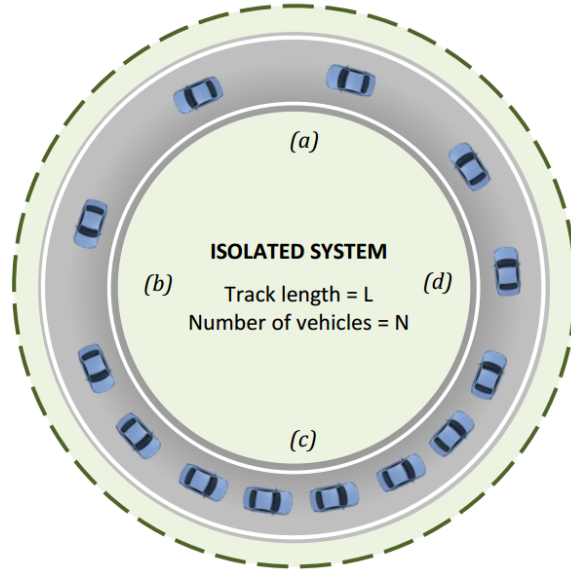


Figure 3.1: Single-lane closed road system under consideration showing (a) vehicles in free flow, (b) vehicles transitioning from free flow to jammed state (joining a cluster), (c) vehicles stuck inside a traffic jam (cluster), and (d) vehicles transitioning from jammed state to free flow.

process in terms of the probability distribution of the states, using a master equation as follows:

master equation

$$\frac{d}{dt}P(r, t) = \sum_{r' \neq r} \{w(r', r)P(r', t) - w(r, r')P(r, t)\} \quad (3.1)$$

where $w(r', r)$ denotes the transition probability rate of going from state r' to state r , i.e. the cluster size changes from r' to r , $P(r', t)$ denotes the probability that r' vehicles are stuck in a cluster at time t , $w(r, r')$ denotes the transition probability rate of going from state r to state r' , and $P(r, t)$ denotes the probability that r vehicles are stuck in a cluster at time t . Under the assumption that only one vehicle may join or leave the traffic jam at any time instant t , i.e. the state r can only transition to neighboring states ($r - 1, r$, or $r + 1$), the master equation reduces to:

$$\begin{aligned} \frac{d}{dt}P(r, t) = & w(r - 1, r)P(r - 1, t) + w(r + 1, r)P(r + 1, t) \\ & - \{w(r, r + 1) + w(r, r - 1)\} P(r, t) \end{aligned} \quad (3.2)$$

Mahnke et al. further develop the master equation approach to study the dynamics of the expected cluster size $\langle r \rangle$, which is given by:

$$\langle r \rangle = \sum_r rP(r, t) \quad (3.3)$$

Through simple algebraic operation on Equation 3.2, the following equation for the dynamics of the expected cluster size $\langle r \rangle$ is obtained:

$$\begin{aligned} \frac{d}{dt}\langle r \rangle &= \frac{d}{dt} \sum_r r P(r, t) \\ &= \sum_r r \left[w_+(r-1)P(r-1, t) + w_-(r+1)P(r+1, t) \right. \\ &\quad \left. - \{w_+(r) + w_-(r)\} P(r, t) \right] \end{aligned} \quad (3.4)$$

where $w_+(r)$ denotes the transition probability rate of a vehicle joining a cluster of size r from free flow and creating a cluster of size $(r+1)$, $w_-(r)$ denotes the transition probability rate of a vehicle leaving a cluster of size r and creating a cluster of size $(r-1)$, and $\langle \cdot \rangle$ denotes the expectation operator. Further expanding the expression under the summation sign in Equation 3.4 and using the boundary conditions:

$$\begin{aligned} \frac{d}{dt}P(0, t) &= w_-(1)P(1, t) - w_+(0)P(0, t) \\ \frac{d}{dt}P(N, t) &= w_+(N-1)P(N-1, t) - w_-(N)P(N, t) \end{aligned} \quad (3.5)$$

the dynamics of the expected cluster size are obtained to be:

$$\frac{d}{dt}\langle r \rangle = \langle w_+(r) \rangle - \langle w_-(r) \rangle \quad (3.6)$$

Further simplification of Equation 3.6 can only be performed by making some additional assumptions. Specifically, the mean-field approximation is applied to the expected value of the transition probability rates at a given cluster size r , such that $\langle w(r) \rangle \approx w(\langle r \rangle)$. As a result, the dynamics of the expected cluster size can be written as:

*mean-field
approximation*

$$\frac{d}{dt}\langle r \rangle = w_+(\langle r \rangle) - w_-(\langle r \rangle) \quad (3.7)$$

3.3.2 Transition probability rates

In order to completely describe the vehicle cluster dynamics, it is necessary to know the functional form of the transition probability rates used in Equation 3.7. The transition probability rate $w_+(r)$ of a vehicle joining a cluster of size r is defined as the inverse of the time taken for a vehicle in free flow to join a cluster. Further, the time taken for a vehicle to join a cluster (t_{join}) is dependent of the car-following or adaptive cruise control algorithm employed, as well as the initial spacing in free flow. Since typical vehicle spacings in a traffic jam are of the order of 1 to 2 m, a following vehicle is said to have ‘joined’ a cluster when it attains this spacing value [109]. Similarly, the transition probability rate $w_-(r)$ of a vehicle leaving a cluster of size r is

defined as the inverse of the time taken to accelerate out of a cluster into free flow traffic. Further, this time taken for a vehicle to leave a cluster (t_{leave}) is determined using a simple constant acceleration model as described in [110][111], and is assumed to be constant for both human-driven and ACC-enabled vehicles.

Mahnke and Pieret present an expression for $w_+(r)$ by assuming that vehicle join the cluster by moving at constant speed and ‘colliding’ with the cluster, irrespective of the driver’s efforts to maintain a safe velocity and distance from the preceding vehicle during the ‘collision’ process [109]. This simple approximation, while a good first step towards modeling self-organizing traffic jams, does not reflect the true driver behavior while approaching a cluster. Instead, as shown in the next section, new transition probability rates are determined based on car-following or ACC algorithms to more accurately describe driver behavior.

3.4 NEW TRANSITION PROBABILITY RATES

In the presented master equation approach, new transition rates are derived based on car-following models to accurately represent driver behavior. While the presented analysis uses a specific car-following algorithm, in general one could use any algorithm for which the analytical expressions for $w_+(r)$ and $w_-(r)$ can be evaluated. Though the list of such car-following algorithms is probably limited in number, the analytical procedure presented here does provide deeper insight into the effects of ACC penetration on the formation of self-organized traffic jams. Consequently, it is a potentially useful tool for studying how increasing ACC penetration influences the ensemble dynamics of traffic jams. The following subsections discuss the car-following algorithm employed, the procedure for calculating the new transition probability rates, and the associated assumptions.

3.4.1 General Motors’ car-following model

One of the popular, validated and intuitively simple car-following algorithms is the General Motors’ (GM) fourth model proposed by the General Motors Research Group around 1960 [84][90]. The model determines the acceleration control effort to be applied to the vehicle by using three variables: the headway to the leading vehicle, the relative velocity between the following vehicle and the leading vehicle, and the absolute velocity of the following vehicle. Specifically,

$$\ddot{x}_j(t + \tau) = \alpha \frac{\dot{x}_j(t) - \dot{x}_{j-1}(t)}{x_j(t) - x_{j-1}(t)} \dot{x}_j(t + \tau) \quad (3.8)$$

where $x_j(t)$ denotes the position of the following vehicle entering the cluster, $x_{j-1}(t)$ denotes the position of the leading vehicle (i.e. the ve-

hicle at the tail-end of the cluster), α denotes the sensitivity of the driver of the vehicle entering the cluster, and τ denotes the reaction time of the driver. For the sake of brevity, the spacing between vehicles $x_j(t) - x_{j-1}(t)$ is represented by $h(t)$ in the remainder of this chapter. Figure 3.2 depicts the different variables that will be used in the development of the analytical framework.

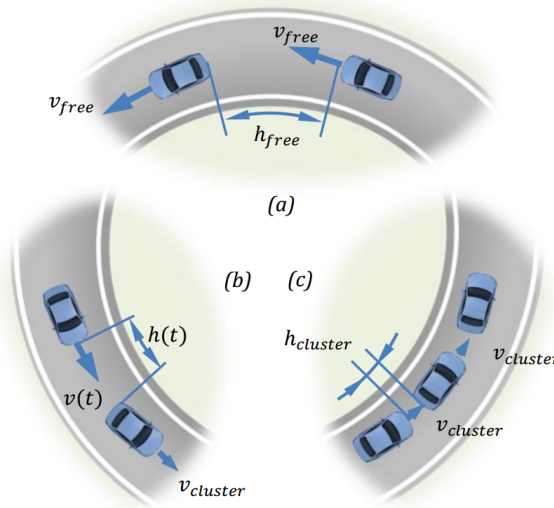


Figure 3.2: Description of variables used in analysis. (a) Vehicles in free flow (h_{free} = free flow headway, v_{free} = free flow velocity; (b) Vehicles transitioning from free flow to jammed state (joining a cluster): $h(t)$ = headway as a function of time, $v(t)$ = velocity as a function of time; (c) Vehicles stuck inside a traffic jam (cluster): $h_{cluster}$ = headway inside a cluster, $v_{cluster}$ = velocity inside a cluster.

The driver sensitivity (α) is typically indicative of the alertness of the driver while following a preceding vehicle. Low driver sensitivity might represent a ‘sleepy’ driver who takes longer to react to maneuvers, such as braking, performed by the leading vehicle. On the other hand, high driver sensitivity might represent an ‘alert’ driver, who is cognizant of any maneuvers performed by the leading vehicle and tends to take any necessary action well in advance. When considering the scenario of a vehicle entering a cluster, the range of admissible driver sensitivities is determined using typical traffic conditions and comfortable deceleration standards set by the American Association of State Highway and Transportation Officials (AASHTO). The typical traffic flow is assumed to have free flow velocity of about 25 m/s (about 55 miles/hour), free flow headway of about 100 m, and cluster velocity of about 0 to 2 m/s. Further, the maximum permissible deceleration is limited to 3.4 m/s², according to AASHTO standards. The admissible driver sensitivities that may be used with the GM fourth model under such constraints are determined by simulating the process of entering a cluster for vehicles with varying driver sensitivities. Figure 3.3 depicts the acceleration profile for a vehicle entering

driver sensitivity

AASHTO

a cluster while using the GM fourth model as the ACC algorithm. The acceleration profiles suggest that the algorithms with low driver sensitivity react much later than algorithms with high driver sensitivity. Only those driver sensitivities for which maximum deceleration during the process of entering the cluster is within the range of values suggested by the AASHTO roadway usage standard are considered for further analysis. The simulations were repeated for different values of driver sensitivity and the maximum deceleration observed during each simulation was recorded.

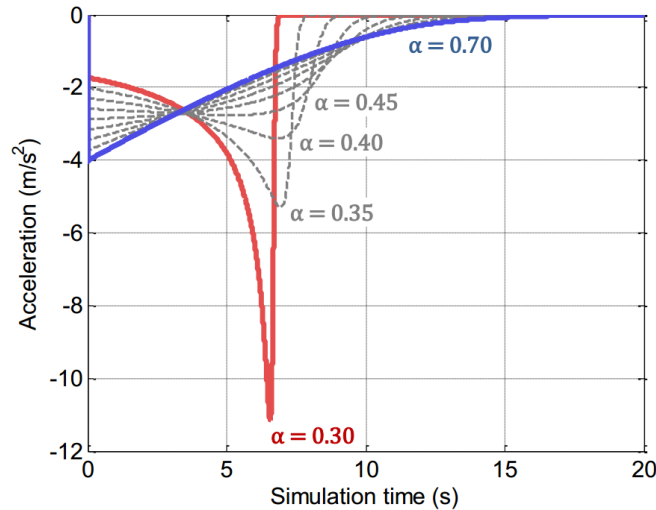


Figure 3.3: Acceleration profiles for a vehicle entering a cluster with the GM fourth model serving as the ACC algorithm with varying driver sensitivities. A driver model with low driver sensitivity ($\alpha = 0.3$) reacts later than a driver with high driver sensitivity ($\alpha = 0.7$).

Figure 3.4 shows the maximum deceleration observed during the process of entering a cluster for vehicles with various driver sensitivities. Driver sensitivities that lie approximately in the range $[0.4, 0.6]$ are admissible values for use in the GM fourth model because they approximately agree with the AASHTO recommended maximum deceleration limit of -3.4 m/s^2 . With this insight, the GM car-following model can now be used to determine the transition probability rates associated with it.

3.4.2 Derivation of new transition probability rates

Section 3.3 discussed that the transition probability rate for a vehicle joining a cluster may be defined as the inverse of the time taken to join a cluster. Since all parameters relevant to the GM fourth car-following model have been specified, Equation 3.8, which is the nonlinear ordinary differential equation describing the applied acceleration effort, can now be solved for the time taken for a vehicle to join a cluster, using the initial and boundary conditions specified by typical traf-

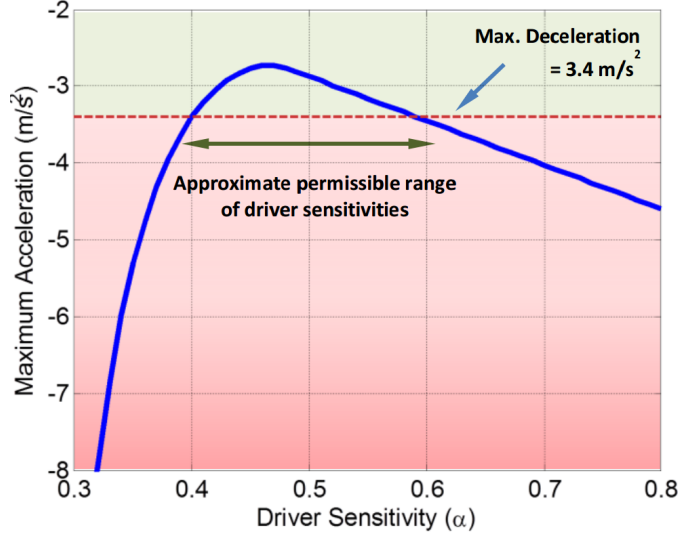


Figure 3.4: Maximum observed deceleration during simulation of a vehicle joining a cluster in typical traffic conditions, with varying driver sensitivities. The range of admissible driver sensitivities is approximately $[0.4, 0.6]$.

fic flow conditions. Rewriting Equation 3.8 in terms of the headway $h(t) = x_j(t) - x_{j-1}(t)$ and neglecting the reaction time τ , we get:

$$h\ddot{h} = \alpha(\dot{h} - v_c)\dot{h} \quad (3.9)$$

where v_c denotes the velocity of the leading vehicle. In the specific case of a vehicle entering a traffic jam, the leading vehicle is the one at the tail-end of a vehicle cluster and its velocity v_c is assumed to be constant. Equation 3.9 may be re-written as follows:

$$\frac{\ddot{h}}{\dot{h}} = \alpha \frac{\dot{h} - v_c}{h} \quad (3.10)$$

which after some simplification results in:

$$\frac{d}{dh} \left(\dot{h} \right) = \alpha \frac{\dot{h} - v_c}{h} \quad (3.11)$$

$$\text{or,} \quad \frac{d\dot{h}}{(\dot{h} - v_c)} = \alpha \frac{dh}{h} \quad (3.12)$$

Integrating both sides of 3.12 yields:

$$\ln(\dot{h} - v_c) = \alpha \ln(h) + \ln(c) \quad (3.13)$$

$$\text{or,} \quad \dot{h} - v_c = ch^\alpha \quad (3.14)$$

Using boundary conditions corresponding to typical free flow traffic, i.e. free flow velocity v_{free} and free flow headway h_{free} , the constant c is calculated to be $c = -k = -v_{free}/h_{free}^\alpha$. Substituting the value of c back into Equation 3.14 and rearranging the terms, we get:

$$dt = \frac{dh}{v_c - kh^\alpha} \quad (3.15)$$

In order to determine the transition probability rate ($w_+(r)$) of joining a traffic jam with r vehicles in it, the time taken to join a vehicle cluster from free flow needs to be derived. The derivation for time taken to reach the tail end of an existing vehicle cluster, starting from free flow headway, is included below. Integrating both sides of [Equation 3.15](#), we get:

$$\int_0^t dt = \int_{h_{free}}^{h(t)} \frac{h_{free}^\alpha}{v_c h_{free}^\alpha - v_{free} h^\alpha} dh \quad (3.16)$$

$$\text{or,} \quad t = \frac{1}{v_c} \int_{h_{free}}^{h(t)} \left\{ 1 + \frac{v_{free} h^\alpha}{v_c h_{free}^\alpha - v_{free} h^\alpha} \right\} dh \quad (3.17)$$

$$\text{or,} \quad t = \frac{h(t) - h_{free}}{v_c} - \frac{1}{v_c} \int_{h_{free}}^{h(t)} \left\{ \left(1 - \frac{v_c h_{free}^\alpha}{v_{free} h^\alpha} \right)^{-1} \right\} dh \quad (3.18)$$

Now realizing that as the vehicle approaches a traffic jam, its headway decreases with time, I.e. $\dot{h} < 0$, one can deduce the following from [Equation 3.15](#):

$$\dot{h} = v_c - \frac{v_{free} h^\alpha}{h_{free}^\alpha} < 0 \quad (3.19)$$

$$\text{or,} \quad \frac{v_c h_{free}^\alpha}{v_{free} h^\alpha} < 1 \quad (3.20)$$

Using the Maclaurin series expansion of $(1 - x)^{-1}$ for $|x| < 1$, i.e.

$$\frac{1}{1 - x} = 1 + x + x^2 + x^3 + \dots \quad (3.21)$$

the expression in [Equation 3.18](#) can be operated upon to get:

$$t = \frac{h(t) - h_{free}}{v_c} - \int_{h_{free}}^{h(t)} \frac{1}{v_c} \left\{ 1 + \left(\frac{v_c h_{free}^\alpha}{v_{free} h^\alpha} \right) + \left(\frac{v_c h_{free}^\alpha}{v_{free} h^\alpha} \right)^2 + \left(\frac{v_c h_{free}^\alpha}{v_{free} h^\alpha} \right)^m + \dots \right\} dh \quad (3.22)$$

$$\text{or,} \quad t = \frac{h(t) - h_{free}}{v_c} - \frac{1}{v_c} \left\{ 1 + \left(\frac{v_c h_{free}^\alpha}{v_{free}} \right) \frac{h^{1-\alpha}}{1-\alpha} + \left(\frac{v_c h_{free}^\alpha}{v_{free}} \right)^2 \frac{h^{1-2\alpha}}{1-2\alpha} + \dots \right\}_{h=h_{free}}^{h=h(t)} \quad (3.23)$$

Equation 3.23 holds true for all $m\alpha \neq 1 (m \in \mathbb{Z}^+)$. However, in case $m\alpha = 1$, the integral of the corresponding m^{th} term can be modified accordingly to yield an expression in terms of $\ln(h)$. Simplifying Equation 3.23 and using the limits of integration corresponding to headway in free flow traffic (h_{free}) and headway inside a vehicle cluster ($h(t)$), the following expression is obtained:

$$t_{join} = \frac{1}{v_c} \sum_{m=1}^{\infty} \left\{ \frac{1}{1 - m\alpha} \left(\frac{v_c}{\kappa} \right)^m \left(h_{free}^{1-m\alpha} - h_c^{1-m\alpha} \right) \right\} \quad (3.24)$$

where t_{join} denotes the time taken to join a cluster, v_c denotes the velocity of the vehicle at the tail-end in the cluster (also the leading vehicle for the vehicle joining the cluster), m refers to the m^{th} term in the series expansion, α denotes the driver sensitivity in the GM fourth car following model, $\kappa = v_{free}/h_{free}^\alpha$ denotes a driver dependent constant, and h_c denotes the headway inside a cluster and is known to be approximately constant at about 1 meter through experimental observations [79][109].

Unfortunately, the expression for t_{join} is a hypergeometric series with no closed-form solution. However, it is observed that as an increasing number of terms are used to evaluate t_{join} , i.e. the series is truncated at higher orders of m , the hypergeometric series quickly converges to the true solution obtained from numerical simulation. Figure 3.5 depicts the convergence of the hypergeometric series to the exact solution. As can be observed, the approximate solution is comparable to the exact solution for even as few as two terms.

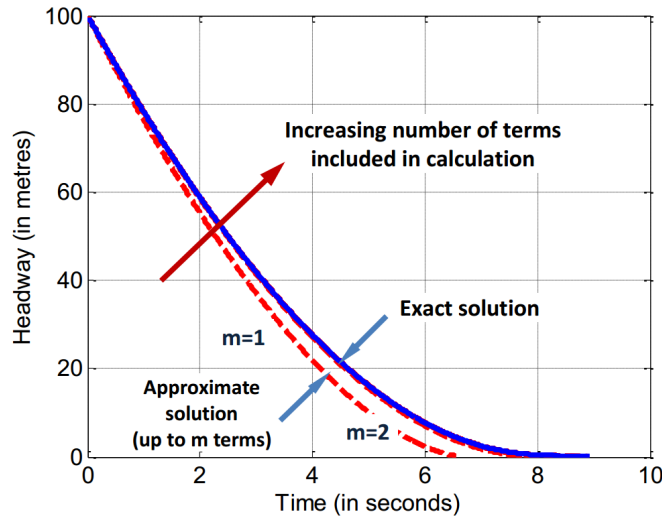


Figure 3.5: Time taken to join a cluster (t_{join}) using the expression derived from the GM fourth model nonlinear ODE. The truncated hypergeometric series quickly converges to the exact solution as more terms are included.

An additional key insight of this work is to recognize that the hypergeometric series is constrained by the range of admissible driver

sensitivities. Considering the range of admissible driver sensitivities, it is observed that a closed-form exact solution of the hypergeometric series t_{join} can be approximated by using the first term of the series (t_1) and an appropriate truncation ratio (ζ), such that $t_{join} = \zeta t_1$. Figure 3.6 depicts the variation in the truncation ratio, which is the ratio of the exact solution obtained from numerical solution (using up to 40 terms in the hypergeometric series) and the approximate solution obtained using only the first term of the series, as a function of driver sensitivity (α). Thus, when the driver sensitivity of the car following algorithm is known, Figure 3.6 may be used to determine the correct truncation ratio and, consequently, the approximate time (t_{join}) taken to join the vehicle cluster.

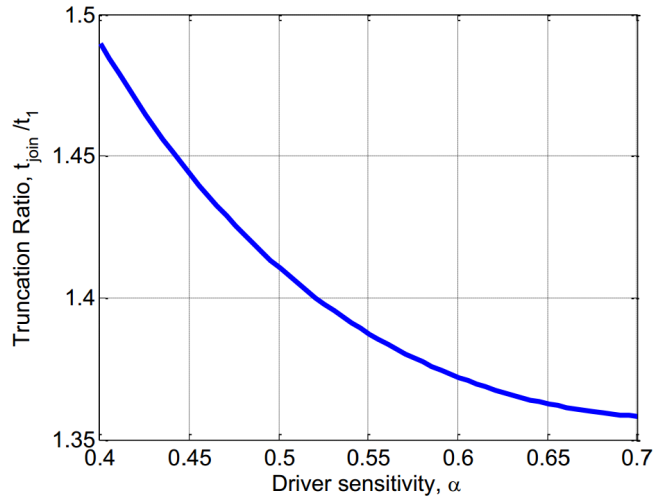


Figure 3.6: Range of admissible driver sensitivities limits the variation of the truncation ratio, $\zeta = t_{join}/t_1$. Based on the driver sensitivity α of the car-following algorithm, an appropriate value of $\zeta(\alpha)$ can be used to approximate the time taken to join a cluster.

As mentioned earlier, the transition probability rate is defined as the inverse of the time taken to join a cluster. Thus, the new transition probability rate for a vehicle joining a cluster is given by:

$$w_+(r) = \frac{1}{t_{join}} = \frac{1}{\zeta t_1} = \frac{\kappa(1-\alpha)}{\zeta} \left(\frac{1}{h_{free}^{1-\alpha} - h_c^{1-\alpha}} \right) \quad (3.25)$$

The transition probability rate for leaving a cluster is determined using a constant acceleration model and is assumed to be constant for both ACC-enabled and human-driven vehicles. The acceleration of a vehicle starting out of a cluster and moving into free flow is determined by modeling it as a vehicle starting from rest. From experimental observations of traffic [111], this acceleration is found to be 2.5 m/s² on an average and the corresponding time taken to leave the cluster based on typical traffic conditions is 7.5 to 10 seconds. As a result, $w_-(r)$ is approximately equal to 0.1 s⁻¹. Thus, new transition

probability rates that better describe actual driver behavior have been obtained and further analysis based on the vehicle cluster dynamics as described by Equation 3.6 can be performed.

3.5 STEADY-STATE ANALYSIS

The vehicle cluster dynamics discussed in Section 3.3 may be used to perform a steady-state analysis to determine the expected size of a stable cluster or traffic jam. This section will discuss how the expected cluster size varies as a function of traffic density in steady-state conditions, for both single species and multi-species environments.

3.5.1 Steady-state analysis for single species environments

As is evident from Equation 3.6, the steady-state condition for a stable cluster size is $w_+ \langle r \rangle = w_- \langle r \rangle$. Since $w_+ \langle r \rangle$ is a function of the free flow headway (h_{free}), as derived from the GM fourth model and described in Equation 3.25, and $w_- \langle r \rangle$ has been assumed to be constant, the steady-state condition can be used to determine an expression of h_{free} as follows:

$$[h_{free}]_{ss} = \left\{ h_c^{1-\alpha} + \frac{t_{leave} \kappa (1-\alpha)}{\zeta} \right\}^{1/(1-\alpha)} \quad (3.26)$$

Additionally, physical constraints such as the finite length of the closed road and finite vehicle length can also be used to determine the free headway. These two expressions for free flow headway, one obtained from the steady-state condition and the other from physical constraints, can then be equated as follows:

$$[h_{free}]_{ss} = \frac{L - Nl - (\langle r \rangle - 1)h_c}{N - \langle r \rangle + 1} \quad (3.27)$$

where l denotes the length of a vehicle. Further, assuming that the expected cluster size is large, so that $\langle r \rangle - 1 \approx \langle r \rangle$, dividing the numerator and denominator on the right hand side by L , and with some rearrangement, the following expression that relates the expected cluster size to the traffic density is obtained:

$$\langle r \rangle^* = \frac{k^* \left([h_{free}]_{ss} + l \right) - l}{[h_{free}]_{ss} - h_c} \quad (3.28)$$

where $\langle r \rangle^* = \langle r \rangle l / L$ denotes the normalized expected cluster size, and $k^* = Nl / L$ denotes the dimensionless traffic density on the closed ring road. Equation 3.28 indicates that the relationship between stable cluster size and the dimensionless traffic density is linear in nature. Further, since the cluster size cannot be less than zero, Equation 3.28 also indicates that there exists a critical density k_c at

which vehicle clusters or self-organized vehicle clusters first begin to appear. Substituting $\langle r \rangle^* = 0$ in Equation 3.28 yields an expression for dimensionless critical density for traffic flow:

$$k_c^* = \frac{l}{[h_{free}]_{ss} + l} \quad (3.29)$$

Figure 3.7 shows the steady-state phase plot of the normalized stable cluster size plotted against the dimensionless density for a traffic flow consisting of a single species, i.e. a single type of driver model (GM fourth model with driver sensitivity $\alpha = 0.4$). The solid line depicts the stable cluster size for a given density. It is observed that in this scenario, the analytical results predict that the dimensionless critical density, or the density at which vehicle clusters begin to form spontaneously, is approximately $k_c^* = 0.1$. It is argued that this value of the driver sensitivity is reasonably representative of human drivers since experimental data from German highways (shown in Figure 3.8) also indicates that the dimensionless critical density for humans, as observed from the fundamental diagram of traffic flow, is approximately 0.1. In the next subsection we discuss the selection of the appropriate driver sensitivity for ACC-enabled vehicles and the methodology for introducing ACC-enabled vehicles in the analysis framework.

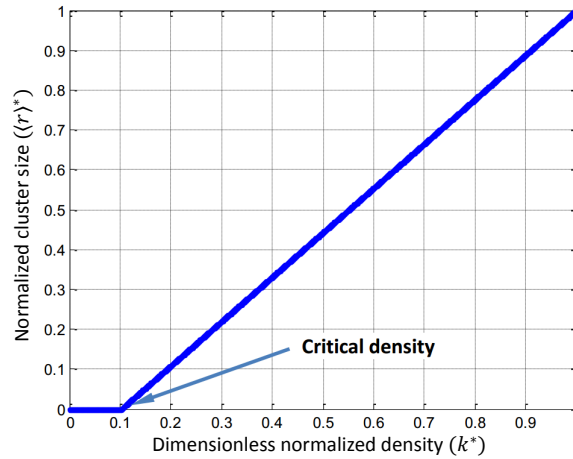


Figure 3.7: Steady-state phase portrait of normalized cluster size versus dimensionless density consisting of a single driver species based on GM fourth model with $\alpha = 0.4$. The solid line indicates the stable cluster sizes or traffic jams. Clusters or traffic jams first begin to appear when the dimensionless density reaches a critical value of $k_c^* \approx 0.1$.

3.5.2 Introduction of ACC-enabled vehicles into traffic flow

The single-lane closed ring system is now considered with traffic consisting of a mixture of ACC-enabled and human-driven vehicles.

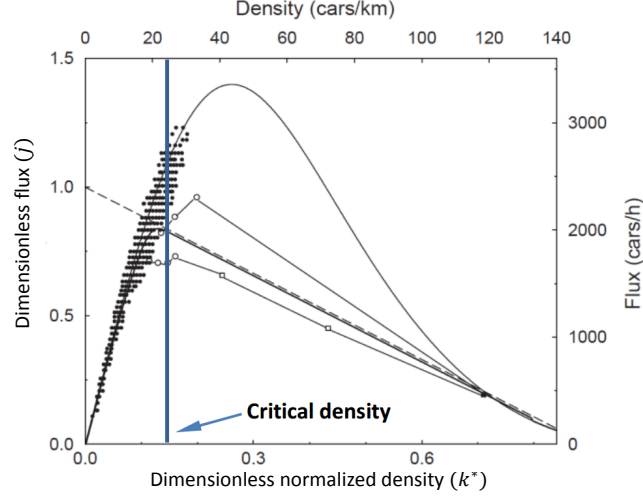


Figure 3.8: Experimental data for traffic flow consisting solely of human drivers on German highways. Dots indicate experimental observations [6]. The observed dimensionless critical density is close to 0.1 [7].

Let the fraction of ACC-enabled vehicles on the closed road be p . Assuming that the population of vehicles on the closed road is large enough, such that the proportion of ACC-enabled and human-driven vehicles outside the cluster remains constant, then the effective transition probability rates are given by:

$$w_+^{\text{EFF}}(r) = (1 - p)w_+^{\text{H}}(r) + pw_+^{\text{ACC}}(r) \quad (3.30)$$

$$w_-^{\text{EFF}} = \frac{1}{t_{\text{leave}}} \quad (3.31)$$

where $w_+^{\text{H}}(r)$ denotes the transition probability rate of joining a cluster for a human-driven vehicle with $\alpha_{\text{H}} = 0.4$, and $w_+^{\text{ACC}}(r)$ denotes the transition probability rate of joining a cluster for an ACC-enabled vehicle with $\alpha_{\text{ACC}} = 0.7$. The rationale behind picking the driver sensitivity value for human drivers has already been presented in the previous subsection.

In contrast, the choice of driver sensitivity for ACC-enabled vehicles is motivated in part by the reasoning that, whereas human drivers are typically performing multiple tasks while driving and may be less alert to sudden changes in the traffic stream, ACC algorithms are performing the sole task of driving and continually monitoring the road ahead. ACC algorithms are expected to be more sensitive and alert to changes in the traffic stream and thus are assigned a higher driver sensitivity value. Another motivating factor for choosing $\alpha_{\text{ACC}} = 0.7$ is the desire to obtain a closed-form solution for the expected vehicle cluster size. This is discussed in the next subsection in relation to the steady-state analysis for mixed traffic

3.5.3 Steady-state analysis for multi-species environment

The sensitivity value for ACC-enabled vehicles is determined from the necessity of obtaining a closed-form solution for the analysis. When the expressions for individual transition probabilities $w_+^H(r)$ and $w_+^{\text{ACC}}(r)$ are substituted in the effective transition probability rate $w_+^{\text{EFF}}(r)$, and the steady-state condition $w_+^{\text{EFF}}(r) = w_-^{\text{EFF}}(r)$ is considered, the following equation is obtained:

$$h_{free}^{1-\alpha_H} h_{free}^{1-\alpha_{\text{ACC}}} - a_2 h_{free}^{1-\alpha_H} - a_1 h_{free}^{1-\alpha_{\text{ACC}}} + a_0 = 0 \quad (3.32)$$

where the coefficients are functions of h_c , t_{leave} , p , α_{ACC} , and α_H and are given by:

$$a_2 = h_c^{1-\alpha_{\text{ACC}}} + (1 - \alpha_{\text{ACC}}) p t_{leave} \kappa_H / \zeta(\alpha_{\text{ACC}}) \quad (3.33)$$

$$a_1 = h_c^{1-\alpha_H} + (1 - \alpha_H)(1 - p) t_{leave} \kappa_{\text{ACC}} / \zeta(\alpha_H) \quad (3.34)$$

$$a_0 = h_c^{1-\alpha_H} h_c^{1-\alpha_{\text{ACC}}} + (1 - \alpha_H)(1 - p) t_{leave} \kappa_H h_c^{1-\alpha_{\text{ACC}}} / \zeta(\alpha_H) \\ + (1 - \alpha_{\text{ACC}}) p t_{leave} \kappa_{\text{ACC}} h_c^{1-\alpha_H} / \zeta(\alpha_{\text{ACC}}) \quad (3.35)$$

where $\zeta(\cdot)$ and κ are functions of driver sensitivity, α , as discussed earlier.

In the depicted general form, Equation 3.32 is a transcendental equation and can only be solved using numerical or graphical methods. In order to obtain an analytical solution for the steady-state free headway, the transcendental equation is reduced to an algebraic equation (quadratic, cubic or bi-quadratic) by enforcing a constraining relation on the values that α_H and α_{ACC} may simultaneously assume. One such relation that reduces Equation 3.32 into a cubic equation and thus allows a closed-form solution is $(1 - \alpha_H) = 2(1 - \alpha_{\text{ACC}})$ i.e. $\alpha_{\text{ACC}} = 0.5(1 + \alpha_H)$. It may be observed that, once this substitution is made, arbitrary choices of driver sensitivities cannot be made in further analysis. This is due to the fact that the choices are restricted by two constraints, viz. the maximum acceptable deceleration, and a constraining relation between α_{ACC} and α_H which is a consequence of the need to obtain a closed-form solution. A number of values of driver sensitivities $(\alpha_H, \alpha_{\text{ACC}})$ such as (0.35, 0.675), (0.4, 0.7) etc. which satisfy the relation $\alpha_{\text{ACC}} = 0.5(1 + \alpha_H)$ also lie approximately in the range defined by maximum acceptable deceleration based on AASHTO standards.

Thus, the relation $\alpha_{\text{ACC}} = 0.5(1 + \alpha_H)$ may be used as an approximation, together with this restricted set of values, to reduce Equation 3.32 into a cubic form as follows:

$$\left(h_{free}^{1-\alpha_{\text{ACC}}}\right)^3 - a_2 \left(h_{free}^{1-\alpha_{\text{ACC}}}\right)^2 - a_1 \left(h_{free}^{1-\alpha_{\text{ACC}}}\right) + a_0 = 0 \quad (3.36)$$

The expression for steady-state free headway $[h_{free}]_{ss}$ in a multi-species environment is obtained by solving the cubic Equation 3.36.

Next, the steady-state free headway expression is substituted into [Equation 3.28](#) to obtain a relationship between expected cluster size and traffic density in a multi-species environment. The implications of the above analysis in both single species and multi-species traffic environments are discussed in the next section, along with some experimental results from mesoscopic simulations of traffic flow.

3.6 RESULTS AND MESOSCOPIC SIMULATIONS

This section discusses the obtained analytical results for both single species and multi-species environments, and their interpretations with respect to real-life traffic flows. Additionally, mesoscopic simulations of vehicle cluster dynamics are presented and are shown to validate the obtained analytical results.

3.6.1 Results for single species traffic flow

In the previous section it was mentioned that the expression for steady-state free headway obtained from [Equation 3.36](#) may be substituted in [Equation 3.28](#) to obtain the relationship between expected normalized cluster size and dimensionless density in a multi-species environment. The resulting relationship may be plotted as a phase portrait to illustrate the cluster dynamics as a function of the proportion of ACC-enabled vehicles on the closed road. [Figure 3.9](#) shows the steady-state phase portraits for two special cases: (i) when the vehicle population consists of only human-driven vehicles ($p = 0.0, \alpha = 0.4$), and (ii) when the vehicle population consists of only ACC-enabled vehicles ($p = 1.0, \alpha = 0.7$). The figure suggests that the traffic operates at higher critical densities, and consequently higher traffic flows, when it consists of only ACC-enabled vehicles as compared to when it consists of only human-driven vehicles. The relationship between cluster size and density in a single-species environment is validated by performing a Monte Carlo simulation using the mesoscopic level definition and dynamics of the system state. Specifically, the cluster formation process is modeled as a one-dimensional random walk where the cluster size grows or shrinks based on the new transition probabilities derived in [Section 3.4](#).

[Figure 3.10](#) shows that the mesoscopic simulation matches the analytical results but is valid only up to dimensionless density $k^* = 0.8$. This can be explained by studying the method for calculating free headway from physical constraints, as described in [Equation 3.27](#). It is evident that as $N \rightarrow L/l$, the numerator on the right-hand side of [Equation 3.27](#) becomes smaller, and represents the limit of bumper-to-bumper traffic. Any further subtraction due to the presence of the cluster headway term, $(\langle r \rangle - 1)h_{cluster}$, will cause the free headway to become negative. Thus, the simulation indicates that present form of

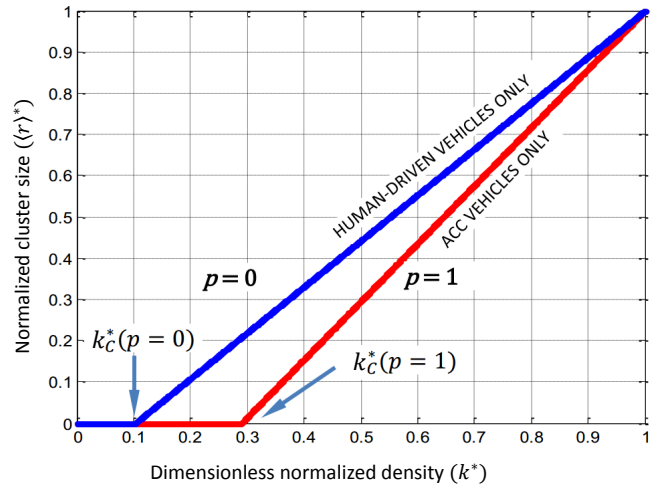


Figure 3.9: Steady-state phase portrait describing analytical results for special cases of mixed traffic. Traffic consists of (i) human-driven vehicles only ($p = 0.0$), and (ii) ACC-enabled vehicles only ($p = 1.0$).

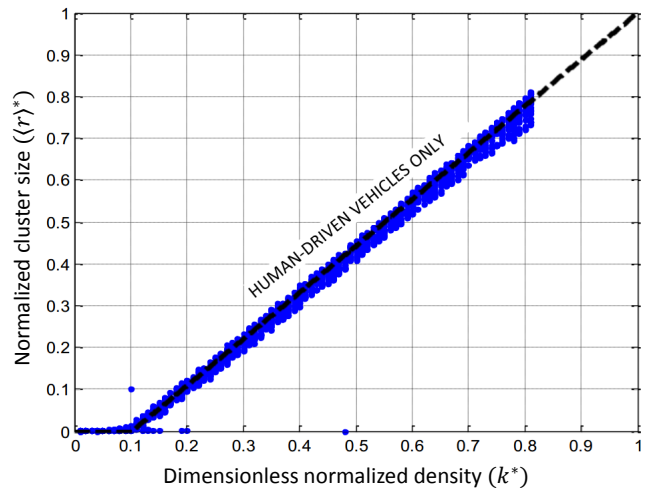


Figure 3.10: Monte Carlo simulation validates the analytical results obtained for the relationship between normalized cluster size and dimensionless density, for a single species environment. Thick dashed line denotes analytical solution. Solid dots indicate the mean steady-state cluster sizes obtained from the simulation.

the analysis may not be applicable for extremely high density traffic. However, it may be realized that situations in which the traffic flow reaches extremely high densities are not expected to be observed too often. The analysis is largely supported by the simulations in the remaining scenarios, especially for determining the critical density at which vehicle clusters (or traffic jams) first appear.

3.6.2 Results for multi-species or mixed traffic flow

In a multi-species environment, it is of greater interest to observe the trends in critical density as a function of the proportion of ACC-enabled vehicles in the mixed traffic flow. Figure 3.11 shows these trends as obtained from the analytical results. It is observed that as the proportion of ACC-enabled vehicles on the road is increased, the critical density increases and this increase is not uniform. Specifically, as the proportion of ACC-enabled vehicles in the traffic flow increases, the traffic flow becomes increasingly sensitive to changes in vehicle population proportions.

For example, consider the two scenarios in Figure 3.11 that depict the traffic system operating at the same threshold (Δk) away from the critical density, but in two very different regimes. In predominantly human driver traffic in the jam-free regime (operating point A), a small change in vehicle proportion (Δp) does not change the state of the traffic flow, which continues to operate in the jam-free regime. On the other hand, if the same change of vehicle proportion is introduced in predominantly ACC traffic in the jam-free regime (operating point B), it causes the traffic flow to change from a jam-free state to a self-organized jam or congested state.

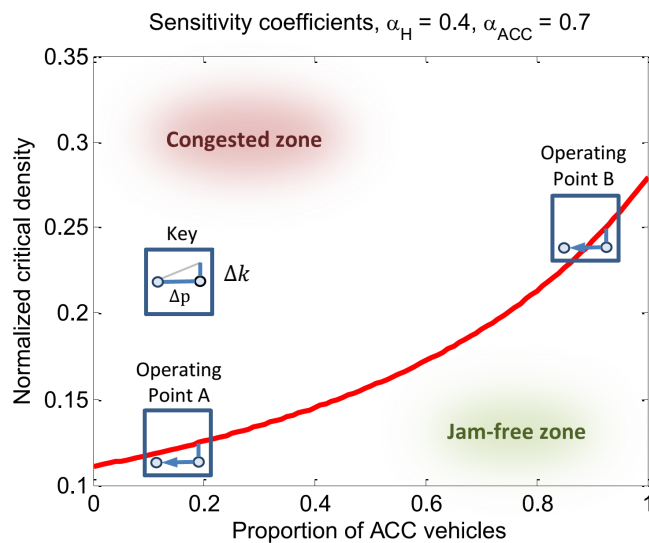


Figure 3.11: Increased ACC penetration results in an increase in the critical density at which traffic jams first appear. Points A and B operate at the same threshold (Δk) away from the critical density line. Identical changes in vehicle proportion (Δp) produce different results at the operating points.

The same trend can be observed by studying the sensitivity of the the critical density to the proportion of ACC-enabled vehicles, which is defined as follows:

$$\text{Sensitivity, } s(p_0) = \left(\frac{dk_c^*}{dp} \right)_{p=p_0} \quad (3.37)$$

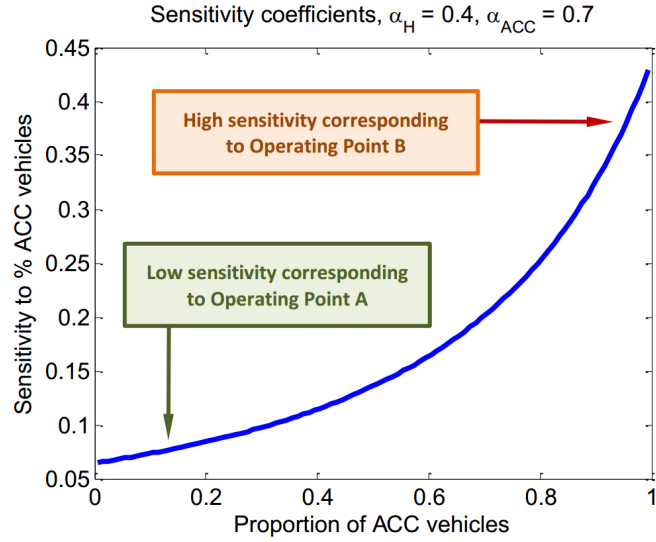


Figure 3.12: Sensitivity of critical density to ACC penetration. Traffic flows with high ACC penetration are up to 10 times more susceptible to the formation of self-organized traffic jams, as compared to traffic flows with low ACC penetration.

Figure 3.12 indicates that for roadways operating at or near peak flow capacity, traffic systems with very high ACC penetration are up to 10 times more susceptible to congestion caused by self-organized traffic jams as compared to traffic systems with very low ACC penetration. In other words, in medium-to-high density traffic, the introduction of a small percentage of human-driven vehicles into a predominantly ACC-enabled vehicle population is more likely to cause a *phantom* traffic jam as compared to the introduction of the same percentage of human-driven vehicles in an already predominantly human-driven population.

In the previous subsection, it was shown that the analytical results for critical density are well supported by the mesoscopic simulations. Extending the analysis to multi-species systems, Monte Carlo simulations are used to determine the normalized critical density as the proportion of ACC-enabled vehicles on the road increases. Figure 3.13 shows the Monte Carlo simulation results with 1000 iterations and varying percentage of ACC-enabled vehicles in the traffic stream. The isolines on the contour map indicate the number of iterations (out of a total 1000 iterations) in which a vehicular cluster was observed. The simulations indicate that the lower bound of the contour map

appears to agree very well with the analytical result for normalized critical density, which is depicted using the dashed line in Figure 3.13.

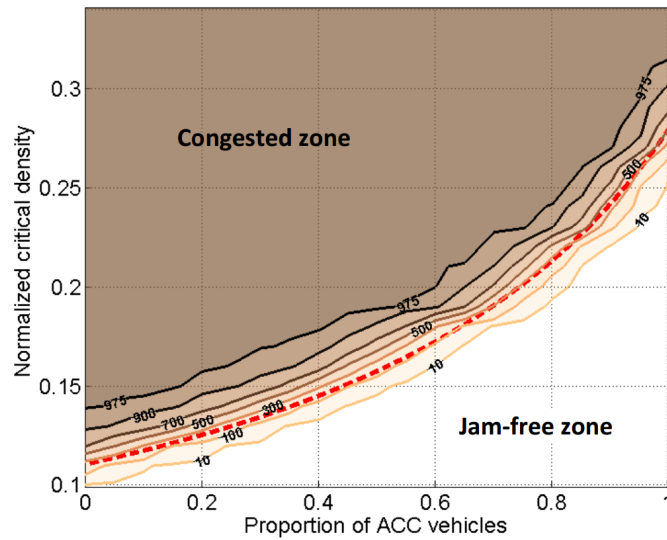


Figure 3.13: Results from the Monte Carlo simulation for mixed traffic flow appear to agree with the analytical results. Isolines indicate number of simulation (out of 1000 total iterations) that resulted in a vehicular cluster (self-organized traffic jam). Dashed line indicates normalized critical density from analytical results.

3.7 CONCLUSIONS, CONTRIBUTIONS AND BROADER IMPACTS

In this chapter, a master equation-based analytical methodology was developed to study the influence of varying vehicular population demographics on the ensemble dynamics. Specifically, the goal of the study was to assess the impact of introduction of ACC-enabled vehicles on the dynamics of self-organized traffic jams. Figure 3.13 indicates that, as the percentage of ACC-enabled vehicles in the traffic stream is increased, the critical density also increases correspondingly. In other words, as more ACC-enabled vehicles join the traffic stream, the density at which vehicle clusters begin to spontaneously appear increases. This indicates that the traffic flow can operate at higher densities and consequently higher flow rates. Additionally, the study also found that while increased ACC penetration may allow the traffic system to operate at increased densities and flows, it comes at a cost. As ACC penetration increases, a small increase in the percentage of human drivers may be enough to cause congestion. In other words, in a predominantly ACC traffic system, introduction of human-driven vehicles may cause a rapid reduction of critical density, resulting in a self-organized traffic jam.

The key contribution of the work presented in this chapter is that it enables the development of a closed-form solution that directly relates the penetration of ACC-enabled vehicles on the critical density at which self-organized traffic jams first begin to appear. The development of an analytical solution reduces reliance on simulation-based approaches, which, though useful, do not provide as significant an insight as analytical solutions. From a broader perspective, the knowledge gleaned from the analysis presented in this chapter may be used to improve upon and design better ACC algorithms that take into account the functional relationship between ACC penetration and traffic jam dynamics. This knowledge could mitigate the environmental, financial and productivity losses arising due to self-organized traffic jams.

GENERALIZED ISING MODEL TO STUDY EFFECTS OF DRIVER ALGORITHMS ON VEHICLE CLUSTER DISTRIBUTION

AUTHOR'S NOTE This chapter borrows significant content from the author's publication titled "Statistical mechanics-inspired framework for the study of mixed traffic flows on highway congestion" published in *Proceedings of the American Control Conference, 2014* held in Portland, Oregon.

In [Chapter 3](#), the discussion primarily revolved around the steady-state behavior of the vehicular cluster as a function of ACC penetration rate. One of the key assumptions made in this study was that only a single cluster is formed on the closed ring-road environment. In many situations, this may not be the case, and since the absence of large clusters could be offset by the presence of several smaller clusters, knowledge of the distribution of cluster sizes can be as important as that of the presence or absence of clusters.

In this chapter, a new microscopic modeling technique inspired by principles from the field of statistical mechanics is used to obtain the distribution of vehicle cluster sizes. Specifically, the generalized Ising model is used to simulate the traffic flow at a microscopic scale. The simulation results indicate that traffic systems dominated by ACC-enabled vehicles exhibit a higher probability of formation of moderately-sized clusters as compared to traffic systems dominated by human-driven vehicles. However, the trend is reversed for formation of large-sized clusters, i.e. traffic systems dominated by human-driven vehicles display a higher propensity of large cluster formation as opposed to ACC-dominated traffic systems. These qualitative results hold significance for algorithm design and traffic control, since it may be easier to predict and take countermeasures for large localized clusters as opposed to several smaller clusters spread across various locations on a highway.

4.1 INTRODUCTION

As mentioned earlier in [Chapter 2](#), the formation of self-organized clusters is of interest not only in the transportation research community, but also in several other domains. Self-organized cluster formation is a fairly common phenomenon which occurs across a wide range of fields, including nucleation in binary alloys, herding behavior of organisms (such as in a school of fish), and transport of granu-

lar media [12]. Intelligent vehicles have the potential not only to affect the steady state cluster sizes, as discussed in Chapter 3, but also to affect the cluster size distributions, as will be shown in the following work.

Traditionally, microscopic numerical simulations have served well to provide some insight into self-organized traffic dynamics as a function of driver behaviors [86]. These simulation approaches utilize models that represent the driving behavior of humans to varying degrees of accuracy. However, some approaches, such as the cellular automata (CA) [13][107] or totally asymmetric simple exclusion process (TASEP) models, significantly simplify the driver behavior to rules that are independent of physical interpretation of model parameters. Other approaches, such as those that use detailed car-following models (e.g. General Motors [90] or optimal velocity models [112]), may cause the simulations to be computationally expensive and memory intensive. Consequently, it is desirable to have a simulation approach that is more detailed than CA or TASEP models and builds upon physical principles, while simultaneously being computationally amenable to parametric studies. The generalized Ising model provides such an approach. The included study builds upon work presented in [39] [113] and utilizes the simple, yet immensely popular Ising model and its generalized forms, to study traffic flow and vehicle cluster dynamics as a function of ACC penetration.

The remaining sections of this chapter discuss the following:

- the problem with known parameters values typically used to represent the state of highway traffic flow,
- the generalized Ising model of traffic flow, wherein self-organized traffic jams manifest as a result of a non-equilibrium process in the presence of an external field with repulsive interactions between vehicles, and
- the Monte-Carlo simulations as well as the calibration of the generalized Ising model.

In the remainder of this work, the term ‘ACC-enabled’ and ‘computer algorithm-driven’ will be used interchangeably.

4.2 PRIOR WORK

While the study of traffic flow dynamics is a rich and vibrant field, statistical mechanics-based approaches to address the problem have received less attention than others. In the following subsections, statistical mechanics-based techniques to study traffic flow dynamics are discussed briefly.

4.2.1 *Statistical mechanics-based techniques*

One of the earliest attempts to use statistical mechanics to study traffic flow dynamics dates back to the work of [Prigogine and Andrews](#) in 1960, who modeled traffic flow using the kinetic theory of gases [4]. For a long period after their work, statistical mechanics was not used within the transportation research community, but recently these approaches have witnessed a resurgence [38][39][114][115]. However, in the context of analyzing changes in traffic flow dynamics as a consequence of driver behavior, these techniques have primarily been limited to single species environments [116][113]. The work presented here extends the statistical mechanics-based approach to a multi-species environment that can model both human-driven and ACC-enabled vehicles via the use of the generalized Ising model (or the Potts model). The generalized Ising model presented here is able to provide better simulation fidelity (as compared to CA or TASEP models), while operating with reduced computational complexity (as compared to numerical simulations with car-following models).

4.2.2 *Limitations of the Ising model*

The statistical mechanics-based approach proposed by Sopasakis and his colleagues models traffic flow using the Ising model, and as such is limited in its predictive capacity by the limitations of the Ising model itself [39]. Specifically, the possible states σ that a site in the Ising model can assume is limited to two. In other words, in an Ising model formulation, a site on a road can either be empty ($\sigma = 0$) or be occupied by a vehicle ($\sigma = 1$). However, if additional states are required, such as when studying traffic systems with more than one type of driver algorithm, the Ising model needs to be extended for the analysis. Fortunately, there exist extensions of the Ising model – such as the generalized Ising model in which a site can assume any integer number of states – which can be used to model mixed traffic systems. Details about the two-state Ising model are provided in [Appendix A](#).

4.3 PROBLEM SETUP

This section discusses the problem setup, which is essentially an exercise in establishing variables that describe the physical system, i.e. traffic, and relating them to model parameters of the generalized Ising model. The following subsections first describe an idealized traffic system selected for study, followed by the model structure that will be used for simulation-based numerical analysis.

4.3.1 Traffic system description

In order to study the effects of driver algorithms on vehicle cluster formation, a traffic system is often idealized as a single-lane closed ring-road without on- or off-ramps. While a road with open boundary conditions, i.e. with on- and off- ramps, may better represent reality, the closed ring-road idealization of the traffic system enforces periodic boundary conditions and greatly simplifies the ensuing analysis and simulations [114]. The closed ring-road is assumed to be of length L and is occupied by M vehicles. The vehicles are assumed to be physically identical with length of $d_v = 5.5$ m, which may be considered the upper limit for the overall length of passenger cars and vans. Additionally, the vehicles are assumed to maintain a safe spacing of $d_0 = 2.5$ m when stationary, which may be evaluated from the typical jam density of approximately 125 vehicles/km in highway traffic [79]. Consequently, the spatial extent occupied by each vehicle when it is stationary is given by $d_s = d_v + d_0 = 8$ m. Later, some of these vehicles will be modeled as being driven by humans, whereas other will be modeled as being driven by computer algorithms.

Next, the typical traffic system is described quantitatively by some commonly observed traffic parameters, which are known to be representative of single-lane highways [79]. The free flow velocity (v_f), which is the speed of vehicles at low densities, is assumed to be 25 m/s (or 90 km/h). The maximum flow of vehicles in the lane, or lane capacity, (q_{max}) is assumed to be 1800 veh/h. The backward wave speed (u) represents the speed at which a wave propagates backwards in the traffic stream and is assumed to be -6 m/s (or -19.6 km/h). The next subsection discusses the specific prerequisites and model structure needed to analyze the system using the generalized Ising model.

4.3.2 Space partitioning and lattice structure of traffic system

As a first step towards modeling the system, the roadway is partitioned into individual non-overlapping sites, so that the sites span the entire length L of the roadway. This process is known as *space partitioning* and results in the partition $S = \{s_1, s_2, \dots, s_N\}$ of the road such that:

space partition

$$\bigcup_{i=1}^N s_i = S \text{ and } s_i \cap s_j = \phi \quad (4.1)$$

where s_i denotes the i^{th} site on the road, and ϕ denotes the empty set. In the presented work, the length of each site is assumed to be $d_s (= d_v + d_0)$, i.e. the space occupied by a vehicle when it is stationary. Thus, if the roadway is occupied at maximum density, it would result in stationary vehicles parked a distance d_0 away from each

other, and occupying a total space of $N(d_v + d_0) = L$. The maximum density is referred to as *jam density* (k_{jam}) in the traffic flow literature [79]. Other values for the length of an individual site are also possible, but the current value ($d_s = 8$ m) is chosen since it makes physical sense and also corresponds directly to the jam density ($k_{jam} = 1/d_s$), a physically observable quantity. The collection of sites that represents the ring road forms a one-dimensional lattice, and the setup is referred to as the *lattice structure* of the system. The terminology is borrowed from physical systems such as lattice gases, whose analysis often relies on statistical mechanics techniques [117].

The next step in the problem setup addresses a framework for assigning the *system microstate*, so that its evolution can be tracked during numerical simulations. Specifically, this requires assigning a state σ_i to each individual site $s_i \in S$. Since the goal of this work is to analyze mixed traffic flow, a specific site s_i can be in one of three states, i.e. $\sigma_i \in \Sigma = \{0, 1, 2\}$, where the set Σ is referred to as the *alphabet* of the system. It is assumed that $\sigma_i = 0$ represents a site that is vacant, $\sigma_i = 1$ represents a site that is occupied by a human-driven vehicle, and $\sigma_i = 2$ represents a site that is occupied by an ACC-enabled vehicle [116]. A schematic representation of the partitioning of the ring road is included in Figure 4.1. In this discretized version of the road, white sites indicate that no vehicle is present, filled sites (gray) indicate that a human-driven vehicle currently occupies that site, and filled sites (black) indicate that an ACC-enabled vehicle currently occupies that site.

system microstate

The system microstate then encapsulates the state information of all N sites as a vector $\sigma = \{\sigma_1, \sigma_2, \dots, \sigma_N\}$. Given the space partition $S = \{s_1, s_2, \dots, s_N\}$ of the system and the set of states $\Sigma = \{0, 1, 2\}$ that each individual site can assume, the total number of possible microstates of the traffic system is given by $|\Sigma|^{|S|} = 3^N$. The microstate contains complete information of the entire system at any given instant of time. The next section builds upon the microstate and lattice structure discussed here to create a framework for simulating the traffic system.

4.4 GENERALIZED ISING MODEL FORMULATION

In this section, a simulation framework that can mimic the dynamics of a single-lane closed ring-road system is developed. As mentioned earlier in Section 4.2.2, while the Ising model allows for a statistical mechanics-based treatment of the formation of traffic jams, it does not allow for distinguishing between different driver behaviors. In the following work, the use of the generalized Ising model removes this limitation and allows us to conduct a numerical analysis of the effects of different driver behaviors on the formation of self-organized vehicle clusters, or traffic jams. In the following subsections, the model parameters that help distinguish between driver algorithms, as well

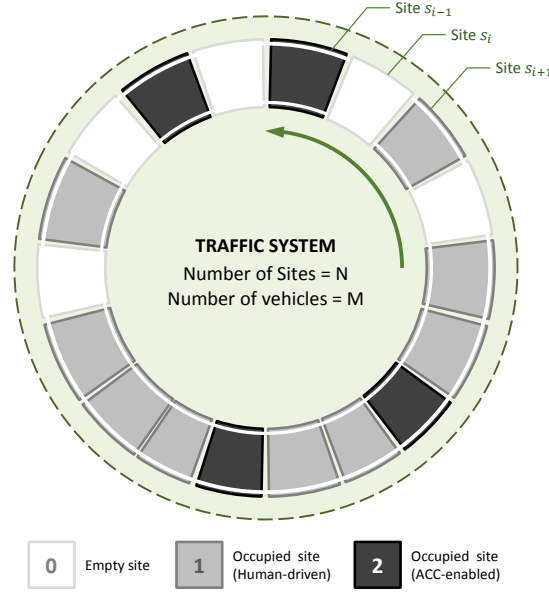


Figure 4.1: Discretized version of traffic system for statistical mechanics-based numerical analysis. Arrow indicates direction of travel. Vehicles travel in direction of reducing site number. Three states, $\sigma_i \in \Sigma = \{0, 1, 2\}$, are possible for each site in accordance with the generalized Ising model approach.

as the means to simulate the system microstate dynamics, will be discussed in detail.

One of the foundational constructs of the generalized Ising model, and statistical mechanics in general, is the idea of the *Hamiltonian*. The Hamiltonian represents the energy of the system in any given microstate, and consequently can be used to determine system dynamics, if the energy evolution scheme within a system is known. The expression for the Hamiltonian is given by:

Hamiltonian

$$H(\sigma) = -B \sum_{i=1}^N \sigma_i - \sum_{\{i,j\}} J_{ij} \sigma_i \sigma_j \quad (4.2)$$

where $j \neq i$ and $i, j \in \{1, 2, \dots, N\}$. In the expression, B represents an external field that is acting on the entire system, J_{ij} represents the interaction strength between sites i and j , and $\{i, j\}$ represents a pair of neighboring sites.

Now, in a traffic system, drivers do not typically interact with every other driver on the road. Drivers, either human or computer algorithms, are often privy to only local information up to a certain 'look-ahead' distance (d_l) downstream of their location. In the current context of analyzing traffic flow dynamics, this implies that interactions between sites on the road are restricted to a few downstream sites

within a defined neighborhood. Mathematically, the forward-looking neighborhood $\mathcal{N}(s_i)$ can be expressed as:

$$\mathcal{N}(s_i) = \{s_j : d(s_i, s_j) \leq d_l, j < i\} \quad (4.3)$$

where $d(s_i, s_j) = |(i - j)d_s|$ denotes the distance between sites s_i and s_j , and d_s is the size of an individual site. Note that the neighborhood $\mathcal{N}(s_i)$ does not include sites upstream from the site s_i , i.e. sites for which $j > i$. Also note that due to the closed ring structure, the neighborhood for numbered sites such as s_1 is appropriately re-defined to include forward-looking sites such as s_N, s_{N-1}, s_{N-2} , and so on.

As a consequence of the local nature of driver response, the forward motion of a vehicle from a site s_i to the adjacent downstream site s_{i-1} should only depend on the states of the sites in the neighborhood $\mathcal{N}(s_i)$, rather than the entire microstate σ . To reflect this understanding, the Hamiltonian can be re-framed for the current context to read as:

$$H(s_i) = -B\sigma_i - \sum_{s_j \in \mathcal{N}(s_i)} J_{ij}\sigma_i\sigma_j \quad (4.4)$$

where $H(s_i)$ denotes the energy associated with a particular site s_i and is a function of the state of the neighboring sites only. The site-based Hamiltonian $H(s_i)$ governs the probability of a vehicle moving from one site to another. A key differentiating feature between the TASEP models mentioned in [Section 4.1](#) and the statistical mechanics-inspired model presented here is that the latter uses a site-based Hamiltonian determine the system evolution. Specifically, the components of the Hamiltonian such as the external field and interaction strength can be related to physical processes, which helps provide meaning to the probability with which a vehicle moves forward. This is quite unlike the TASEP models which, though simple and useful, make it relatively difficult to relate hopping probabilities to physical processes. The next few subsections discuss explain details about the Hamiltonian, its individual components, and how it can be used to determine system dynamics.

4.4.1 *External field*

The role of the external field in traffic flow dynamics can be understood by drawing parallels between Prigogine's original interpretation of traffic flow based on the kinetic theory of gases and the expression presented in [Equation 4.4](#). In Prigogine's gas kinetic theory of traffic flow, competing forces are at play that push and repel vehicles [4]. The external field corresponds to Prigogine's 'relaxation' term and is the driving force that 'pushes' vehicles forward. The stronger the external field, the greater the tendency of the vehicles

to keep moving forward. The external field acts equally on all vehicles, irrespective of whether they are driven by humans or computer algorithms (i.e. ACC enabled). However, the states of sites occupied by human-driven vehicles ($\sigma_i = 1$) and those occupied by ACC-enabled vehicles ($\sigma_i = 2$) are different by design. Thus, the expression for the field may be altered slightly as follows:

$$B = \begin{cases} B_0, & \text{if } \sigma_i = 1 \\ B_0/2, & \text{if } \sigma_i = 2 \end{cases} \quad (4.5)$$

so that the field component of the Hamiltonian is equal in both cases, i.e. $B\sigma_i = B_0 > 0$, irrespective of the state σ_i of the site s_i . Here, the parameter B_0 can be related to the speed limit of the roadway. From a physical perspective, a high value of the external field parameter B_0 corresponds to a larger driving force acting on the system which, in turn, can be said to correspond to a higher speed limit. This relation is made evident when the model is calibrated in [Section 4.5.1](#).

4.4.2 Interaction strength

The role of the interaction strength on traffic flow dynamics can also be understood by reviewing Prigogine's gas kinetic theory of traffic flow. Specifically, the interaction strength J_{ij} is representative of the 'collision' term in Prigogine's work and is a measure of 'repulsion' faced by vehicles as they approach another vehicle [4]. The greater the magnitude of the interaction term between a vehicle and a preceding vehicle, the slower it will approach that preceding vehicle. To produce a repulsive effect with downstream vehicles, the interaction strength must be negative, i.e. $J_{ij} < 0$, for $j < i$. As interaction with upstream vehicles is not considered, so $J_{ij} = 0$ for $j > i$. The precise nature of the interactions is assumed to follow an inverse-square law as follows:

$$J_{ij} = \begin{cases} \frac{J_0}{(d(s_i, s_j))^2}, & \text{if } s_j \in \mathcal{N}(s_i) \\ 0, & \text{otherwise} \end{cases} \quad (4.6)$$

where the interaction coefficient J_0 is a constant, and $d(s_i, s_j)$ represents the distance between sites as discussed earlier in [Section 4.4](#). The inverse-square law representation for the interaction strength chosen here is in accordance with prior work [118], which has shown that such interactions produce long range order via a continuous phase transition in the one-dimensional Potts model, similar to the phase transitions observed in traffic flow [74]. Other interaction laws, such as where the interaction strength is inversely proportional to the distance between the sites, yield discontinuous (or first-order) phase transitions, which are uncharacteristic of traffic flow [118][119].

From a physical perspective, the interaction coefficient J_0 can be related to driver sensitivity or alertness. An alert driver, such as a computer algorithm, may respond sooner to the presence of a cluster downstream, and may correspondingly have a higher magnitude of the interaction coefficient as compared to an inattentive driver, such as a distracted human. In the next subsection, the use of interaction strength to model driver behaviors and algorithms is discussed in more detail.

4.4.3 Modeling driver behavior via interactions

It is known that the behaviors of vehicles when they are accelerating from rest [111] or decelerating to a stop [120] are quite different. Consequently, the interaction coefficients for vehicles entering or exiting a cluster are designed to be different as well, and are postulated to be:

$$J_0 = \begin{cases} J_{\text{in}}, & \text{if } k_i - k_l < 0 \\ J_{\text{out}}, & \text{if } k_i - k_l > 0 \end{cases} \quad (4.7)$$

where $J_{\text{in}} < 0$ represents the interaction coefficient for vehicles entering a region of higher local density, $J_{\text{out}} < 0$ represents the interaction coefficient for vehicles exiting a region of higher local density, s_l is the nearest occupied site within the neighborhood $\mathcal{N}(s_i)$, i.e. $\sigma_l \neq 0$, and k_i denotes the dimensionless local density at site s_i , and is defined as:

$$k_i = \frac{1}{|\mathcal{N}(s_i)|} \sum_{s_j \in \mathcal{N}(s_i)} \mathbb{1}_{\mathcal{N}(s_i)}(s_j) \quad (4.8)$$

where $|\mathcal{N}(s_i)| = \mathcal{N}$ represents the cardinality of the neighborhood set, and $\mathbb{1}_A(\cdot)$ represents the indicator function for elements belonging to the set A . The use of the local density to determine the interaction coefficient can be better understood by using [Figure 4.2](#) as an aid. The dimensionless local density represents the density of vehicles present in the neighborhood of a particular site. In the scenario where the local density k_l at site s_l is neither greater nor less than the local density k_i at site s_i , the interaction coefficient is chosen randomly with uniform distribution.

Now, the key innovation of the presented work is the ability to model various driver algorithms and behavior, and observe their effects on the formation of vehicle clusters, within a statistical mechanics framework. Different driver behaviors are implemented by changing the manner in which vehicles interact with one another. Consider that a computer algorithm is designed so that it attempts to avoid contributing to the growth of self-organized vehicle clusters whenever possible. Let the interaction coefficient associated with this algorithm be denoted by J_0^{ACC} , whereas the interaction coefficient associated with

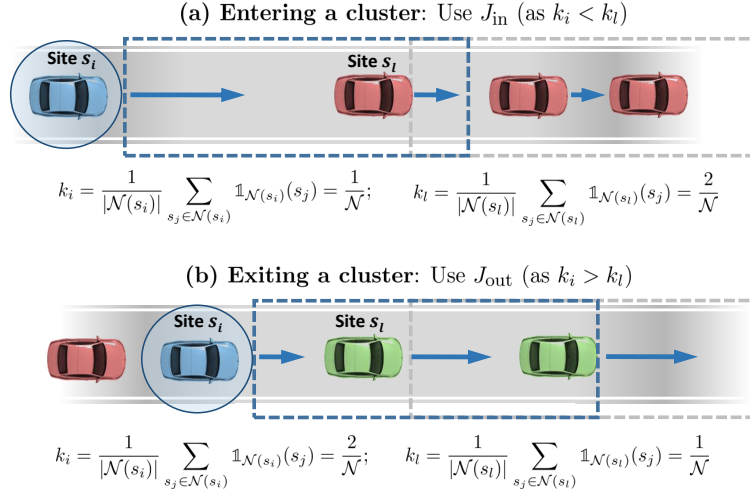


Figure 4.2: Interaction coefficients for vehicles determined using differences in local density. Dashed box denotes the neighborhood for the respective vehicles. (a) Difference in local density is negative for a vehicle (circled) entering a cluster. (b) Difference in local density is positive for a vehicle (circled) exiting a cluster.

a human-driven vehicle be denoted by J_0^{H} . An appropriately modeled qualitative difference between the coefficients J_0^{H} and J_0^{ACC} can result in reduced congestion incidents due to formation of self-organized vehicle clusters. For example, an ACC-enabled vehicle approaching a vehicular cluster will attempt to avoid contributing to the cluster growth. In the context of the current model, this behavior may be associated with the ACC-enabled vehicles experiencing greater repulsion near the cluster, as compared to human-driven vehicles. Mathematically, the behavior can be realized by the following relation between the interaction coefficients:

$$|J_{\text{in}}^{\text{ACC}}| > |J_{\text{in}}^{\text{H}}| \quad (4.9)$$

where $J_{\text{in}}^{\text{ACC}}$ and J_{in}^{H} denote the interaction coefficient while entering a cluster for an ACC-enabled and a human-driven vehicle, respectively. Similarly, an ACC-enabled vehicle exiting a vehicular cluster will attempt to leave it as quickly as possible so as not to contribute to the cluster growth. In the context of the current model, this behavior may be associated with the ACC-enabled vehicles experiencing less repulsion from vehicles downstream of the cluster, as compared to human-driven vehicles. Mathematically, the behavior can be realized by the following relation between the interaction coefficients:

$$|J_{\text{out}}^{\text{ACC}}| < |J_{\text{out}}^{\text{H}}| \quad (4.10)$$

where $J_{\text{out}}^{\text{ACC}}$ and $J_{\text{out}}^{\text{H}}$ denote the interaction coefficient while exiting a cluster for an ACC-enabled and human-driven vehicle, respectively. The next subsection describes how the Hamiltonian can be used to study the evolution of the traffic system.

4.4.4 Exchange dynamics

One of the first steps while studying the evolution of the traffic system is to identify the type of dynamics that will govern this evolution. In the statistical mechanics literature, two types of dynamics are popular, viz. the spin flip dynamics and the spin exchange dynamics [121]. In *spin flip dynamics*, a particular site flips from one state to another, without affecting the remainder of the system. Spin flip dynamics may be useful when modeling vehicles that are entering or leaving the system, such as at on- or off-ramps. For example, the state at the last site on the edge of the system may flip from $\sigma_N = 1$ at time t to $\sigma_N = 0$ at time $t + 1$, to indicate that a vehicle has left the system. However, in the current context, it is evident that the total number of vehicles is conserved on the closed ring-road, i.e. no vehicles are leaving the system. As a result, the sites can only exchange their states to model the forward motion of vehicles, so *exchange dynamics* are chosen to model system evolution. Specifically, exchange dynamics imply that if a vehicle moves from site s_i at time t to s_{i-1} at time $t + 1$, then the states of these sites are exchanged. For example, if at time t the states are given by $\{\sigma_i, \sigma_{i-1}\}_t = \{1, 0\}$, then at time $t + 1$ the states will be $\{\sigma_i, \sigma_{i-1}\}_{t+1} = \{0, 1\}$, i.e. the states have exchanged and the vehicle has moved forward. Further, the current implementation of exchange dynamics stipulate that state exchange may only take place with an adjacent and *vacant* downstream site, i.e. the exchange *may* occur if:

$$\sigma_i \neq 0 \text{ and } \sigma_{i-1} = 0 \quad (4.11)$$

With knowledge of the exchange dynamics, the only missing component to begin a study of the system evolution is the rate at which these exchanges take place. The next subsection discusses the development of transition probability rates and their significance in relation to the modeling of non-equilibrium (or far-from equilibrium) processes.

4.4.5 Transition probability rates

Parallels can be drawn between the problem of modeling of traffic dynamics using the Potts model, and the study of driven Ising lattice gases [107][117]. Systems that are driven by external fields, such as a temperature or concentration gradient, typically operate far-from-equilibrium. Such systems can exhibit steady-state behavior, though such a state may be one of continuous flux. Mathematically, such systems cannot be described by a stationary probability distribution. It is immediately evident that certain traffic behavior, such as formation of self-organized vehicle clusters or 'stop-and-go' waves, belong to a

spin flip dynamics

exchange dynamics

class of far-from-equilibrium systems because their microstate probability distributions are non-stationary.

The non-stationary nature of the probability distributions of far-from-equilibrium systems has a direct impact on how the transition probability rates are determined. Far-from-equilibrium systems do not necessarily obey the condition of detailed balance [74]. Consequently, the transition probability rates have to be determined on the basis of observations of specific physical phenomena occurring in the system. For example, since vehicles are not expected to move backward in a traffic system, the associated transition probability rate of a vehicle moving to an adjacent and vacant *upstream* site is assumed to be zero. Such observations allow reasoned estimates to be made about potential transition probability rates. Mathematically, the transition probability rate (w) in this scenario is given by:

*far-from-equilibrium
systems
detailed balance*

$$w(\sigma \rightarrow \sigma') = 0$$

$$\text{where, } \sigma = \{\sigma_1, \sigma_2, \dots, \sigma_{i-1}, 1, 0, \sigma_{i+2}, \dots, \sigma_N\} \quad (4.12)$$

$$\sigma' = \{\sigma_1, \sigma_2, \dots, \sigma_{i-1}, 0, 1, \sigma_{i+2}, \dots, \sigma_N\}$$

i.e. σ' represents a microstate where the vehicle at site s_i has moved to the upstream site s_{i+1} , while the states $\{\sigma_1, \sigma_2, \dots, \sigma_{i-1}, \sigma_{i+2}, \dots, \sigma_N\}$ remain unchanged. On the other hand, the microstate transition probability rate for the scenario where a vehicle at site s_i (denoted by site state $\sigma_i = 1$) moves to the adjacent and vacant downstream site s_{i-1} (denoted by the site state $\sigma_{i-1} = 0$) is given by:

$$w(\sigma \rightarrow \sigma') = c_0 \cdot \exp(-\beta H(s_i))$$

$$= c_0 \cdot \exp\left(\beta B \sigma_i + \beta \sum_{s_j \in \mathcal{N}(s_i)} J_{ij} \sigma_i \sigma_j\right) \quad (4.13)$$

$$\text{where, } \sigma = \{\sigma_1, \sigma_2, \dots, \sigma_{i-2}, 0, 1, \sigma_{i+1}, \dots, \sigma_N\},$$

$$\sigma' = \{\sigma_1, \sigma_2, \dots, \sigma_{i-2}, 1, 0, \sigma_{i+1}, \dots, \sigma_N\},$$

$$c_0 = \text{pre-exponential factor, and}$$

$$\beta = k_i$$

The expression in Equation 4.13 is similar to the reaction rate postulated for Arrhenius dynamics [39]. The parameter β is assumed to be proportional to the local density and is conceptually analogous to its interpretation in other physical systems. For example, in a ferromagnet, $\beta \propto 1/T$, where T denotes the temperature. Consequently, a high value of β corresponds to a low temperature T , in which case the magnetic moments are forced to align with their neighboring moments. Similarly, in a traffic system, a high value of β corresponds to

a high value of local density k_i , in which case the vehicles are not free to move and are forced to ‘align’ with the slow-moving or stationary states of their neighbors.

Now the expression for the transition probability rates can be used to determine the probability with which a randomly selected vehicle will transition from site s_i to the site s_{i-1} :

$$P(\sigma_{t+1} = \sigma' | \sigma_t = \sigma) = \min\{1, w(\sigma \rightarrow \sigma')\} \quad (4.14)$$

which is similar to the expression for the acceptance probability employed in the Metropolis-Hastings algorithm [122]. The following sections use the statistical-mechanics inspired framework built here to numerically simulate and analyze the effects of driver algorithms of formation of self-organized vehicular clusters.

4.5 MONTE CARLO SIMULATIONS

In order for the developed framework to accurately reflect the evolution of self-organized vehicular clusters, the values of the model parameters must be chosen carefully. The following subsection discusses the model calibration procedure.

4.5.1 Calibration of parameters

The calibration procedure of the presented model is performed in a traffic scenario whose evolution is theoretically and empirically well known. The traffic system, i.e. the closed ring-road, is populated with human-driven vehicles so that they form a queue, such as one that may form at a signalized intersection, to yield a moderate-density scenario with a normalized density $k^* = k/k_{jam}$. At time $t = 0$, the queue is allowed to dissipate and the system evolution is compared with known results from the Lighthill-Whitham-Richards (LWR) model of traffic flow [75][76] as well as the representative traffic parameters described in Section 4.3.1. Specifically, as the vehicles begin to exit a queue, they discharge at maximum capacity (q_{max}) and attain free flow velocity (v_f). At the same time, a backward wave moving with speed u can be seen to develop, both at the beginning of the queue (due to vehicles leaving the cluster) and at the end of the queue (due to vehicles entering the cluster after traversing the ring-road). The model parameters c_0 , B , J_{in}^H , and J_{out}^H should be such that the simulation behavior matches these known representative values of the traffic parameters.

The calibration procedure is performed in two steps. In the first step, the parameters c_0 and B are calibrated to yield the free flow velocity calculated via the speed of the first vehicle exiting the queue. The queued traffic system is simulated several times for different values of c_0 and B and the free flow velocities obtained by exiting ve-

*Potts model
calibration - first
step*

hicles are shown in Figure 4.3. Assuming that vehicles are nearly stationary ($v \approx 0.5$ m/s) when the external driving field is absent ($B = 0$), and using the representative value of free flow velocity $v_f = 25$ m/s for highways, the calibrated parameters for the traffic system are found to be $c_0 = 0.05$ and $B = 125$. Vehicles cannot be assumed to be completely stationary when the external field is absent because in that scenario c_0 evaluates to zero, implying that the transition probability rate is identically zero. Other alternative choices for the parameter calibration, such as $c_0 = 0.1$ and $B = 100$, also appear to be valid candidates. However, the minimum speed that can be modeled with this set of parameters is $v_f = 1$ m/s. Consequently, the choice of parameters relies in part on the trade-off one is willing to accept between the ability to model low free flow speeds, and the sensitivity of the free flow speed to changes in the external field parameter (which is higher in the range $B \in [0, 150]$ as compared to $B \in [150, \infty)$).

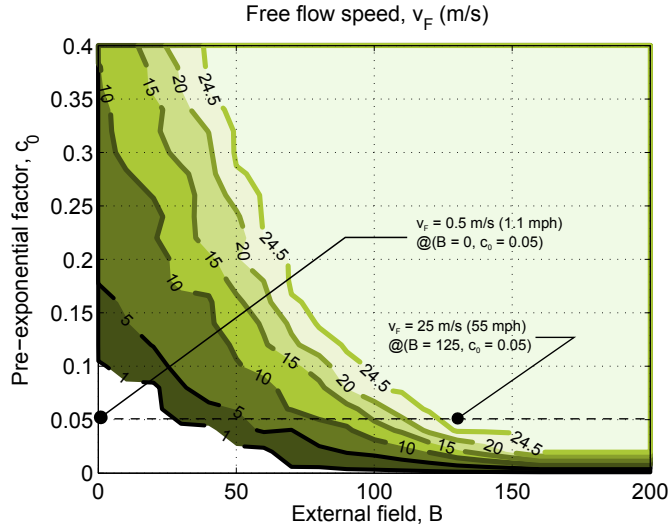


Figure 4.3: Calibration of generalized Ising model parameters B and c_0 to match free flow speed on a highway ($v_f = 25$ m/s). Contours indicate free flow speeds (m/s) obtained with corresponding set of model parameters. The values are chosen to be $B = 125$ and $c_0 = 0.05$.

In the second step of the calibration procedure, the calibrated values of B and c_0 are used to evaluate the appropriate values of J_{in}^H and J_{out}^H . The queued traffic system is simulated for a range of interaction coefficients and the resulting backward wave speeds are plotted as shown in Figure 4.4. The contours in this figure indicate specific values of backward wave speed that are observed in simulation for various pairs of values of the interaction coefficients J_{in}^H and J_{out}^H . The backward wave speeds are then compared for both scenarios, when a vehicle is exiting a cluster (u_{out}) (Figure 4.4(a)), and when it is entering a cluster (u_{in}) (Figure 4.4(b)). According to the LWR theory, for a queued traffic system on a closed ring-road populated with human-

*Potts model
calibration - second
step*

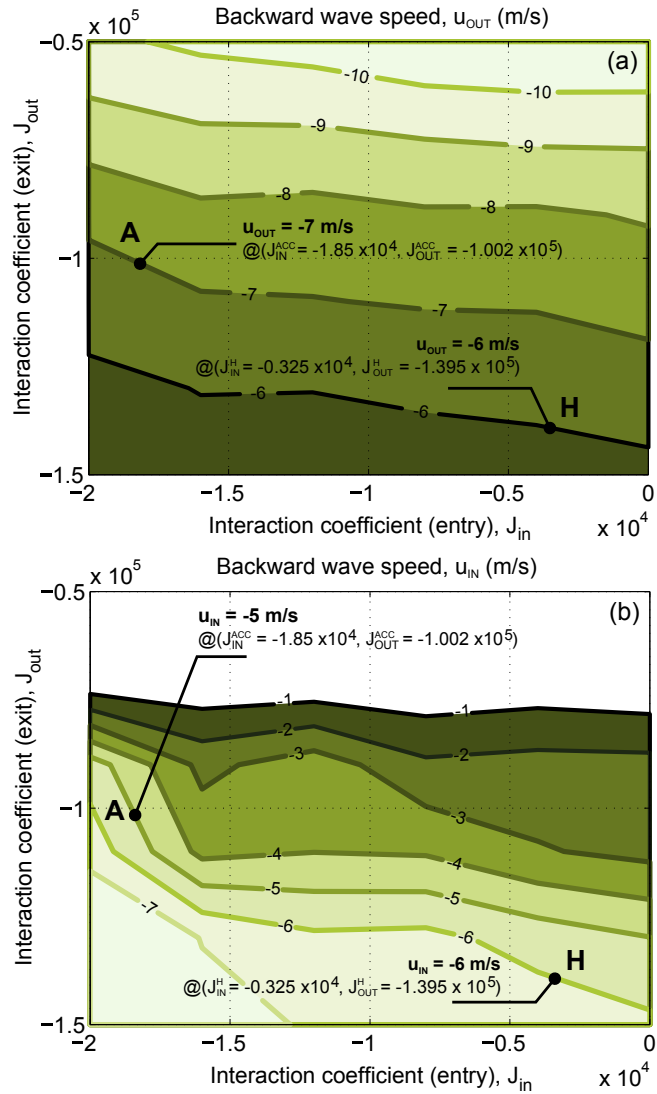


Figure 4.4: (a) Backward wave speed (u_{out}) evaluated for vehicles exiting a cluster. (b) Backward wave speed (u_{in}) evaluated for vehicles entering a cluster. Parameters J_{in} and J_{out} are calibrated to match backward wave propagation speeds for both human-driven (H) and ACC-enabled (A) vehicles, evaluated using $B = 125$ and $c_0 = 0.05$. Contours indicate backward wave speeds (m/s) obtained with corresponding set of model parameters.

driven vehicles, the values of (u_{out}) and (u_{in}) should be identical and equal to -6 m/s. Point H in [Figure 4.4](#) indicates the parameter values ($J_{\text{in}}^{\text{H}} = -0.325 \times 10^4 \text{ m}^2$, $J_{\text{out}}^{\text{H}} = -1.395 \times 10^5 \text{ m}^2$) for which the backward wave speeds ((u_{in}) and (u_{out})) match empirically observed speeds of -6 m/s in real-world traffic systems, as discussed in [Section 4.3.1](#).

Finally, the interaction coefficients for ACC-enabled vehicles can also be hypothesized from [Figure 4.4](#). As discussed in [Section 4.4.3](#), ACC-enabled vehicles with appropriately designed algorithms are expected to exit clusters faster so as to avoid contributing to the growth of self-organized clusters. If such vehicles exit the cluster faster, the backward wave speed (u_{out}) will have a larger magnitude, implying a higher cluster dissipation rate. Similarly, such vehicles are also expected to enter clusters at a slower rate to avoid increasing cluster size. As a result, the backward wave speed (u_{in}) will have a smaller magnitude, implying a higher cluster dissipation rate. Using the second step of the calibration procedure already performed for human-driven vehicles, and the qualitative relationships described in [Equation 4.9](#) and [Equation 4.10](#), the values of the backward wave speeds for a traffic system comprising only ACC-enabled vehicles are assumed to be $u_{\text{out}} = -7$ m/s and $u_{\text{in}} = -5$ m/s. Point A in [Figure 4.4](#) indicates the calibrated parameter values ($J_{\text{in}}^{\text{ACC}} = -1.85 \times 10^4 \text{ m}^2$, $J_{\text{out}}^{\text{ACC}} = -1.002 \times 10^5 \text{ m}^2$) for the associated backward wave speeds.

These parameters enable us to carry out the Monte Carlo simulations to mimic traffic flow dynamics in a mixed traffic flow. A simulation of the queued traffic system with the calibrated model parameters is shown in [Figure 4.5](#). It must be noted that these parameter values for the ACC-enabled vehicles provide us with only a qualitative assessment of the effects of increased ACC penetration. The pseudocode for the Monte Carlo algorithm used in the study is included in [Algorithm 1](#).

4.5.2 Simulation results

With the appropriate model parameters, and the transition probability rates developed in [Section 4.4.5](#), the traffic system was simulated as a closed-ring road with $N = 500$ sites. The number of vehicles populating the ring-road were varied to create scenarios where the normalized density $k^* = k/k_{\text{jam}}$ varies from 0.1 to 0.9 in steps of 0.1. Additionally, the levels of penetration for ACC-enabled vehicles were varied from 0% to 100%, in steps of 10%. The simulation was run for a real-time equivalent of one hour to allow for transients to die off, so that steady state cluster distribution could be observed. The system was updated in a random-parallel fashion, i.e. all sites were updated at each time step, but the order within each time step update was chosen randomly.

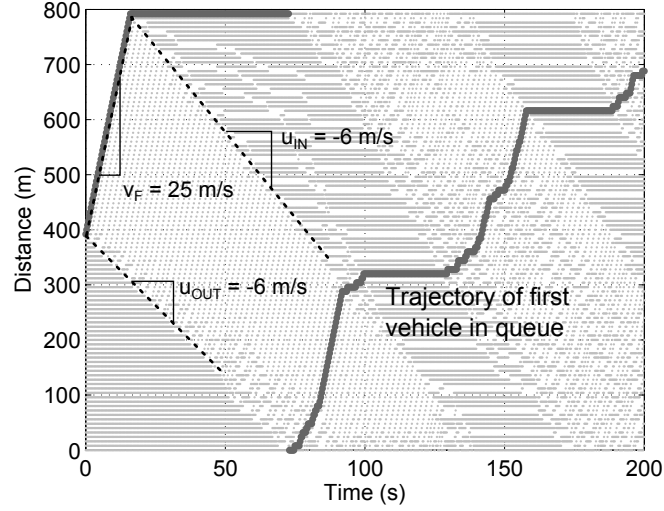


Figure 4.5: Queued traffic system is simulated with $k^* = 0.5$, $c_0 = 0.05$, $B = 125$, $J_{\text{in}}^H = -0.325 \times 10^4$, and $J_{\text{out}}^H = -1.395 \times 10^5$. Use of a queued traffic system helps ensure that calibrated model parameters lead to behavior that mimics real-life and agrees with existing theory (LWR model).

Algorithm 1 SIMULATING TRAFFIC FLOW DYNAMICS WITH MARKOV CHAIN MONTE CARLO ALGORITHM

- 1: Uniformly distribute M vehicles across N available sites to set up initial microstate σ
 - 2: **while** time \leq ENDTIME **do**
 - 3: **for** all sites $s_i \in S$ **do**
 - 4: **if** $\sigma_i \neq 0$ and $\sigma_{i+1} = 0$ **then**
 - 5: calculate the site-based Hamiltonian $H(s_i)$
 - 6: calculate transition probability rate $w = \exp(-\beta H(s_i))$
 - 7: select a random number $r \sim U(0, 1)$
 - 8: **if** $r < \min(1, w)$ **then**
 - 9: exchange states σ_i and σ_{i+1}
 - 10: accept new microstate
 - 11: **end if**
 - 12: **end if**
 - 13: **end for**
 - 14: time \leftarrow time + 1
 - 15: **end while**
-

The Monte Carlo simulations yield a probability mass function $f_R(r)$ which denotes the probability that a vehicle cluster of size $R = r$ exists in the traffic system in steady state. Then, the joint probability mass function $f_{VR}(v, r)$ which denotes the probability that a randomly selected vehicle $V = v$ is in a vehicular cluster of size $R = r$ can be expressed as follows:

$$f_{VR}(v, r) = f_{V|R}(V = v | R = r) f_R(r) \quad (4.15)$$

where $f_{V|R}(V = v|R = r)$ denotes the probability of selecting a vehicle V that lies in a cluster, given that a cluster of size R exists in the traffic system. The conditional probability is found to be:

$$f_{V|R}(V = v|R = r) = \frac{r}{M} = r^* \quad (4.16)$$

where M is the total vehicular population on the closed ring-road, and r^* denotes the normalized cluster size. The associated random variable R^* may be expressed in terms of the random variable R as $R^* = R/M$. The resulting joint probability distribution $f_{VR}(v, r)$ is plotted for varying values of density for which the Monte Carlo simulations were performed. Extremely high values of density ($k^* \in [0.6, 1.0]$) are not usually observed in traffic, and no significant cluster formation trends were observed in the simulations for low values of density ($k^* \in [0.1, 0.3]$). Consequently, the probability distribution $f_{VR}(v, r)$ is plotted in [Figure 4.6](#) for the range of density values $k^* \in [0.4, 0.6]$, where significant cluster distribution trends were observed as a function of ACC penetration. The figure does not include 'clusters' of size $r^* = 1/M$, since they correspond to individual vehicles that are not part of a larger cluster, and which skew the results disproportionately. The implications of these results and the conclusions that can be drawn from them are discussed in the next section.

4.6 RESULTS

The simulation results included in [Figure 4.6](#) describe the probability of a randomly selected vehicle being present in a cluster of a particular size. The trends observable in these results, while not definitive, can still be used to draw qualitative conclusions pertaining to the effect of ACC penetration of the formation of clusters and cluster distributions. One trend that is immediately evident is that cluster distributions for predominantly human-driven traffic systems are skewed to the right (towards large-sized clusters), whereas those for predominantly ACC-populated traffic systems are skewed to the left (towards moderately-sized clusters), across all densities shown in the figure. For example, in the plot corresponding to $k^* = 0.6$ in [Figure 4.6](#) consider the dotted line, which represents 100% ACC penetration, and the thick solid line, which represents a population of 100% human-driven vehicles. It is evident that there exists a noticeable right-leaning skew in the human-driven vehicle population indicating a propensity towards formation of larger clusters. On the other hand, the dotted line on the same figure, a noticeable skew towards the left is seen, indicating a propensity towards formation of smaller clusters for ACC-dominated vehicular populations. Thus, the probability that a randomly selected vehicle is present in a large-sized cluster is higher for traffic systems consisting predominantly of human-driven vehicles

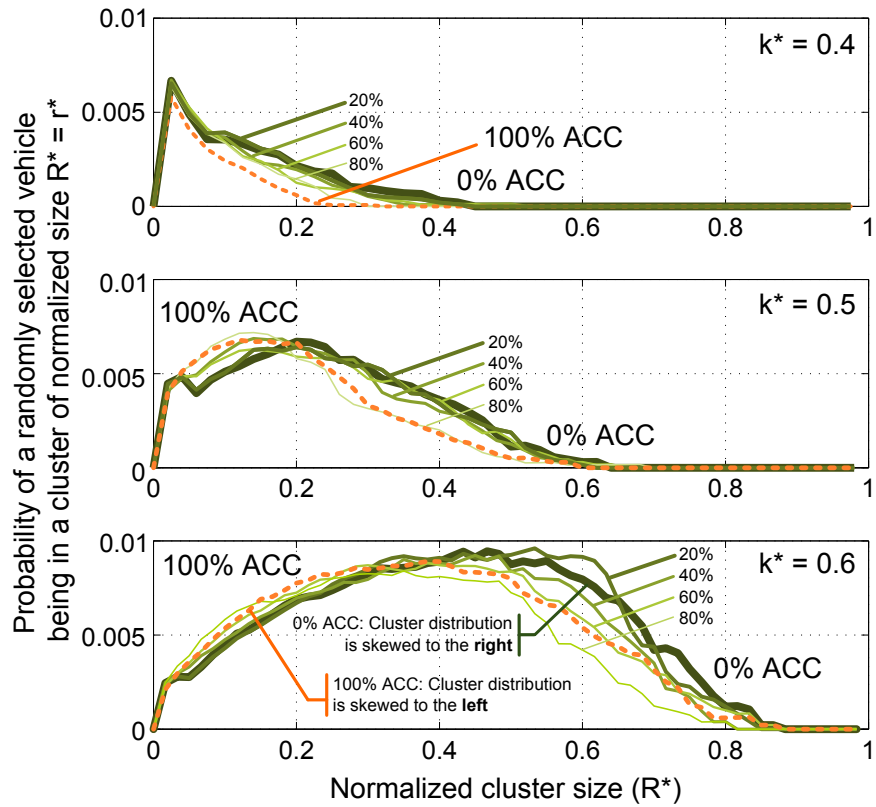


Figure 4.6: Probability of a randomly selected vehicle lying in a cluster of size r^* for varying levels of ACC penetration and densities of interest. Lines of decreasing thickness indicate increasing levels of ACC penetration. Dotted line corresponds to a traffic system consisting entirely of ACC-enabled vehicles. Clusters of size $r^* = 1/M$ (or $r = 1$) not shown in the distribution.

as opposed to ACC-enabled vehicles. Similarly, the probability that a randomly selected vehicle is present in a moderately-sized cluster is higher for traffic systems consisting predominantly of ACC-enabled vehicles.

4.6.1 *Conclusions and broader impacts*

These qualitative results may have significant implications for autonomous vehicle design, traffic control and guiding policy decision-making. Specifically, from a traffic control perspective, it is easier to design and manage highway elements to counter localized bottlenecks that could result in large clusters. On the other hand, having several moderately-sized clusters that may appear at random across a large swathe of highway may require the development of more elaborate traffic control techniques. However, these findings are only applicable to traffic systems operating at moderate densities ($k^* \in [0.4, 0.6]$). In contrast, our previous research has indicated that ACC penetration is quite advantageous at lower densities ($k^* \in [0, 0.3]$) since it raises the critical density at which jams first begin to appear and enables higher flows [114].

In addition, the inclusion of ACC-enabled vehicles in traffic systems operating at moderate densities might increase the risk of collisions. Specifically, the presence of several smaller self-organized vehicle clusters in predominantly ACC-enabled traffic flow may lead to an increase in ‘stop-and-go’ behavior. Each such stopping maneuver carries with it the risk of collision or disruption of traffic flow, especially from human drivers. Further, increased numbers of acceleration and deceleration cycles may also lead to an increase in the release of greenhouse gases and other harmful emissions, though such an impact has not been quantified here. In conclusion, it was found that the generalized Ising model could satisfactorily simulate the traffic dynamics of mixed traffic flows, and that these simulation reveal interesting effects of driver algorithms on the formation of self-organized vehicular clusters.

Part II

INFLUENCE VIA SUBSPACE SELECTION

In [Part I](#) of this dissertation, the underlying scheme adopted to influence ensemble dynamics was the modification of population demographics. While such an approach for influencing self-organizing systems is extremely useful from the perspective of analyzing dynamics, it is quite impractical if the goal is to control the ensemble dynamics or guide them along a desired trajectory. In Part II of this dissertation, an alternative approach will be considered which requires only a small number of agents to influence the ensemble. Specifically, this part deals with the selection of appropriate regions of the state space within which to initiate a control effort so as to influence the ensemble dynamics/mesostate. These regions are closely related to controllable sets discussed in [Section 2.2.2](#) and are referred to as *influential subspaces* in this dissertation. In [Chapter 5](#), results from the kinematic wave theory are used to determine analytical expression for the extent of the influential subspaces of connected vehicles in the traffic flow, given a specific set of admissible control policies. In [Chapter 6](#), a more formal control-theoretic approach is adopted to identify the influential subspaces via a combinatorial search. In either case, the underlying principle is the **identification of a novel agent-specific influential subspace where control actions can influence the ensemble dynamics.**

INFLUENTIAL SUBSPACES OF CONNECTED VEHICLES

AUTHOR'S NOTE This chapter borrows significant content from the author's publication titled "Event horizons and influential subspaces of connected vehicles" submitted to *IEEE Transactions on Intelligent Transportation Systems* in June 2014.

Work presented in [Part I](#) focused on the ability to influence ensemble dynamics via population modification. This chapter focuses on an alternative approach to studying influence. In this chapter, a preliminary introduction to the novel concepts of influential subspaces and event horizons is provided. These concepts are then applied to highway traffic containing connected vehicles. Herein, an influential subspace of a connected vehicle is defined as the region of a highway where the vehicle has the ability to influence the macroscopic traffic flow so as to drive it to a pre-determined macrostate within a specified time. The event horizon marks the spatial extent of the influential subspace, beyond which vehicles cannot escape or avoid a traffic jam. Analytical expressions for the influential subspace and event horizon are derived using the Lighthill-Whitham-Richards theory of traffic flow. Included results describe the extent of the influential subspace as a function of traffic flow conditions and for pre-specified driving algorithms of the connected vehicles. The analysis of the results includes several key takeaways that may be helpful for guiding policy decisions related to connected vehicle technology.

5.1 INTRODUCTION

Recent years have witnessed significant attention directed towards technologies that allow vehicle-to-vehicle (v2v) and infrastructure-to-vehicle (I2V) communication. While v2v technologies hold the potential to improve passenger safety (by detecting imminent collisions) and reduce driver effort (by using cooperative adaptive cruise control algorithms), and I2V technologies could increase the efficiency of the traffic system, there are some key questions related to these developments that remain unanswered. Given the increasing ability to inform drivers about nearby traffic conditions, it becomes natural to ask the following questions: can an individual driver use such information to positively affect traffic flow? And which drivers in a traffic network have the most influence on traffic flow, i.e. *where* and *to whom* should this information be delivered?

It is these questions that have led the authors to introduce a new concept with regards to connected vehicles in highway traffic – the influential subspace – and the related notion of event horizons on the roadway. The *influential subspace* of a connected vehicle is defined as the region of a highway where the vehicle has the ability to influence the macroscopic traffic flow so as to drive it to a pre-determined macrostate within a specified time interval. The problem of individual agents acting locally to affect global (or macroscopic) behavior is not restricted to traffic systems alone – it is applicable to several engineered, physical, social, and biological systems – and a general formulation will be presented in the next chapter. For now, attention is focused on applying this novel concept to the problem of connected vehicles approaching self-organized jams in highway traffic.

5.2 PRIOR WORK

Current research in connected vehicles focuses on issues such as communication protocols and vehicular network topologies [123][124], and their role in the reliable and continuous dissemination of information across a vehicular ad hoc network (VANET) [125] [126]. More specific to the current context, several researchers have focused on message propagation and the probability of receiving a message from a connected vehicle as a function of distance [126][127]. However, very little emphasis has been placed on the regions of the highway where the transmitted information may actually be useful. While the aforementioned research is extremely important from an implementation viewpoint, understanding how connected vehicles can use information to impact traffic flow is also essential to help fully realize the technology’s potential. The present work hopes to correct this imbalance by addressing the problem of identifying the regions of the highway where the transmitted information is of use.

Significant research effort has also been directed towards understanding the impact that driving algorithms and strategies have on traffic flow. For example, as shown in Chapter 3, the impact of increasing penetration rates of adaptive cruise control-enabled vehicles on traffic flow has been analytically predicted [114]. Shladover et al. have experimentally studied the behavior of a platoon of connected vehicles equipped with cooperative adaptive cruise control (CACC) algorithms [128], and Monteil et al. have performed the stability analysis of cooperative highway traffic [129]. More recently, Nishi et al. have studied the effect of individual driving strategies on traffic flow, and specifically on jam absorption [94]. Each of these studies briefly touches upon various aspects of how individuals might affect macroscopic traffic flow dynamics. However, these research efforts do not address the problem of identifying spatial regions of the roadway where such driving algorithms could actually influence the macro-

scopic traffic flow. The following section presents a simple thought experiment and the framework within which the concept of influential subspaces will be introduced.

5.3 INFLUENTIAL SUBSPACES AND EVENT HORIZONS

Some basic knowledge of an agent and a macrostate, in the context of multi-agent systems, is a prerequisite for understanding the concepts of the influential subspace and event horizon. An agent represents an independent entity capable of controlling its own behavior, though such behavior may be influenced by neighboring agents that are part of the multi-agent system. The macrostate is a reduced-order quantitative representation of the multi-agent system that takes into account all agents that constitute the system.

5.3.1 Notion of agents and macrostate in a traffic system

To better understand these concepts when the multi-agent system under consideration is traffic flow, consider the following example with reference to [Figure 5.1](#). In this scenario, each vehicle is an agent that is controlled either by a human or a computer algorithm, such as adaptive cruise control (ACC). The macrostate may be chosen in a manner that ‘best’ represents the state of the system. The discussion on macrostate selection is a matter for another place and time, but some insights can be gained from [\[21\]](#). For now, it suffices to say that the macrostate ψ is defined herein as the number of vehicles that are not in free flow, i.e. the number of vehicles that are not moving at free flow velocity v_f . Mathematically, this may be expressed as:

$$\psi = \sum_{a \in A} \mathbb{1}_a \quad (5.1)$$

where a represents an individual agent (i.e. an individual vehicle), A represents the set of all agents (i.e. the entire vehicular population), and $\mathbb{1}_a$ represents the indicator function defined as follows:

$$\mathbb{1}_a = \begin{cases} 1, & v(a) \neq v_f \\ 0, & v(a) = v_f \end{cases} \quad (5.2)$$

where $v(a)$ denotes the velocity of agent a . Traditionally, since the quantity ψ is observed at the scale at which vehicle clusters form, it is referred to as the *mesostate* rather than the macrostate [\[114\]](#). This is done to avoid confusion with existing notions of macroscopic traffic flow variables such as flow (q) and density (k), which are observed at an even coarser scale. However, in this chapter, the variables ψ , q , and k are all referred to as macroscopic variables, since the scale-based distinction between them does not serve a significant purpose here.

5.3.2 A thought experiment

With the prerequisites in place, we can begin a thought experiment, using Figure 5.1 as a reference. The roadway in the figure represents a single-lane highway segment in which vehicles move left to right and no passing is allowed. The speed limit on the highway is the free flow velocity v_f , and no vehicle travels faster than this speed. In this work, the only admissible control policy (or driver algorithm) for a connected vehicle is assumed to be slowing down for a short period upon receiving information of a downstream jam, and then speeding up again. Specific details pertaining to when the vehicle slows down and speeds up, and which speed it slows down to, will be discussed in Section 5.4.

It is assumed that a self-organized traffic jam has formed on one section, so that vehicles in this region are in a jammed state J and are *not* moving at the free flow velocity v_f . In other words, the macrostate of the traffic system at this instant of time is given by $\psi(t) = \psi_0 \neq 0$. It is generally desirable that all vehicles move at free flow velocity so that passengers can reach their destination in the least amount of time, which implies that the desired macrostate is $\psi(t) = \psi_d = 0$. Now, consider the impact that a connected vehicle receiving information on downstream traffic conditions could have on the self-organized traffic jam, and by extension the macrostate $\psi(t)$, for each of the four regions outlined in Figure 5.1.

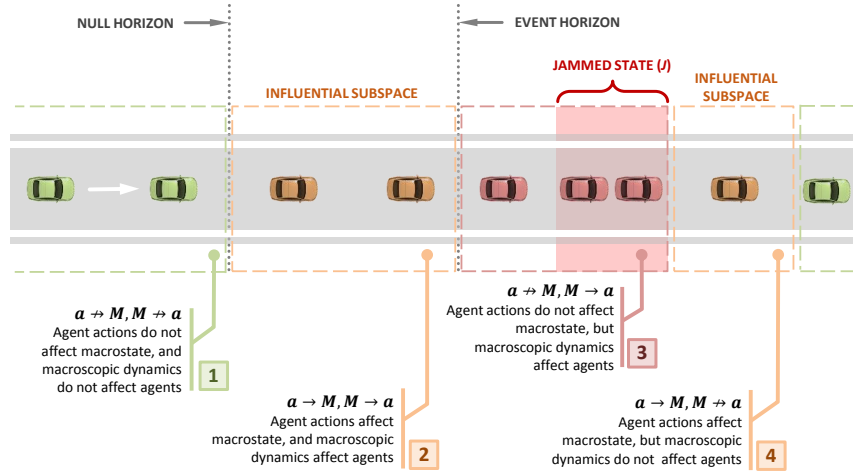


Figure 5.1: Thought experiment for understanding the concept of influential subspaces of connected vehicles, and event horizons in highway traffic. White arrow indicates direction of travel. The letter M relates to the macrostate, whereas a relates to individual agents.

In region 1 of Figure 5.1, a connected vehicle (a_{cv}) is situated well upstream of the traffic jam. At this location, even if this connected vehicle receives information pertaining to the jam, its driving algorithm, which may include slowing down to a pre-specified speed v_s

($< v_f$) to avoid the jam, it will not be able to positively effect the jammed state – the jam would have dissipated by the time the connected vehicle moves downstream. In other words, the actions of the agent a_{cv} in region 1 have no beneficial impact on the dynamics of the macrostate ψ . Region 1 is said to extend up to the *null horizon*, which is a location on the roadway upstream of which the admissible driving algorithm of the connected vehicle has no positive effect on the dynamics of the macrostate ψ . Transmitting traffic information to connected vehicles in this region serves no useful purpose in terms of improving the macroscopic dynamics, i.e. dissipating the jam and driving the macrostate to $\psi_d = 0$.

DEFINITION A *null horizon* represents a spatial location upstream of the traffic jam on a highway, *upstream* of which a connected vehicle cannot use its admissible driving algorithm (or control policy) to positively influence the macroscopic traffic flow dynamics, i.e. drive the macrostate to the pre-determined state ψ_d .

Null horizon

In region 2, a connected vehicle a_{cv} is situated upstream of the traffic jam, but downstream of the null horizon. If this connected vehicle receives traffic information, it may modify its driving behavior and choose an admissible control policy that helps mitigate the jam growth. For example, in the current discussion, an admissible control policy allows the connected vehicle to slow down for a short period before speeding up again. In this scenario, fewer vehicles would enter the jammed state, resulting in faster jam dissipation, and the connected vehicle may manage to avoid the traffic jam altogether. Thus, transmitting traffic information to connected vehicles in this region does serve a useful purpose as it may help drive the macrostate to $\psi_d = 0$ within a specified time t_d . Thus, region 2 represents the *influential subspace*.

DEFINITION The *influential subspace* of a connected vehicle is defined as the region of a highway where the vehicle has the ability to positively influence the macroscopic traffic flow so as to drive the traffic macrostate ($\psi(t)$) to a pre-determined improved state (ψ_d) within a specified time (t_d), with the given set of admissible control policies.

Influential subspace

Seasoned control theorists may notice a similarity between the definition of the influential subspace and a controllable set [47]. However, these concepts are distinct and a mathematically rigorous definition will appear in [Chapter 6](#). In the meanwhile, it should be noted that the influential subspace is defined for *an individual agent*, and is a func-

tion of the current macrostate ($\psi(t)$), the pre-determined macrostate that we desire to reach (ψ_d), and the specified time within which to reach it (t_d). It is also expected that not all locations within the influential subspace have equal influence on the macrostate, and there may exist some specified times t_d for which an influential subspace does not exist. Specifically, the locations that are close to the boundary of the influential subspace, e.g. near the null horizon, may have less influence on the macroscopic dynamics. Similarly, connected vehicles located in close proximity to the traffic jam may also have very little influence. For example, consider connected vehicles in region 3, which is immediately upstream of the traffic jam. Even if these vehicles receive advance warning of the jammed state that exists downstream, they are incapable of avoiding and contributing to the growth of the jam. Thus, vehicles in this region have no positive influence on the macrostate ψ , i.e they cannot drive the system to the macrostate $\psi_d = 0$ within a specified time t_d . Transmitting traffic information to them serves no useful purpose as well, unless, of course, they act as routers for propagating the message further upstream to connected vehicles inside the influential subspace. It is instructive to note that not all vehicles in region 3 are in the jammed state yet.

The boundary between regions 2 and 3 proves to be quite interesting. It represents the demarcation point on the roadway between locations where connected vehicles can influence the macrostate, and locations where they cannot. Specifically, once a connected vehicle is in a region inside the demarcation point, it cannot influence the macroscopic dynamics. Additionally, it can also not escape the traffic jam by using its driving algorithm, i.e. it helplessly ‘falls into’ the traffic jam. By drawing a weak analogy between traffic jams and high density astronomical regions in time-space, i.e. black holes, which possess a boundary beyond which light cannot escape and ‘falls into’ the black hole, the authors decided to christen this demarcation point as the ‘*event horizon*’. Event horizons on the highway are situated upstream of the traffic jam and indicate the location beyond which transmitted traffic information may become useful for connected vehicles to affect the macrostate ψ . The event horizon, along with the null horizon, marks the spatial extent of the largest influential subspace for any possible specified time t_d .

DEFINITION An *event horizon* represents a spatial location upstream of the traffic jam on a highway, *downstream* of which a connected vehicle cannot use its admissible driving algorithm (or control policy) to positively influence the macroscopic traffic flow dynamics, i.e. drive the macrostate to the pre-determined state ψ_d .

Event horizon

Finally, region 4 is also of interest. If a vehicle in region 4 decides to exit the traffic jam slower than at the free flow velocity, then it may influence the macroscopic dynamics as well. For example, if the exiting vehicle decides to stop completely, the traffic jam will continue to grow (as passing is not allowed). However, it is not influential in the sense that a vehicle in this region cannot drive the macrostate to the pre-determined state $\psi_d = 0$. However, if the pre-determined state had been $\psi_d > \psi_0$, then this region would be considered as an influential subspace. In practice, it may be important to identify such ‘influential’ subspaces as well, so that connected vehicles in these regions may be informed not to execute maneuvers that drive the system to an undesirable macrostate. Regions upstream of region 4 belong in the same category as region 1; they cannot influence the macroscopic dynamics, i.e. their driving algorithms cannot drive the system to the pre-determined macrostate $\psi_d = 0$ in the specified time t_d .

This concludes the thought experiment. The concepts of influential subspace and event horizon have been established by means of a simple example. The next section discusses the problem setup and some basic postulates of the Lighthill-Whitham-Richards (LWR) model of traffic flow [75][76] that will be used to later develop analytical solutions for the influential subspace and event horizon.

5.4 PROBLEM SETUP

The problem is set up as a single-lane highway where no passing is allowed. A triangular relationship between flow and density is assumed, and representative values of traffic flow parameters such as maximum flow ($q_{max} = 1800$ veh/hr), jam density ($k_J = 110$ veh/km), and free flow velocity ($v_f = 90$ km/hr) are used to construct the fundamental diagram of traffic flow (Figure 5.2). A self-organized or spontaneous traffic jam is assumed to form on the highway and vehicles upstream of the jam approach it at a free flow velocity. The state of the traffic flow (A) upstream of the jam is defined by flow q_A and density k_A ; additional traffic states, such as capacity flow (C) and jammed state (J), are indicated on the fundamental diagram in Figure 5.3. The analysis uses standard results of the Lighthill-Whitham-Richards (LWR) model by drawing time-space diagrams to identify the time taken for the traffic flow to reach the pre-determined macrostate $\psi_d = 0$, i.e. the state when all vehicles are moving in free flow.

The connected vehicles are assumed to possess an event-triggered control policy or driving algorithm. For example, the event of receiving traffic information pertaining to a downstream traffic jam triggers a control action that causes the connected vehicle to slow down to a velocity v_S . The state of traffic flow (S) associated with the velocity v_S is given by flow q_S and density k_S , and is also shown in Figure 5.3. To keep the analysis simple, only two connected vehicles are considered

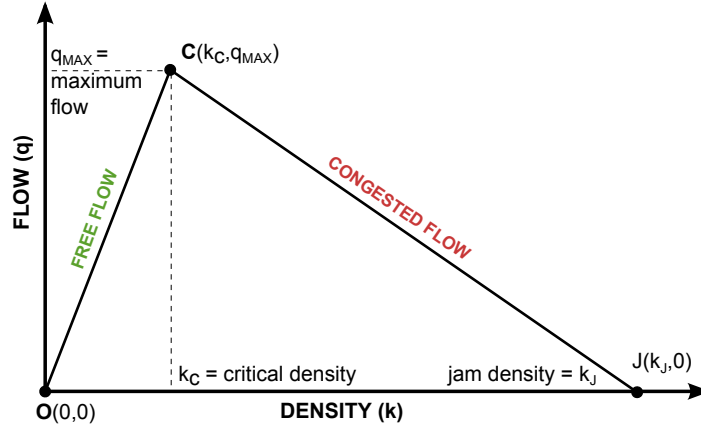


Figure 5.2: Fundamental diagram of traffic flow for single species traffic. State of traffic flow is defined using macroscopic variables such as flow (q) and density (k). Traffic states C and J are depicted as the critical and jammed states in the diagram, respectively. Slopes in the figure indicate speeds. Slope of segment OC is v_F , the free flow speed.

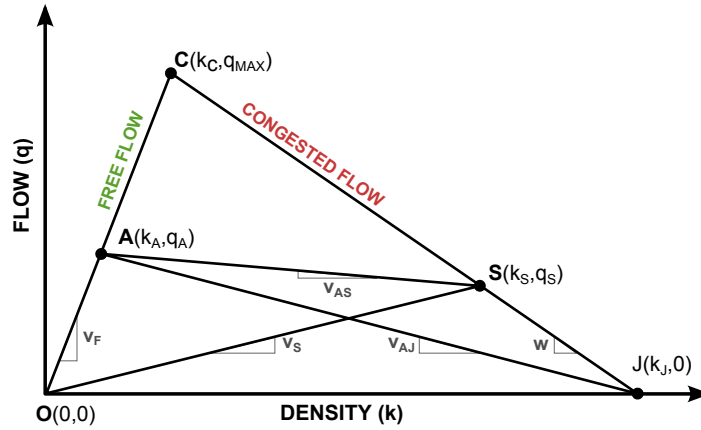


Figure 5.3: Fundamental diagram of traffic flow for slow and fast moving traffic. Traffic states A and S are depicted on the free flow and congested flow branches of the diagram, respectively. Slopes in the figure indicate speeds. Slope of segment OA is v_F , the free flow speed. Slope of segment OS is v_S , the reduced speed at which the connected vehicle drives to avoid the jam. v_{AS} denotes the interface speed between states A and S which may co-exist on neighboring regions of the highway.

in the presented work. Without loss of generality, let us assume that at time $t = 0$, the first connected vehicle (cv_1) enters the jam and sends an alert signal indicating a jammed state to the connected vehicle cv_2 situated upstream, which receives the signal instantaneously.

The admissible control policy (or driving algorithm) of the connected vehicle cv_2 is defined as follows: the reception of the alert signal from cv_1 causes an event-triggered control action in the second connected vehicle (cv_2), which slows down to a pre-determined

speed v_s as selected by the driver or dictated by an inbuilt cruise control algorithm. When cv_1 exits the traffic jam at time $t = t_{\text{EXIT}}$, it sends another alert signal upstream. This alert results in a second event-triggered control action in cv_2 due to which it speeds up to free flow velocity v_f . Depending on the location of the second connected vehicle cv_2 , the combined event-triggered control actions of slowing down and speeding up may or may not have an effect on the macrostate ψ . The next section discusses several explanatory cases similar to the ones described in [Figure 5.1](#), as well as analytical solutions for the influential subspace and event horizon.

5.5 ANALYTICAL SOLUTION OF INFLUENTIAL SUBSPACES OF CONNECTED VEHICLES

For the following discussion, the traffic system is assumed to be operating at traffic state A given by $q_A = 900$ veh/hr and $k_A = 10$ veh/km. It is assumed that the first connected vehicle cv_1 enters the spontaneous traffic jam of initial length $x_q = 500$ m at time $t = 0$, and immediately sends an alert signal to upstream vehicles. Upon receiving the signal, the second connected vehicle cv_2 is assumed to slow down to a predetermined speed $v_s = 10$ km/hr in order to avoid the traffic jam. This results in a slow-moving state S given by $q_S \approx 733$ veh/hr and $k_S \approx 73$ veh/km. Space-time diagrams based on the kinematic wave theory of the LWR traffic flow model are drawn for four scenarios where the vehicles cv_1 and cv_2 are separated by different distances, as shown in [Figure 5.5](#), and the diagram elements are explained in [Figure 5.4](#). These diagrams are discussed in detail in the following subsection.

5.5.1 Interpretation of time-space diagrams

The time-space diagram shown in [Figure 5.4](#) represents different states of the traffic system as it evolves over time. Dashed lines in the diagrams represent traffic jam evolution in the absence of any connected vehicles. These dashed lines extend up to the time $t = t_0$, indicating the duration of the self-organized traffic jam in the absence of connected vehicles. Additionally, at time $t = 0$, the system macrostate, i.e. the number of vehicles not in free flow, can be evaluated using the density k_J of jammed state J , and the initial length x_q of the traffic jam, as follows:

$$\psi(t = 0) = k_J x_q \quad (5.3)$$

If necessary, the above expression can be extended to incorporate additional congested states, such as S , when they appear in the traffic system. However, the elegant framework of the time-space diagrams

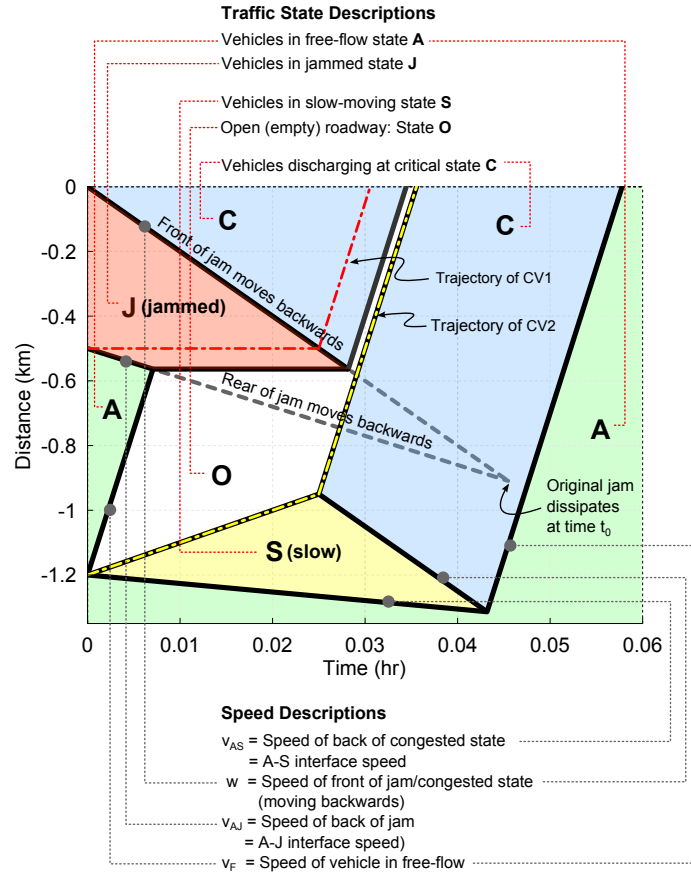


Figure 5.4: Description of traffic states and interface speeds in the time-space diagram. Dashed line indicates jam evolution without connected vehicles. Dash-dotted lines are vehicle trajectories of connected vehicles.

eliminates the need for an elaborate analysis in favor of a geometric treatment of the diagrams, as discussed later in Section 5.5.2.

The time-space diagrams can be closely related to the regions discussed with reference to Figure 5.1. Specifically, the cases (a) and (b) in Figure 5.5 correspond to region 3 that was discussed in the thought experiment. In these cases, where the vehicle cv_2 is in very close proximity to the jammed state, its control actions have no effect on the time it takes to reach the desired macrostate $\psi_d = 0$. In other words, the time t_J taken for the system to reach the state $\psi_d = 0$ remains unchanged despite of the presence of connected vehicles, as evinced by the overlap of the dashed and solid lines in Figure 5.5(a-b).

Figure 5.5(c) corresponds to region 2 in Figure 5.1, where the actions of vehicle cv_2 cause the traffic system to reach the desired macrostate ψ_d earlier as compared to cases (a) and (b). Specifically, the slow-moving state S vanishes at time t_S , whereas the jammed state J vanishes at time $t_J < t_S$, implying that all vehicles in the system are in free flow by time t_S . Thus, there is a net reduction in the time taken for the traffic flow to reach the desired macrostate ψ_d , as

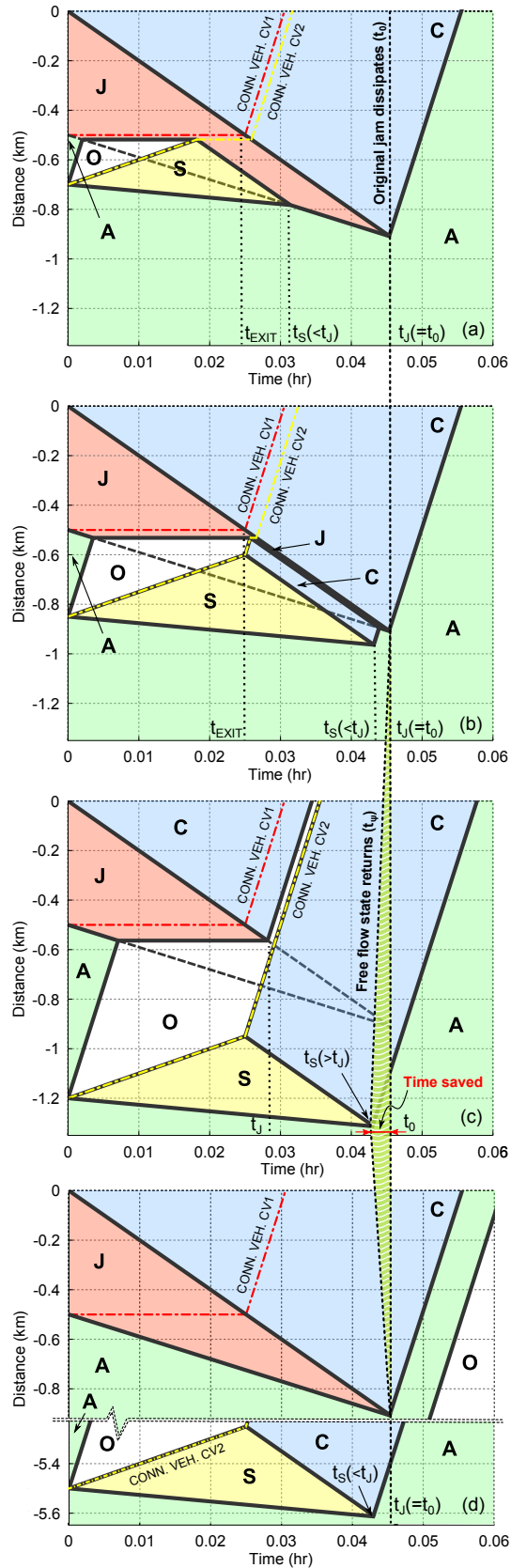


Figure 5.5: Space-time diagram for connected vehicles separated by (a) 200 m, (b) 350 m, (c) 700 m, and (d) 5000 m, for $v_s = 10$ km/hr and $x_q = 500$ m. Figure(c) shows the time saved with this control policy.

compared to cases (a) and (b). Finally, Figure 5.5(d) corresponds to region 1 of Figure 5.1, where the actions of vehicle cv2 have no impact on the time taken to reach the macrostate $\psi_d = 0$, since the jammed state J dissipates and all vehicles return to free flow condition of their own accord.

5.5.2 Analytical solution of influential subspaces

Mathematically, the time taken for the traffic system to reach the pre-determined macrostate $\psi_d = 0$, where all vehicles are in free flow, is given by:

$$t_\psi = \max\{t_J, t_S\} \quad (5.4)$$

where t_J denotes the time taken for the jammed state J to dissipate, and t_S represents the time taken for the slow-moving traffic state S to vanish. In other words, the time taken to reach the pre-determined macrostate ψ_d is governed by which of state J or S persists for a longer period of time. The underlying mechanism to evaluate the times t_J and t_S relies on the interface speeds (slopes in the time-space diagram) and the intersection points between the different traffic states.

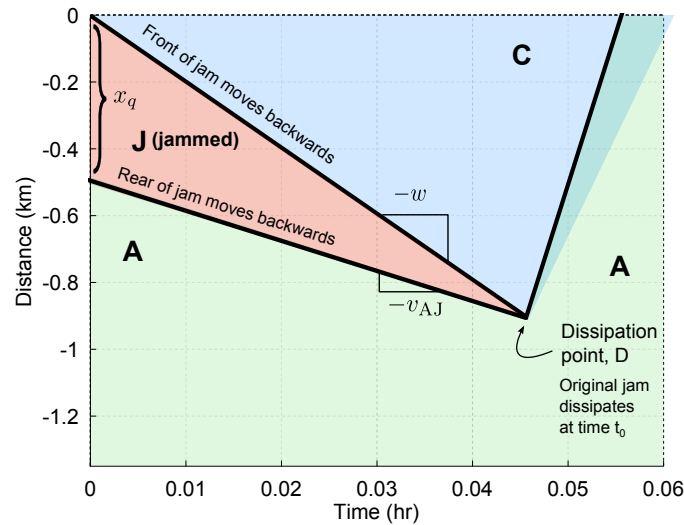


Figure 5.6: Evaluation of dissipation time t_0 in a simple jam dissipation scenario.

For example, consider the scenario where a pre-existing traffic jam dissipates of its own accord. In this case, the time-space diagram will take the form as shown in Figure 5.6. Consequently, the time t_0 taken for the jammed state J to dissipate may be evaluated using the location of the dissipation point where the interfaces between states A

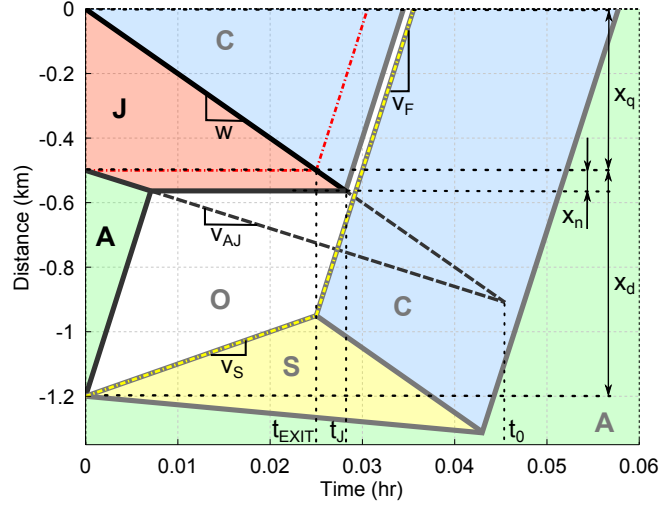


Figure 5.7: Evaluation of t_J using time-space diagram. Only relevant quantities needed for deriving analytical solution are labeled. Note that the interface speeds between states are derived from the fundamental diagram of traffic flow.

and J , and states J and C meet. The location x_D of the dissipation point D using the interface between states J and C is given by:

$$x_D = x_{JC} = -w \cdot t_0 \quad (5.5)$$

Similarly, the location of the dissipation point from the $A - J$ interface is given by:

$$x_D = x_{AJ} = -x_q - v_{AJ} \cdot t_0 \quad (5.6)$$

But $x_D = x_{JC} = x_{AJ}$, so the dissipation time t_0 is evaluated to be:

$$t_0 = \frac{x_q}{w - v_{AJ}} \quad (5.7)$$

In a very similar fashion, the analytical expressions for t_J and t_S can be calculated from geometric considerations of [Figure 5.5](#), as discussed below.

Expression for dissipation time of jammed state J

First, consider the evaluation of t_J with reference to [Figure 5.7](#) (or [Figure 5.5\(c\)](#)). In this scenario, the time taken for the jammed state J to dissipate is a function of the original queue length x_q at time $t = 0$, the distance x_d between the connected vehicles at time $t = 0$, and the traffic state A that exists upstream of the jammed state J . The expression for t_J in [Figure 5.7](#) is given by:

$$t_J = \frac{x_q + x_n}{w} \quad (5.8)$$

where x_n is the length of the roadway occupied by the vehicles between the two connected vehicles at the jam density, and w is the

backward wave speed obtained from the triangular fundamental diagram. The quantity x_n is determined by assuming that the number of vehicles is conserved on the roadway. Specifically, under this assumption, the number of vehicles between the two connected vehicles cv_1 and cv_2 can be calculated to be:

$$\begin{aligned} \text{Number of vehicles between } cv_1 \text{ and } cv_2 &= x_d k_A \\ &= x_n k_J \end{aligned} \quad (5.9)$$

so that x_n is given by:

$$x_n = x_d \frac{k_A}{k_J} \quad (5.10)$$

where x_d is the distance between the connected vehicles cv_1 and cv_2 at time $t = 0$. Consequently, the expression in Equation 5.8 can be expanded to yield:

$$t_J = \frac{x_q + x_d k_A / k_J}{w} \quad (5.11)$$

However, this expression is correct only for a specific region of the roadway, for which analytical expressions can be found by analyzing Figure 5.7. Note that the expression for t_J in Equation 5.8 first becomes valid in a situation similar to Figure 5.7, i.e. when the second connected vehicle just manages to avoid the jammed state J . As the location of the second connected vehicle is pushed further upstream, the expression stays valid till a situation somewhat similar to Figure 5.5(d) occurs. In this situation, the last vehicle ahead of the vehicle cv_2 just manages to avoid the jammed state J , and the expression Equation 5.8 is no longer valid. These two situations essentially correspond to event and null horizons, respectively, and yield the maximum possible spatial extent of the influential subspace. To evaluate the lower spatial limit, i.e. in the case when cv_2 just manages to avoid the jammed state J (Figure 5.7), the expressions Equation 5.8 or Equation 5.11 first become valid if:

$$x_d - x_n \geq v_s t_{\text{EXIT}} + v_f (t_J - t_{\text{EXIT}}) \quad (5.12)$$

where $t_{\text{EXIT}} (= x_q / w)$ represents the time at which the first connected vehicle cv_1 exits the jammed state J . The expression in Equation 5.12 may be expressed in terms of roadway characteristics as follows:

$$x_d - x_n \geq v_s \frac{x_q}{w} + v_f \left(\frac{x_q + x_d k_A / k_J}{w} - \frac{x_q}{w} \right) \quad (5.13)$$

$$\text{or, } x_d - x_n \geq v_s \frac{x_q}{w} + v_f \left(\frac{x_d k_A / k_J}{w} \right) \quad (5.14)$$

where ξ_e corresponds to the lower spatial limit for the validity of expression Equation 5.11. In relation to the terminology developed

in the thought experiment, this lower spatial limit corresponds to the *event horizon*. For $x_d \leq \xi_e$, the connected vehicle cannot impact the dynamics of macrostate ψ .

RESULT The *event horizon* ξ_e represents the location after which downstream connected vehicles cannot affect the dynamics of the macrostate ψ . The event horizon can be calculated as follows:

Analytical expression for event horizon

$$\xi_e = \left\{ 1 - \left(1 + \frac{v_f}{w} \right) \frac{k_A}{k_J} \right\}^{-1} \left\{ v_s \frac{x_q}{w} \right\} \quad (5.15)$$

The upper spatial limit for the validity of expression [Equation 5.11](#) is evaluated in the scenario when the second connected vehicle cv2 is sufficiently upstream so that last vehicle just ahead of it reaches the jammed state at time t_0 , i.e. when the jam is just about to dissipate of its own accord. Thus, the upper spatial limit can be evaluated by a simple condition given by:

$$x_q + x_n \leq wt_0 \quad (5.16)$$

$$\text{or, } \frac{k_A}{k_J} x_d \leq wt_0 - x_q \quad (5.17)$$

$$\text{or, } x_d \leq \frac{k_J}{k_A} (wt_0 - x_q) = \xi_n \quad (5.18)$$

where ξ_n corresponds to the upper spatial limit for the validity of expression [Equation 5.11](#). In relation to the terminology developed in the thought experiment, this upper spatial limit corresponds to the *null horizon*. For $x_d \geq \xi_n$, the connected vehicle cannot impact the dynamics of macrostate ψ .

RESULT The *null horizon* ξ_n represents the location after which upstream connected vehicles cannot affect the dynamics of the macrostate ψ . The null horizon can be calculated as follows:

Analytical expression for null horizon

$$\xi_n = \frac{k_J}{k_A} (wt_0 - x_q) \quad (5.19)$$

On the other hand, in [Figure 5.5\(a\)](#), (b), and (d), the expression for t_j is obtained quite simply from the original jam dissipation time t_0 evaluated in the absence of any connected vehicles. The jam evolution trajectory is indicated using dashed lines in [Figure 5.5](#) and [Figure 5.7](#).

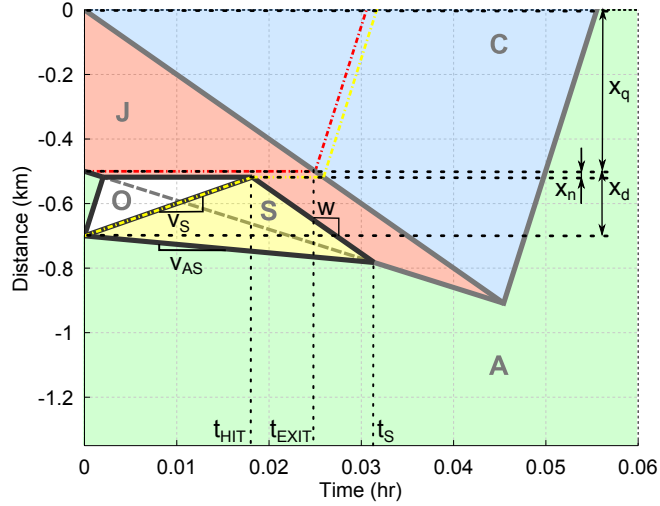


Figure 5.8: Evaluation of t_s using time-space diagram. Only relevant quantities needed for deriving analytical solution are labeled.

In these scenarios, the jam dissipation time $t_J = t_0$, and is found as follows:

$$\begin{aligned} \text{Distance traveled} &= wt_0 = x_q + v_{AJ}t_0 \\ \implies t_0 &= \frac{x_q}{(w - v_{AJ})} \end{aligned} \quad (5.20)$$

where v_{AJ} represents the interface speed between traffic states A and J . Consequently, the expression for time taken for dissipation of the jammed state J is given by combining the expressions in Equation 5.11, Equation 5.14, Equation 5.18, and Equation 5.20 to yield:

$$t_J = \begin{cases} \frac{1}{w} \left(x_q + x_d \frac{k_A}{k_J} \right), & \text{if } \xi_e \leq x_d \leq \xi_n \\ x_q / (w - v_{AJ}), & \text{else} \end{cases} \quad (5.21)$$

Expression for dissipation time of slow-moving state S

Similar geometric arguments can be used to determine the expression for the time taken for the slow-moving traffic state S to dissipate. Specifically, consider Figure 5.8 (or Figure 5.5(a)) in order to ascertain the analytical expressions. If the second connected vehicle cv_2 is too close to cv_1 , as depicted in the Figure 5.8, it enters the jam and the dissipation time for state S is governed by the initial separation between cv_1 and cv_2 . In alternative scenarios, when the vehicle cv_2 is further upstream, the dissipation time is constant, as evinced by Figure 5.5(b), (c), and (d). In Figure 5.8, the dissipation time of the slow-moving state can be evaluated by geometric calculations as follows:

$$\begin{aligned} \text{Distance} &= v_S t_{\text{HIT}} - w(t_S - t_{\text{HIT}}) = v_{AS} t_S \\ \implies t_S &= \left(\frac{v_S + w}{v_{AS} + w} \right) t_{\text{HIT}} \end{aligned} \quad (5.22)$$

where t_{HIT} is the time at which the vehicle cv_2 first enters the jammed state J , and v_{AS} is the interface speed between the states A and S . The expression for t_{HIT} can be found using geometric considerations to be:

$$\begin{aligned} t_{\text{HIT}} &= \frac{x_d - x_n}{v_S} \\ &= \frac{x_d}{v_S} \left(1 - \frac{k_A}{k_J} \right) \end{aligned} \quad (5.23)$$

so that the dissipation time t_S of state S when cv_2 is in close proximity to the jam is given by:

$$t_S = \left(\frac{v_S + w}{v_{AS} + w} \right) \left(1 - \frac{k_A}{k_J} \right) \frac{x_d}{v_S} \quad (5.24)$$

On the other hand, in [Figure 5.5\(b\)](#), (c), and (d), where the vehicle cv_2 is further upstream, the dissipation time for the state S can be calculated similarly as follows:

$$\begin{aligned} \text{Distance} &= v_S t_{\text{EXIT}} - w(t_S - t_{\text{EXIT}}) = v_{AS} t_S \\ \implies t_S &= \left(\frac{v_S + w}{v_{AS} + w} \right) t_{\text{EXIT}} \end{aligned} \quad (5.25)$$

where t_{EXIT} is the time at which the first connected vehicle cv_1 exits the jammed state J , and which can be found using geometric considerations to be:

$$t_{\text{EXIT}} = \frac{x_q}{w} \quad (5.26)$$

so that the dissipation time of state S when cv_2 is further away from the jam is given by:

$$t_S = \left(\frac{v_S + w}{v_{AS} + w} \right) \frac{x_q}{w} \quad (5.27)$$

Consequently, by observing the nature of t_S across the various parts of [Figure 5.5](#), it is realized that the value of t_S increases as the distance between the connected vehicles increases (case (a)), but saturates at a constant value in cases (b-d). Thus, the general expression for the dissipation time for the slow-moving state S is simply the minimum of expressions in [Equation 5.24](#) and [Equation 5.27](#), given by:

$$t_S = \left(\frac{v_S + w}{v_{AS} + w} \right) \min \left\{ \left(1 - \frac{k_A}{k_J} \right) \frac{x_d}{v_S}, \frac{x_q}{w} \right\} \quad (5.28)$$

To recapitulate the analysis, the time taken for the traffic system to reach the desired macrostate $\psi_d = 0$, is given by:

$$t_\psi = \max\{t_J, t_S\} \quad (5.29)$$

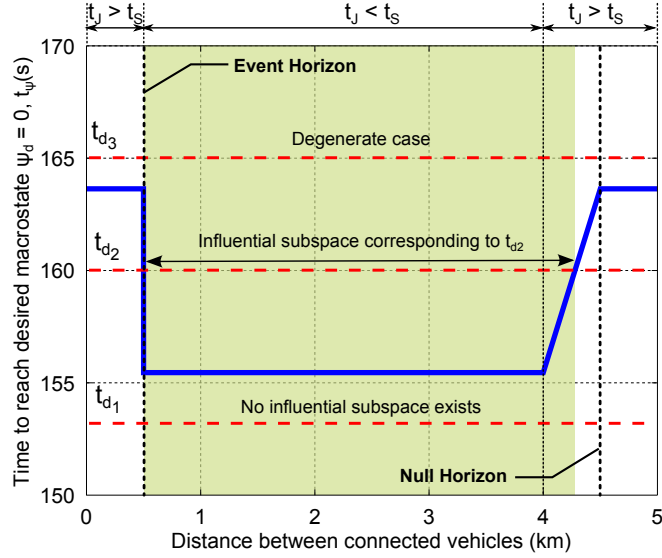


Figure 5.9: Evaluating influential subspace of the second connected vehicle for $x_q = 500$ m and $v_s = 10$ km/hr, given the pre-determined macrostate $\psi_d = 0$ and a specified time t_{d_i} within which to reach it ($i = 1, 2, 3$). Solid line indicates time taken to reach the state $\psi_d = 0$ as a function of distance between connected vehicles.

where the expressions for t_J and t_S are provided in Equation 5.21 and Equation 5.28, respectively. This result is used next to determine the influential subspace of the connected vehicle cv2, given the pre-determined macrostate $\psi_d = 0$ and a specified time t_d within which ψ_d must be attained.

5.6 RESULTS

While the concepts of the event and null horizon are important, they alone cannot help determine the influential subspace of a connected vehicle. Recall that the definition of the influential subspace requires the vehicle control action or algorithm to drive the system to a pre-determined macrostate ψ_d within a specified time t_d . If the macrostate ψ_d cannot be achieved within time t_d , then the connected vehicle cannot be said to be in its influential subspace. In the ongoing example, Equation 5.29 is used to calculate the time taken for the traffic system to reach the macrostate $\psi_d = 0$ for varying distances x_d between the connected vehicles cv1 and cv2. The result is indicated by the solid blue line in Figure 5.9.

Now, consider the following three scenarios. In the first scenario, it is desired that the traffic system be driven to the pre-determined macrostate $\psi_d = 0$ in time $t \leq t_{d_1} = 153$ s. However, as shown in Figure 5.9, there is no spatial location of the second connected vehicle cv2 that satisfies this requirement, so an influential subspace does not exist. It is simply not possible to achieve the desired macrostate within the given time. In the second scenario, it is desired that the

system be driven to $\psi_d = 0$ in time $t \leq t_{d_2}$. Since $t = t_{d_2} = 160$ s intersects t_ψ , this requirement can be satisfied and a solution exists. In this case, if the vehicle cv2 is present approximately between 0.5 km and 4.2 km of the first connected vehicle cv1, the system can be driven to the desired macrostate ψ_d in time $t \leq t_{d_2}$. The third scenario represents a degenerate case, where the system will always reach the pre-determined macrostate ψ_d within time $t_{d_3} = 165$ s, irrespective of the spatial location of the vehicle cv2, as long as the set of admissible control actions remains unchanged. However, other scenarios may exist where this degenerate case is not observed, such as when a self-organized traffic jam is growing in size, or if additional control policies (or driving algorithms) for the connected vehicle are available.

In [Figure 5.9](#), the influential subspace for the vehicle cv2 is determined for very specific values of the variables v_s (slower speed of connected vehicle), x_q (initial jam length), k_A (density of upstream traffic) and t_d (specified time within which to reach pre-determined macrostate ψ_d). However, the analytical solutions developed in [Section 5.5.2](#) allow us to observe more general patterns in the extent of the influential subspace as variables such as v_s , x_q and k_A change.

5.6.1 Dependence on reduced speed v_s

The spatial extent of the influential subspace bears a strong dependence on the control policy (or driving algorithm) adopted by the connected vehicles. Specifically, the slower speed v_s assumed by the vehicle cv2 when it receives an alert signal from a downstream vehicle has a significant effect on the influential subspace, as depicted in [Figure 5.10](#). The figure can be understood as follows: if a connected vehicle desires to drive the traffic macrostate to $\psi_d = 0$ in time $t_d = 133$ s (say; reading contour values), and the admissible driving algorithm is restricted to small range of speeds, say approximately between 40 and 50 km/hr (reading y-axis values), then this goal is achievable only if the connected vehicle cv2 is in its influential subspace, i.e. between 2 and 2.6 km (reading x-axis values) upstream of the vehicle cv1 (i.e. the location of the back of the jam at time $t = 0$). If the time restriction is relaxed so that it is now desired to reach the macrostate ψ_d within time $t_d = 145$ s (say), but no change is made to the admissible driving algorithm, then the influential subspace is also relaxed to approximately between 2 and 3.3 km upstream of the vehicle cv1. Note that these values hold when the other parameters x_q and k_A are held constant at the indicated levels.

From a broader perspective, understanding of this dependence of the influential subspace on the control policy, i.e. the driver algorithm, of the connected vehicle may be helpful in dynamically establishing speed limits in specific regions of the highway. Such dynamic speed

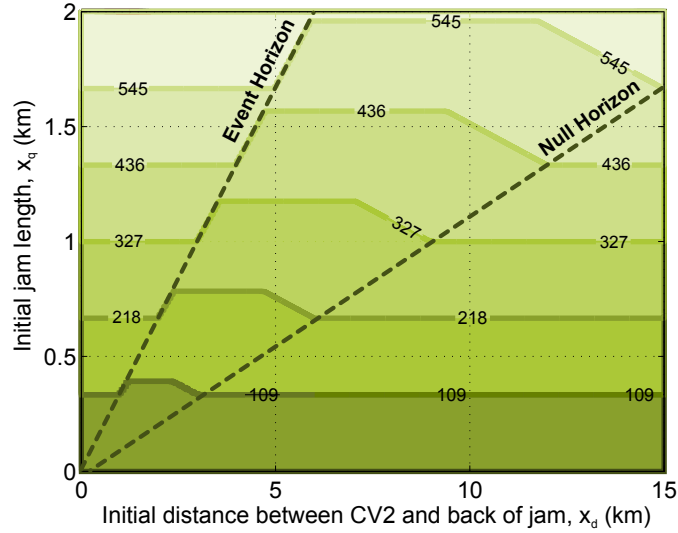


Figure 5.11: Influential subspace is pushed further upstream as initial jam length x_q increases. Other system parameters are held constant: $v_S = 30$ km/hr, and $k_A = 10$ veh/km. Contours represent the time t_d (s) taken to reach the pre-determined macrostate $\psi_d = 0$. The range of values enclosed by the contour reach the macrostate $\psi_d = 0$ in time $t < t_d$, and hence can be used to determine the influential subspace using the x -axis.

increases, the influential subspace, i.e. the region between the event and null horizons, is pushed further away from the start of the jam.

Clearly, the parameter x_q , the length of the self-organized traffic jam, is not under our control like the parameter v_S . However, from a broader perspective, the knowledge of this dependence on x_q is still useful for implementation of connected vehicles technology. Specifically, if the initial jam length can be estimated by infrastructure elements or by the connected vehicle entering the jam, then this information can be transmitted to only those connected vehicles that are in their influential subspace, allowing for reduction in bandwidth requirements.

5.6.3 Dependence on upstream traffic density k_A

The upstream traffic state directly impacts the location of the influential subspace, as indicated in Figure 5.12, where the y -axis has been normalized to show the magnitude of k_A in relation to the critical density k_C . The figure can be understood as follows: if it is desired to drive the traffic flow to the macrostate $\psi_d = 0$ within time $t_d = 316$ s (say; reading contour values), and the normalized upstream traffic density is 0.75 (reading y -axis values), then the influential subspace of the connected vehicle CV2 extends from approximately 1.5 to 9 km (reading x -axis values) upstream of the vehicle CV1 (i.e. the location of the back of the jam at time $t = 0$). Note that these values hold when

the other parameters v_S and x_q are held constant at the indicated levels.

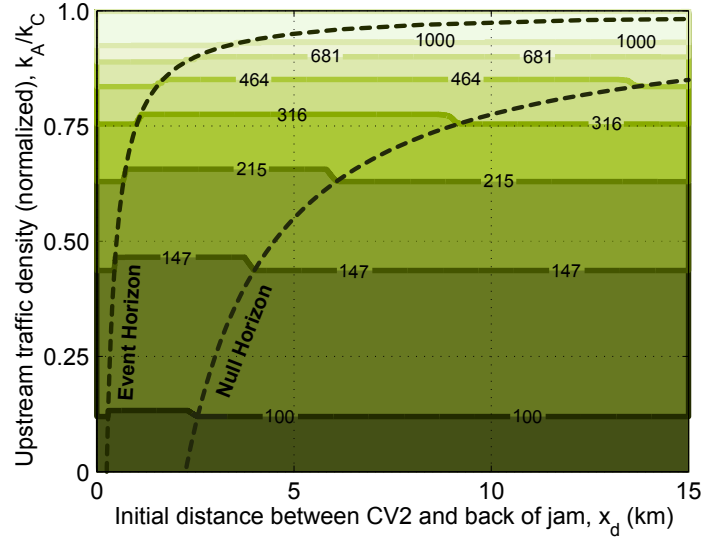


Figure 5.12: Influential subspace vanishes and the event horizon tends to infinity ($\xi_e \rightarrow \infty$), as upstream free-flowing traffic state k_A nears critical density k_C . Other system parameters are held constant: $v_S = 10$ km/hr, and $x_q = 500$ m. Contours represent the time t_d (s) taken to reach the pre-determined macrostate $\psi_d = 0$. The range of values enclosed by the contour reach the macrostate $\psi_d = 0$ in time $t < t_d$, and hence can be used to determine the influential subspace using the x-axis.

In this scenario, it is observed that as the upstream traffic density approaches the critical density, the event horizon tends to infinity. When the upstream traffic is near this critical state, CV2's control policy, i.e. slowing down to v_S when CV1 enters the jam and speeding up to v_f when CV1 exits the jam, has no effect on the macroscopic dynamics, irrespective of the spatial location or the reduced speed of CV2. However, this result is expected to change for systems with more than two connected vehicles, wherein each vehicle may be able to enact a control policy whose cumulative effect across a large set of connected vehicles may be beneficial.

Interestingly, this analysis also highlights certain message hopping requirements for connected vehicles technology to be able to effectively mitigate traffic jams and control macroscopic traffic flow. Specifically, connected vehicles downstream of the event horizon must be able to communicate with at least one connected vehicle upstream of the event horizon, in order to control macrostate dynamics. Let us assume a conservative estimate of the communication range capabilities of Dedicated Short-Range Communications (DSRC) to be about 800 m [130]. Considering traffic flow at the density $k_A = 16$ veh/km (i.e. normalized density of 0.75), the event horizon lies at a distance of 1.2 km from the back of the jam at time $t = 0$ (when CV1 reaches

the jam). Thus, at least two message hops are required across two connected vehicles so that at least one connected vehicle lies beyond the event horizon. As is evident from [Figure 5.12](#), as the event horizon is pushed further back with increasing density, more stringent message hopping requirements are necessary for connected vehicles with given admissible control policies to be able to affect macroscopic traffic flow dynamics.

5.7 CONCLUSIONS, CONTRIBUTIONS AND BROADER IMPACTS

Knowledge of the influential subspace is a critical element for the efficient implementation of connected vehicles technology. Implementation of this technology will have to deal with, among other things, issues such as bandwidth limitations and packet transmission ranges. Consequently, knowledge of the influential subspace can help ensure that bandwidth is not wasted by transmitting packets to vehicles that are not in their influential subspaces. Additionally, the same knowledge can help optimally route packets to vehicles within the influential subspaces and reduce power requirements for transmission equipment. Further, future policy decisions on connected vehicles technology, such as setting dynamic speed limits and understanding message hopping requirements, could be guided by the results discussed in reference to [Figure 5.10](#), [Figure 5.11](#) and [Figure 5.12](#). Other potential applications that may utilize the concept of influential subspaces and event horizons include cooperative adaptive cruise control, where the location of platoon formation, merging, and splitting may be constrained by where such maneuvers influence the traffic macrostate.

SPATIAL DEPENDENCE OF AGENT INFLUENCE IN SELF-ORGANIZING SYSTEMS

AUTHOR'S NOTE This chapter borrows significant content from the author's publication titled "Identification of locally influential agents in self-organizing multi-agent systems" submitted to the *American Control Conference (ACC) 2015* in September 2014.

In the [Chapter 5](#), a thought experiment pertaining to the notion of an influential subspace was presented. Further analysis showed that such influential subspaces could be found in the context of connected vehicles in a highway system where a self-organized traffic jams has formed. More importantly, the work in the previous chapter hinted that, in large-scale multi agent systems (MAS), agent influence on self-organized dynamics may be spatially dependent. In this chapter, such spatial dependence of agent influence on self-organized dynamics is studied in a more formal, control-theoretic perspective.

Current research methods directed towards measuring the influence of specific agents on the dynamics of a large-scale MAS rely largely on the notion of controllability of the full-order system, or on the comparison of agent dynamics with a user-defined macroscopic system property. They, however, do not utilize the information that such systems tend to self-organize, and that their dynamics often reside on a low-dimensional manifold. The proposed framework uses this fact to measure an agent's influence on the macroscopic dynamics. First, the minimum embedding dimension that can encapsulate the low-dimensional manifold associated with the self-organized dynamics is identified using a modification of the method of false neighbors. Second, the minimum embedding dimension is used to guide the Krylov subspace-based model order reduction of the system dynamics. Finally, an existing controllability-based metric is applied to the local reduced-order representation to measure an agent's influence on the self-organized dynamics. The proposed technique is demonstrated by applying it to the problem of vehicle cluster formation in traffic, a prototypical self-organizing system. With this technique, one can identify regions of the state space where an agent has significant local influence on the dynamics of the self-organizing MAS.

6.1 INTRODUCTION

In recent years, there has been significant interest in the self-organized behavior exhibited by large-scale MAS. However, as discussed ear-

lier, it is difficult to control the global (or macroscopic) behavior of self-organizing MAS because (i) an external centralized mechanism to control the macroscopic dynamics of such a large-scale system would likely require significant control effort, and (ii) alternative decentralized approaches would require controlling each agent in a large-scale MAS, which is often not a feasible option. However, macroscopic behavior of self-organizing systems may be *influenced* by controlling a small subset of agents. Such a phenomenon can already be seen at play in several natural-engineered systems, where the self-organizing behavior of a naturally existing large-scale multi-agent system is affected by introduction of a ‘small’ set of artificially-engineered agents [114][131]. Within a MAS, not all agents have the same influence on the system’s macroscopic dynamics. The following work presents a methodology to choose the set of most influential agents with respect to the macroscopic behavior of the naturally existing large-scale MAS. Self-organized vehicle cluster formation is used as a prototypical example to demonstrate this methodology.

6.2 PRIOR WORK

Prior work pertaining to subspace selection and agent selection was reviewed in Section 2.2.2 and Section 2.2.3, respectively. Many such approaches use a combinatorial search strategy to determine the set of agents that maximize an output-based measure, i.e. a pre-specified macroscopic quantity of the network. Within the framework of pinning control [61], Porfiri and di Bernardo have proposed a technique to identify a set of pinned nodes or agents that lead to higher network synchronization strength [60]. Similarly, Patterson et al. have suggested the use of network coherence as the macroscopic quantity to optimize during the combinatorial search [69]. Recent works have also studied the influence of individual agents on macroscopic properties by drawing inspiration from other fields, such as the manipulability measure of influence proposed by Kawashima et al., which draws inspiration from sensitivity-like measures developed for robotic arms [71]. Often, the optimized macroscopic quantity (or output-based measure) is selected based on the user’s understanding of the system dynamics (such as studying synchronization strength in coupled oscillators, or network coherence in consensus problems). However, in systems where the underlying self-organized dynamics are not well understood, approaches that rely on output-based measures may have limited applicability.

Other researchers have approached the problem more directly by attempting to develop measures of influence for individual agents. The influence metrics developed in recent times have largely relied on controllability-based approaches, such as using the determinant, minimum eigenvalue, or other properties of the controllability gram-

mian [67][68][73]. These works follow the rich tradition of some earlier research on measures of controllability from the 1980s [132] [133] [134], which attempted to measure the controllability of linear time-invariant systems of the form:

$$\dot{x} = Ax + Bu \quad (6.1)$$

where $x \in \mathbb{R}^N$ represents the state of the system, u is a scalar input provided to the system, $A \in \mathbb{R}^{N \times N}$, and $B \in \mathbb{R}^{N \times 1}$. These early works were based on carrying out a comparison between controllable and uncontrollable systems. In the following decades, these works were built upon to propose measures of modal controllability [135], for input and output selection [136], as well as actuator and sensor placement on large-scale systems [8][57][137]. More recently, with increasing attention being placed on complex networked systems, the idea of selecting leaders in a multi-agent system using controllability measures has been pursued by researchers [60][138][139]. The underlying commonality between these approaches is the use of eigenvalues or singular values of combinations of the system matrices A and B to develop controllability measures, some of which are discussed below.

measures of controllability

6.2.1 Eising's measure of controllability

In 1984, Eising proposed a measure of controllability (μ_E) based on a distance metric between a controllable system (A, B) and the set S_{UNC} of uncontrollable systems given as [132]:

$$\mu_E = d((A, B), S_{\text{UNC}}) = \min_{s \in \mathbb{C}} \{\sigma_{\min}[sI - A, B]\} \quad (6.2)$$

where σ_{\min} represents the smallest singular value, $s \in \mathbb{C}$ represents a point in the complex plane, and $[sI - A, B]$ represents an augmented matrix based on the Hautus test for controllability. As the metric $d((A, B), S_{\text{UNC}})$ becomes smaller, it becomes harder to control the system (A, B) . This measure may be evaluated numerically, but poses some challenges since numerical methods may lead to a local minimum and yield an incorrect measure of controllability [140].

6.2.2 Hamdan's geometric measure of modal controllability

In 1988, Hamdan and Elabdalla proposed a geometric measure of modal controllability (μ_H), which has its foundations in the Popov-Belevitch-Hautus (PBH) eigenvalue test for modal controllability [135]. Let the left eigenvectors for the single input linear time-invariant system given by Equation 6.1 be denoted by q_i such that:

$$Aq_i = \lambda_i q_i \quad (6.3)$$

and \mathbf{b}_j represent the j^{th} column of \mathbf{B} . If \mathbf{q}_i and \mathbf{b}_j are orthogonal, then the i^{th} mode of the system (\mathbf{A}, \mathbf{B}) is not controllable from its j^{th} input. Hamdan and Elabdalla extended this idea to develop a geometric measure of modal controllability based on the angle between the two one-dimensional subspaces spanned by the vectors \mathbf{q}_i and \mathbf{b}_j . Mathematically, the measure may be written as [135]:

$$\mu_H = \cos(\theta(\mathbf{q}_i, \mathbf{b}_j)) = \frac{|\mathbf{q}_i^T \mathbf{b}_j|}{\|\mathbf{q}_i\| \|\mathbf{b}_j\|} \quad (6.4)$$

A single input system may be re-written as an N input system, i.e. each agent has a distinct controller so that \mathbf{B} is a diagonal matrix, in order to make use of this measure for the agent selection problem.

6.2.3 Degree of controllability

In 1984, [Viswanathan, Longman, and Likins](#) proposed a measure referred to as the degree of controllability [8]. Today, we would recognize this definition in terms of the controllable set of a system. The original definition makes use of the concept of a *recovery region*, which is defined for time t_f as [8]:

$$\mathcal{R} = \{\mathbf{x}(0) : \exists \mathbf{u}(t), t \in [0, t_f], \quad |u_i(t)| \leq 1 \quad (i = 1, 2, \dots, M) \\ \text{such that } \mathbf{x}(t_f) = \mathbf{0}\} \quad (6.5)$$

i.e., the set of all initial conditions $\mathbf{x}(0)$ such that an admissible control effort can drive the system state to $\mathbf{0}$ in time t_f . The *degree of controllability* (μ_D) is then defined as:

$$\mu_D = \rho = \inf \|\mathbf{x}(0)\| \quad \forall \mathbf{x}(0) \notin \mathcal{R} \quad (6.6)$$

In [8], Viswanathan et al. suggest an algorithm for approximating the recovery region/controllable set, followed by using [Equation 6.6](#) to determine the degree of controllability. The algorithm forms the basis of polyhedra-based approaches for determining controllable sets.

6.2.4 Limitations of prior work

These prior works share a common limitation: they do not address the need for a methodology to assess agent influence in *self-organizing* systems. The following work describes such a systematic methodology while incorporating topological considerations arising from the self-organizing nature of the system dynamics. In this work, Eising's measure of controllability is used to assess agent influence due to its ease of use. The entire process is explained through the use of vehicle cluster formation as a prototypical example of self-organization.

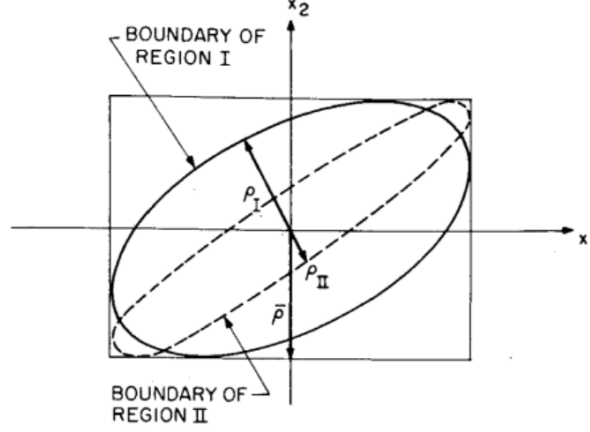


Figure 6.1: The degree of controllability indicates how easy it is control the system. As ρ tends to zero, the system becomes less controllable. At $\rho = 0$ the system is uncontrollable. $\bar{\rho}$ represents the approximate degree of controllability based on a parallelepiped approximation of the recovery region [8].

6.3 A PROTOTYPICAL SELF-ORGANIZING SYSTEM

For this study, vehicle clusters will be generated by simulating driver behavior via the intelligent driver model (IDM) [91]. The primary reason for this choice is that the IDM is one of the few models that can mimic car-following dynamics without requiring an explicit delay term. The absence of an explicit delay term is advantageous because it helps avoid modeling the system via delay differential equations and significantly simplifies the ensuing controllability-based analysis.

6.3.1 Intelligent driver model

As discussed earlier in Section 2.3, the intelligent driver model is expressed as:

$$\dot{x}_i(t) = v_i \quad (6.7)$$

$$\begin{aligned} \ddot{x}_i(t) &= f(x_i, x_{i-1}, \dot{x}_i, \dot{x}_{i-1}, a_i, b_i) \\ &= a_i \left\{ 1 - \left(\frac{v_i}{v_0} \right)^\delta - \left(\frac{s(v_i, \Delta v_i)}{s_i} \right)^2 \right\} \end{aligned} \quad (6.8)$$

where, $s_i = x_i - x_{i-1}$ denotes the spacing between the following and followed vehicles, $\Delta v_i = v_i - v_{i-1} = \dot{x}_i - \dot{x}_{i-1}$ denotes the relative velocity between the following and followed vehicles, $s(v_i, \Delta v_i) = s_0 + v_i T + v_i \Delta v_i / (2\sqrt{a_i b_i})$, a_i denotes the maximum acceleration of the following vehicle, v_0 denotes the maximum vehicle velocity in free flow traffic, s_0 represents the minimum spacing between two stationary vehicles, T denotes the desired time headway maintained by the following vehicle, b_i denotes the comfortable braking deceleration of the following vehicle, and the exponent δ is usually assumed to have a value of 4 [91].

$$\begin{aligned}
\underbrace{\begin{bmatrix} \delta \dot{x}_1 \\ \delta \ddot{x}_1 \\ \delta \dot{x}_2 \\ \delta \ddot{x}_2 \\ \delta \dot{x}_3 \\ \delta \ddot{x}_3 \end{bmatrix}}_{\dot{x}} &= \underbrace{\begin{bmatrix} 0 & 1 & 0 & 0 & 0 & 0 \\ \alpha_{x_i}^{(1)} & \alpha_{\dot{x}_i}^{(1)} & 0 & 0 & \alpha_{x_{i-1}}^{(1)} & \alpha_{\dot{x}_{i-1}}^{(1)} \\ 0 & 0 & 0 & 1 & 0 & 0 \\ \alpha_{x_{i-1}}^{(2)} & \alpha_{\dot{x}_{i-1}}^{(2)} & \alpha_{x_i}^{(2)} & \alpha_{\dot{x}_i}^{(2)} & 0 & 0 \\ 0 & 0 & 0 & 0 & 0 & 1 \\ 0 & 0 & \alpha_{x_{i-1}}^{(3)} & \alpha_{\dot{x}_{i-1}}^{(3)} & \alpha_{x_i}^{(3)} & \alpha_{\dot{x}_i}^{(3)} \end{bmatrix}}_A \underbrace{\begin{bmatrix} \delta x_1 \\ \delta \dot{x}_1 \\ \delta x_2 \\ \delta \dot{x}_2 \\ \delta x_3 \\ \delta \dot{x}_3 \end{bmatrix}}_x + \underbrace{\begin{bmatrix} 0 & 0 & 0 & 0 & 0 & 0 \\ \beta_a^{(1)} & \beta_b^{(1)} & 0 & 0 & 0 & 0 \\ 0 & 0 & 0 & 0 & 0 & 0 \\ 0 & 0 & \beta_a^{(2)} & \beta_b^{(2)} & 0 & 0 \\ 0 & 0 & 0 & 0 & 0 & 0 \\ 0 & 0 & 0 & 0 & \beta_a^{(3)} & \beta_b^{(3)} \end{bmatrix}}_B \underbrace{\begin{bmatrix} \delta a_1 \\ \delta b_1 \\ \delta a_2 \\ \delta b_2 \\ \delta a_3 \\ \delta b_3 \end{bmatrix}}_u \quad (6.9)
\end{aligned}$$

6.3.2 System dynamics

The self-organized vehicle cluster formation is replicated as a system of M vehicles on a closed ring-road of length L in this work. The closed ring-road environment simplifies the problem by avoiding open boundary conditions due to vehicles entering or exiting the system. For the purposes of this work, the system under consideration is restricted to $M = 3$ vehicles on a closed ring road of length $L = 60$ m. This simple construction allows for easier visualization of the system dynamics as compared to a large-scale MAS, while still retaining the ability to demonstrate the proposed framework for identifying locally influential agents. For this system, our interest lies in the evolution of the system state described by the state vector $x = [x_1, \dot{x}_1, x_2, \dot{x}_2, x_3, \dot{x}_3]^T \in \mathbb{R}^6$.

The *local controllability* of the system can be determined by linearizing the system about a current operating point (x_0), and studying the rank of the controllability matrix. It is assumed that each vehicle has the ability to change its acceleration-related parameters, i.e. a_i (the maximum acceleration) and b_i (the comfortable braking deceleration). By controlling such acceleration-related parameters, the agents can potentially influence the self-organized vehicle cluster formation as seen in [114]. Now, the linearization of the 3-vehicle system yields the local evolution equations given by Equation 6.9. In this equation, $\alpha_j^{(i)}$ represents the partial derivative of the acceleration of the i^{th} vehicle with respect to the state variable j at the operating point x_0 , where the acceleration is given by the car-following model in Equation 6.8. For example, $\alpha_{x_i}^{(1)}$ represents $\partial f / \partial x_i$ evaluated for the first vehicle at the operating point x_0 , $\alpha_{\dot{x}_{i-1}}^{(2)}$ represents $\partial f / \partial \dot{x}_{i-1}$ evaluated for the second vehicle at the operating point x_0 , and so on. Similarly, $\beta_k^{(i)}$ represents the partial derivative of the acceleration of the i^{th} vehicle with respect to the input k , evaluated at the operating point x_0 . For example, $\beta_a^{(1)}$ represents $\partial f / \partial a$ evaluated for the first vehicle at the operating point x_0 .

local controllability

6.3.3 Studying agent influence

Agent influence can be determined by studying the minimum singular value of the augmented matrix $[sI - A, B]$ ($s \in \mathbb{C}$), as proposed by Eising in [132]. To study the influence of a specific agent on the system dynamics, the B matrix can be modified appropriately, so that only the specific agent can provide control inputs to the system. For example, in order to measure the influence of vehicle 1 on the system dynamics, one can set $\beta_a^{(2)} = \beta_b^{(2)} = \beta_a^{(3)} = \beta_b^{(3)} = 0$, so that the B matrix reads as:

$$B = B_1 = \begin{bmatrix} 0 & 0 & 0 & 0 & 0 & 0 \\ \beta_a^{(1)} & \beta_b^{(1)} & 0 & 0 & 0 & 0 \\ 0 & 0 & 0 & 0 & 0 & 0 \\ 0 & 0 & 0 & 0 & 0 & 0 \\ 0 & 0 & 0 & 0 & 0 & 0 \\ 0 & 0 & 0 & 0 & 0 & 0 \end{bmatrix} \quad (6.10)$$

In this scenario, only the first agent (or vehicle) may influence the system dynamics via its control actions (or acceleration and deceleration maneuvers). Now, the minimum singular value σ_1 of the augmented matrix $[sI - A, B_1]$ yields a measure of influence of agent 1 on the full-order system dynamics. Comparing the minimum singular value σ_1 with the minimum singular values σ_2 and σ_3 obtained from the corresponding augmented matrices $[sI - A, B_2]$ and $[sI - A, B_3]$ respectively, one can identify the locally most influential agent in the system.

However, the methodology presented up to this point is applicable to all systems, and does not leverage the fact that several multi-agent system exhibit self-organized behavior. Before modifying the presented methodology, we first study the self-organizing behavior of the prototypical system, i.e. self-organized vehicle cluster formation on the closed ring-road. The 3-vehicle system was simulated with model parameters values typically used in the IDM model to model traffic behavior, such as $a = 1 \text{ m/s}^2$, $b = 3.4 \text{ m/s}^2$, $T = 2.5 \text{ s}$, $s_0 = 2 \text{ m}$, and $v_0 = 15 \text{ m/s}$ [91]. The maximum free flow velocity takes into account the sharp turning radius of the ring road. The results of the simulation are included in Figure 6.2, which offers some evidence that spatio-temporal patterns may be present in the system as it evolves over time. This hypothesis is further strengthened when the phase portrait of the system is observed. However, since the system evolves in \mathbb{R}^6 , we can only visualize the phase portrait via projections onto lower-dimensional spaces. For such a visualization, the phase portrait is projected into two \mathbb{R}^3 spaces, one given by the spacing of the vehicles in the system, i.e. $[s_1, s_2, s_3]^T = [x_1 - x_2, x_2 - x_3, x_3 - x_1]^T \in \mathbb{R}^3$, and the other given by the velocities

of the vehicles in the system, i.e. $[v_1, v_2, v_3]^T \in \mathbb{R}^3$. These projections are shown in Figure 6.3 and Figure 6.4 and they exhibit behavior similar to limit cycles, which indicates the presence of an attractor or low-dimensional manifold on which the self-organized dynamics of the system evolve. Since the goal of this study is to identify the agents that have most significant influence on the self-organized dynamics, the next step involves determination of the minimum embedding dimension of the low-dimensional manifold on which these dynamics reside.

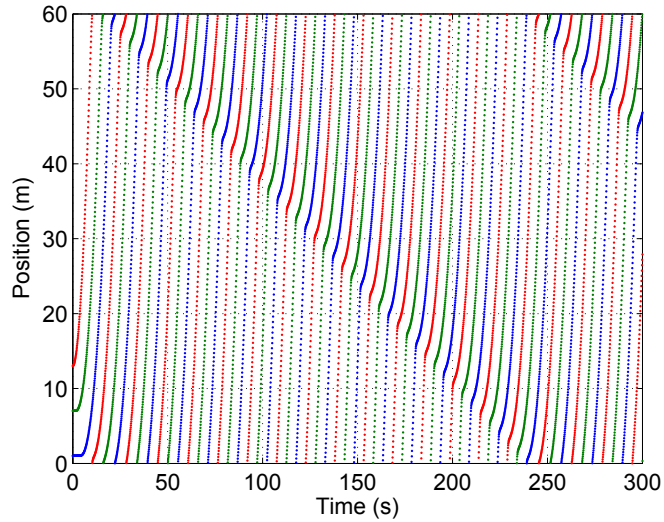


Figure 6.2: Three vehicle system on a ring road with dynamics manifesting as self-organized stop-and-go waves.

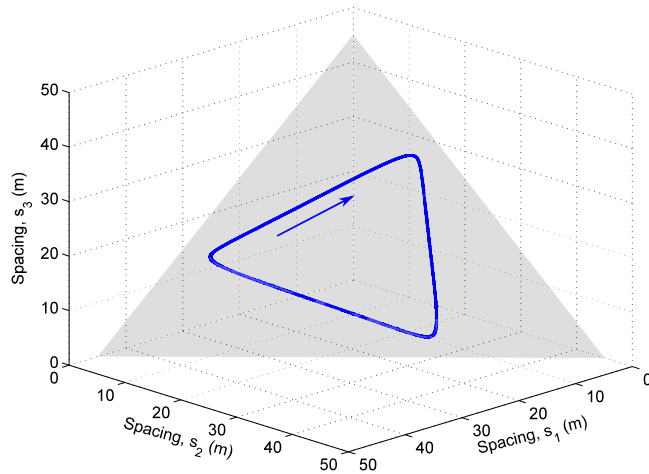


Figure 6.3: Behavior similar to a limit cycle observed in the \mathbb{R}^3 projection given by vehicle spacings $[s_1, s_2, s_3]^T$. Arrow indicates the direction of system evolution. The shaded region indicates the plane in which the limit cycle resides.

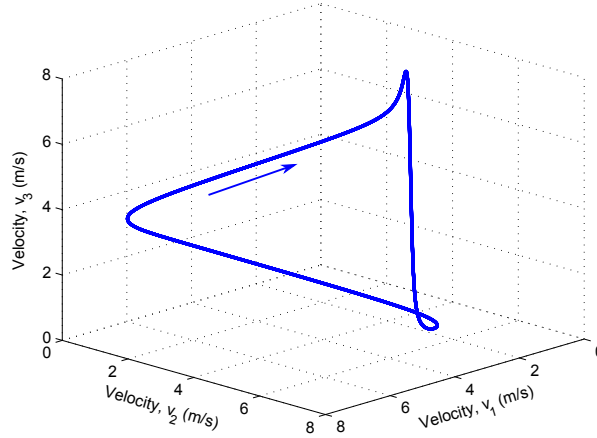


Figure 6.4: Behavior similar to a limit cycle observed in the \mathbb{R}^3 projection given by vehicle velocities $[v_1, v_2, v_3]^T$. Arrow indicates the direction of system evolution.

6.4 MINIMUM EMBEDDING DIMENSION OF LOW-DIMENSIONAL MANIFOLD

The evidence presented in [Figure 6.3](#) and [Figure 6.4](#) indicates that the self-organized dynamics of the multi-agent system may evolve on a low-dimensional manifold in \mathbb{R}^M , where $M \ll N$. Knowledge of the dimension of this manifold can assist with the model order reduction of the linearized system equations presented in [Equation 6.9](#), resulting in a more accurate estimation of the locally influential agents. The use of a reduced-order model also has significant computational advantages for extremely large-scale multi-agent system whose self-organized dynamics may evolve on a manifold of very small dimension.

The dimension of the attractor or low-dimensional manifold can be determined by several methods. While the Hausdorff dimension, or its more practical counterpart, the box dimension, may yield accurate estimates of the attractor dimension, these methods require significant computational resources [\[141\]](#). Moreover, since the ultimate goal is to determine the dimension for a reduced-order model, an upper bound of the attractor dimension serves our purpose equally as well as the exact attractor dimension. Fortunately, there exist methods to determine the upper bound of the attractor dimension that are computationally inexpensive. One such technique is the method of false neighbors developed by [Kennel et al. \[142\]](#). A modification of this method by Cao is utilized in this work and is explained in the following subsection.

6.4.1 Method of false neighbors

The underlying premise of the method of false neighbors is that, when a trajectory residing on an attractor is projected onto an even lower-dimensional manifold, certain points on the trajectory end up closer to each other as a result of geometric constraints rather than dynamics [142]. Such points that are ‘close’ to each other because they have been forced into a lower dimension are known as *false neighbors*. As the dimension of the lower-dimensional manifold is increased, fewer trajectory points are neighbors due to geometry rather than dynamics. In other words, as the dimension of the lower-dimensional manifold increases, the percentage of false neighbors decreases. The dimension at which the percentage of false neighbors drops to zero indicates the minimum embedding dimension d_0 , i.e. the attractor can be embedded in a state space whose dimension is *at least* d_0 . Thus, the minimum embedding dimension can serve as a guide for the reduced-order modeling of large-scale multi-agent systems.

The concept is very intuitive and easier to understand with visual aids. For example, consider the Hénon map, which is a dynamical system described by the following equations:

Hénon map

$$x_{k+1} = 1 - ax_k^2 + y_k \quad (6.11)$$

$$y_{k+1} = bx_k \quad (6.12)$$

where a and b are constants. The attractor for this dynamical system exists in a 2-dimensional space, as is evident from Figure 6.5. Now consider Figure 6.5(b) where the attractor is observed in 1-dimensional space. In this space, both points B and C appear to be neighbors of point A. However, when the attractor is observed (or *embedded*) in 2-dimensional space, it is immediately apparent that the point C is a false neighbor, and appears to be close to point A only due to the geometric constraints forced on the state space. On the other hand, point B is close to point A due to the dynamics of the system, and is referred to as a *true neighbor*.

Evaluation of the minimum embedding dimension requires scalar time series data of the state trajectory $x(t) = [x_1, \dot{x}_1, x_2, \dot{x}_2, x_3, \dot{x}_3]^T$. The scalar time series data can be generated from the state trajectory as follows:

$$\chi(t) = c_1x_1 + c_2\dot{x}_1 + c_3x_2 + c_4\dot{x}_2 + c_5x_3 + c_6\dot{x}_3 \quad (6.13)$$

where $c_i \in \mathbb{R} \setminus \{0\}$. Without loss of generality, we may assume that $c_i = 1 \forall i \in \{1, 2, \dots, 6\}$, since, in principle, this choice does not affect the evaluation of the minimum embedding dimension. Using the seminal work of Takens for state space reconstruction [143], one can generate state trajectories of increasingly higher dimensions until the percentage of false neighbors falls to zero. Specifically, the recon-

*state space
reconstruction*

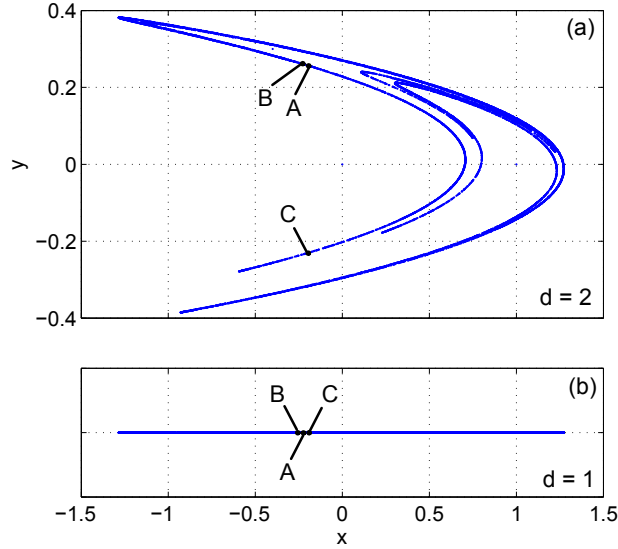


Figure 6.5: False neighbors (e.g. point C) exist when the Hénon map is observed in 1-dimensional space. System was simulated with parameters $a = 1.4$ and $b = 0.3$.

structured state space is developed in the form of multivariate vectors in d -dimensional space as follows:

$$y_s(d) = [\chi(s), \chi(s + \tau), \dots, \chi(s + (d - 1)\tau)]^T \quad (6.14)$$

$$(s = 1, 2, \dots, S - (d - 1)\tau)$$

where $y_s(d)$ represents a d -dimensional reconstructed vector generated at time s , τ is the time delay used in the reconstruction (whose choice depends on the system dynamics [144]), and S represents the length of the scalar time series data set. For example, using $d = 2$, one can generate a two-dimensional time series $y(s) = [\chi(s), \chi(s + \tau)]^T$. If the dimension of the attractor or low-dimensional manifold is $d_0 = 2$, then all reconstructed vectors of dimension $d > 2$ will ideally have no false neighbors. This is exactly what was observed when the dimension of the embedding state space was increased from $d = 1$ to $d = 2$ in the Hénon map example.

However, the method of false neighbors, as originally proposed by Kennel et al., has a few limitations in the form of heuristic choices of thresholds pertaining to what constitutes a ‘close’ neighbor. Consequently, a modification of the method of false neighbors, as proposed by Cao, is used in the following work [145].

6.4.2 Minimum embedding dimension via Cao’s methodology

Cao presented two metrics that draw inspiration from the method of false neighbors, while simultaneously avoiding its limitations [145]. Specifically, a measure of the change in distance between two neigh-

boring points, when the state space is reconstructed using a higher embedding dimension, is evaluated as follows:

$$a(s, d) = \frac{\|y_s(d+1) - y_n(d+1)\|}{\|y_s(d) - y_n(d)\|} \quad (6.15)$$

where $\|y_s(d) - y_n(d)\|$ represents the Euclidean distance between the d -dimensional reconstructed vector y_s and its neighbor y_n at time s , and $\|y_s(d+1) - y_n(d+1)\|$ represents the distance between the same points when reconstructed using a $(d+1)$ -dimensional space. The value of $a(s, d)$ is large for a specific set of false neighbors that are geometrically close in dimension d , but not in dimension $d+1$. The mean value of $a(s, d)$ over the entire time series data set is evaluated as:

$$E(d) = \frac{1}{S - d\tau} \sum_{s=1}^{S-d\tau} a(s, d) \quad (6.16)$$

Realizing that various $a(s, d)$ ceases to vary for $d \geq d_0$, where d_0 represents the minimum embedding dimension, it is observed that $E(d)$ also does not vary for dimensions beyond d_0 . Cao defines the E_1 metric is defined as follows:

$$E_1(d) = \frac{E(d+1)}{E(d)} \quad (6.17)$$

From evaluating the E_1 metric for known attractors of dynamical systems such as the Hénon map, it is observed that the metric tends to unity beyond the minimum embedding dimension d_0 . Similarly, Cao also defines an E_2 metric to distinguish between deterministic and stochastic signals. Specifically, Cao first defines E^* as follows:

$$E^*(d) = \frac{1}{S - d\tau} \sum_{s=1}^{S-d\tau} |x_{i+d\tau} - x_{n+d\tau}| \quad (6.18)$$

where $x_{n+d\tau}$ represents the last entry in the reconstructed state vector $y_n(d+1)$ which is the neighbor of the reconstructed state vector $y_s(d+1)$. The E_2 metric is then defined as follows:

$$E_2(d) = \frac{E^*(d+1)}{E^*(d)} \quad (6.19)$$

The behavior of the $E_2(d)$ metric is similar to that of the $E_1(d)$ metric, i.e. it approaches unity as $d \rightarrow d_0$, where d_0 is the minimum embedding dimension. However, the E_2 metric was primarily designed to identify the minimum embedding dimension for stochastic signals. Cao recommends using both metrics to determine the minimum embedding dimension d_0 .

The minimum embedding dimension is evaluated for the self-organized dynamics of the 3-vehicle system on a closed ring-road. [Figure 6.6](#) indicates the variation in the E_1 and E_2 metrics for reconstructed vectors $y_s(d)$ of increasingly higher dimensions. It is found

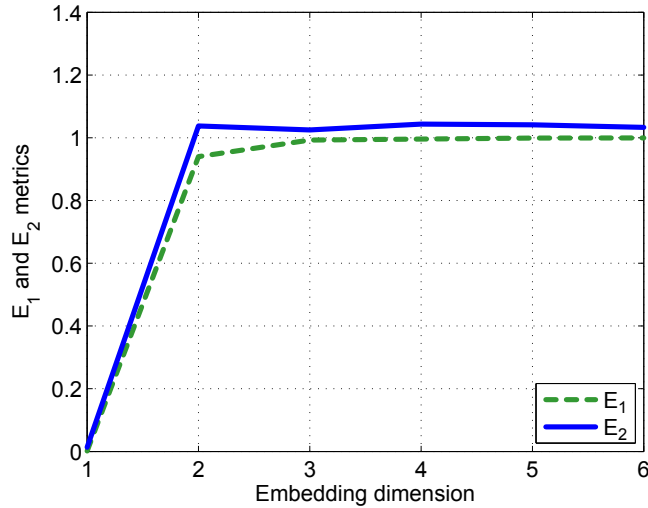


Figure 6.6: Minimum embedding dimension for the self-organized dynamics of the 3-vehicle system is found to be $d_0 = 2$. The minimum embedding dimension is determined via Cao’s method as the dimension at which E_1 and E_2 approach unity.

that both metrics approach unity at $d = 2$, which implies that the self-organized dynamics of the 3-vehicle system can be completely embedded in a low-dimensional manifold of dimension $d_0 = 2$. The next section discussed how this information can be used in the model order reduction of the linearized system (Equation 6.9).

6.5 IDENTIFICATION OF INFLUENTIAL AGENTS

As discussed earlier, the goal of this study is to identify the agents that have the ability to influence the self-organized dynamics of the multi-agent system. In Section 6.3, we discussed a scheme for evaluating agent influence for the full-order linearized system. Since the self-organized dynamics evolve on a low-dimensional manifold, the logical next step is to reduce the full-order linearized system and identify the agent influence in the reduced-order model. The minimum embedding dimension determined in the previous section indicates that the state vector of the reduced-order model should have a dimension $d_0 = 2$.

6.5.1 Model order reduction via Krylov subspaces

Over the years, several methods have been proposed for the model order reduction of large-scale linear and nonlinear systems, such as balanced truncation and Krylov subspace-based methods, to name a few [146]. Balanced truncation reduces the model order by retaining only the controllable and observable states of the system. While this approach is beneficial in many scenarios, we do not know *a priori* if the controllable states will generate a reduced-order model whose

dynamics evolve on the desired low-dimensional manifold. In other words, the relationship between self-organization and controllability is currently unknown and remains an open problem for the research community.

On the other hand, the analytical structure provided by Krylov subspace-based methods can leverage some topological information to obtain a local approximation of the low-dimensional manifold and a reduced-order linearized model. A d -dimensional Krylov subspace for a system such as in Equation 6.9 is defined as follows:

Krylov subspace

$$\mathcal{K}_d(A, b_0) = \text{span}\{b_0, Ab_0, \dots, A^{d-1}b_0\} \quad (6.20)$$

where $A \in \mathbb{R}^{N \times N}$ represents the system matrix of the multi-agent system linearized about the current operating point x_0 , and $b_0 \in \mathbb{R}^{N \times 1}$ represents a *starting vector* used to generate the Krylov subspace [147][148]. The choice of the starting vector is critical in generating a reduced-order model that accurately depicts the system dynamics. Ideally, the starting vector should lie in the invariant subspace in which the dynamics evolve, so that the Krylov subspace can capture the system behavior. Typically, this information is not available, but the current context presents insights which can guide the selection of the starting vector. Specifically, the tangent to the steady-state system trajectory is expected to lie in the local low-dimensional manifold of the system equations. This tangent vector, defined as:

starting vector

$$b_0 = \left[\frac{\partial f^{(1)}}{\partial x_n}, \frac{\partial f^{(1)}}{\partial \dot{x}_n}, \frac{\partial f^{(2)}}{\partial x_n}, \frac{\partial f^{(2)}}{\partial \dot{x}_n}, \frac{\partial f^{(3)}}{\partial x_n}, \frac{\partial f^{(3)}}{\partial \dot{x}_n} \right]^T \quad (6.21)$$

can be evaluated at each time instant t at the current operating point x_0 on the system trajectory. The tangent vector can then serve as the starting vector of the Krylov subspace for model order reduction at each time instant as we traverse over the system trajectory.

An orthonormal basis of the Krylov subspace $\mathcal{K}_d(A, b_0)$ may be used as a projection operator $U = [u_1, u_2, \dots, u_d]$ ($u_i \in \mathbb{R}^N$) to project the dynamics of the full-order system onto the local low-dimensional manifold. In the current context, since the minimum embedding dimension is $d_0 = 2$, the associated projection operator $U \in \mathbb{R}^{6 \times 2}$ obtained by Arnoldi's process is given by:

$$U = \begin{bmatrix} b_0 & b_1 \\ \frac{1}{\|b_0\|} & \frac{1}{\|b_1\|} \end{bmatrix} \quad (6.22)$$

$$\text{with } b_1 = Ab_0 - \frac{\langle b_0, Ab_0 \rangle}{\langle b_0, b_0 \rangle} b_0 \quad (6.23)$$

where $\langle \cdot, \cdot \rangle$ denotes the inner product. The next subsection discusses how this information may be used to identify agents that can influence the self-organized dynamics of the 3-vehicle system.

6.5.2 Influential agents in 3-vehicle system

The reduced-order model of the system described in Equation 6.9 may be obtained through the operations $A_r = U^T A U$ and $B_r = U^T B_i$, so that the reduced-order linearized system equations are:

$$\dot{\psi} = A_r \psi + B_r u \quad (6.24)$$

where ψ represents a low-order state such that $x = U\psi$, and $B_i \in \{B_1, B_2, B_3\}$ depending on the agent i whose influence on the self-organizing dynamics is being assessed. The minimum singular value is evaluated at the current operating point x_0 over the system trajectory for the three different augmented matrices $[sI - A_r, U^T B_1]$, $[sI - A_r, U^T B_2]$, and $[sI - A_r, U^T B_3]$, corresponding to control inputs provided only by vehicle 1, vehicle 2, or vehicle 3, respectively. Figure 6.7 describes the state trajectories as well as the trends in the minimum singular value for each system configuration. The linearized reduced-order system that has the largest minimum singular value helps identify the agent that exerts the most influence on the macroscopic dynamics at a particular instant of time.

Analysis of Figure 6.7 yields some interesting insights that agree strongly with intuition about the 3-vehicle system, and about self-organized traffic jams in general. For example, it is observed that vehicles with large spacings, which represent vehicles in free flow, do not have significant influence on the self-organized dynamics. Additionally, it is also observed that vehicles that are about to enter a cluster (i.e. vehicles whose spacing is decreasing with time), have significant influence over the self-organized dynamics. These results indicate a strong spatial dependence of agent influence and agree with intuition as well as similar results from previous related research on connected vehicles [116].

6.6 CONCLUSIONS, CONTRIBUTIONS AND BROADER IMPACTS

In this chapter, a methodology for assessing the influence of specific agents on the self-organized dynamics of a large-scale multi-agent system was proposed. The methodology made use of existing knowledge of controllability metrics and model order reduction, and coupled it with the novel application of the minimum embedding dimension to identify agent influence on self-organized dynamics. Approaching the problem from a topological perspective also provided a solution to the selection of an appropriate starting vector for the Krylov subspace-based model order reduction process.

The methodology presented here is general enough to be applied to any self-organizing system. The technique was applied to a known prototypical problem of self-organizing multi-agent systems, i.e. the self-organized vehicle cluster formation on closed ring roads. The ob-

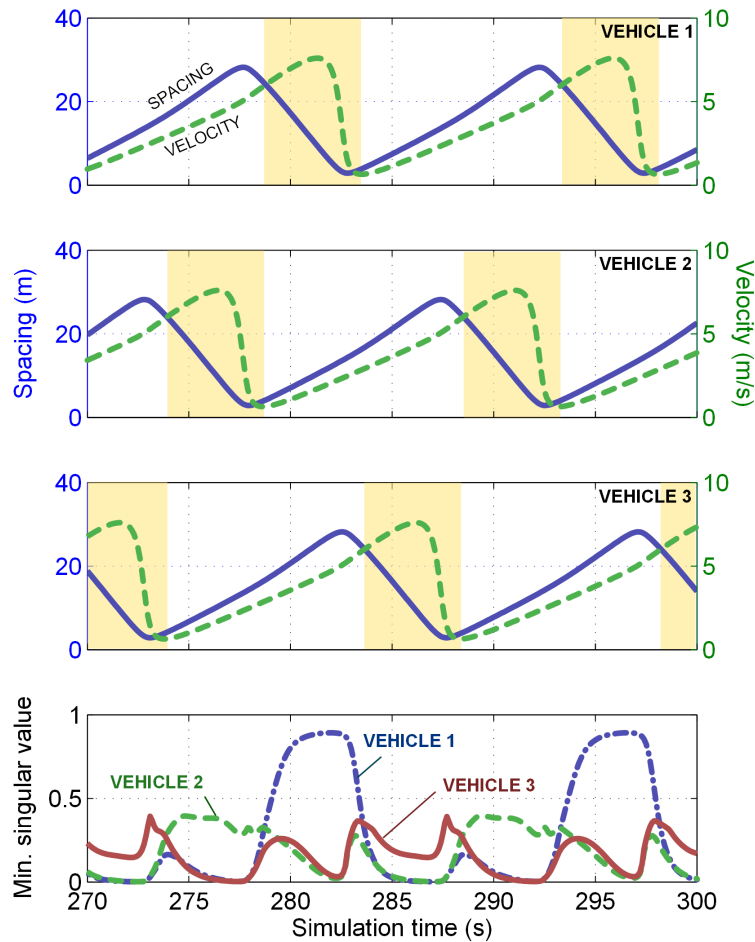


Figure 6.7: State trajectories for the 3-vehicle system. For configurations where different vehicles are designated as controllers, the minimum singular values help identify influential agents. Shaded yellow regions indicate the spatial locations where a particular agent (or vehicle) has the most local influence on the self-organized dynamics of the system.

tained results which identify the most influential agents at any instance of time were found to agree with intuition as well as related previous studies. Specifically, it was found that vehicles in free flow have little influence on the self-organized dynamics, whereas vehicles approaching a cluster are quite influential in this regard. The generality of the proposed approach hopes to propel further research directed towards assessing the role of agent influence in guiding self-organizing behavior.

FUTURE DIRECTIONS

In this final chapter, the approaches presented in [Chapter 3](#) through [Chapter 6](#) are summarized and their key insights are outlined. This chapter also contains details about some unsuccessful, but potential avenues for research, as well as some advice for new researchers in this field. This advice is a result of lessons learnt the hard way, so the author hopes that the researchers who follow find it useful. Finally, this chapter also includes some short-term and long-term potential directions on future work.

7.1 SUMMARY OF WORK

In this dissertation, the problem of influence in self-organizing systems was handled from two fundamentally different approaches, though each used self-organizing traffic jams as the underlying example. In the first approach, encapsulated in [Part I](#), the goal of influencing self-organized behavior of the large-scale MAS, i.e. the traffic jams, was achieved by modifying the natural agent population by introducing artificially engineered agents, i.e. cruise controlled vehicles, into the mix. As the proportion of the cruise controlled vehicles in traffic increased, the self-organizing behavior was affected. Realizing that such an approach does not result in a satisfactory control technique (it is infeasible to control population demographics of large-scale MAS), the same goal was approached from a different perspective in [Part II](#). In [Part II](#), a novel concept of influential subspaces was introduced, which essentially described the spatial dependence of an agent's influence on self-organizing dynamics of a large-scale MAS. This idea was discussed in the context of both, connected vehicles and adaptive cruise controlled (ACC) vehicles, and it was found to be a valid technique to control the self-organized dynamics of vehicular cluster formation. The key insights from this work are presented in the following subsection.

7.1.1 *Key insights*

The key insights obtained from the works discussed in the previous chapters are discussed in this subsection. The reader is requested to take note that the use of the terminology 'ACC' and 'human' is meant to distinguish between good and bad driving behavior, respectively. Specifically, the 'ACC' algorithms used in this work are not fully representative of the current state-of-the-art cruise control algorithms,

but have been modeled to represent our understanding of what good driving or car-following behavior should look like.

At low densities, increased ACC penetration results in higher traffic flows without self-organizing traffic jams

The study has shown that as the percentage of ACC-enabled vehicles in the traffic system is increased the critical density also increases correspondingly. The increase in critical density implies that the density at which vehicle clusters begin to appear is increased. This indicates that the traffic flow can operate at higher densities and consequently higher flow rates, since it is known from the fundamental diagram of traffic flow that, in the free flow regime, the flow increases as the density increases [74].

At low densities, increased ACC penetration results in the traffic system being more susceptible to formation of self-organizing traffic jams

While increased ACC penetration may allow the traffic system to operate at increased densities and flows, it comes at a cost. As ACC penetration increases, a small percentage of drivers with low sensitivities are enough to cause a self-organized traffic jam. In other words, in a predominantly ACC traffic system, introduction of a small percentage of human drivers may cause a rapid reduction of critical density, resulting in a self-organized traffic jam [114].

At moderate densities, higher ACC penetration may complicate traffic control and highway design processes

Numerical simulations indicate that a randomly selected vehicle is more likely to be stuck in a moderately-sized cluster given a predominantly ACC-enabled traffic system, while it is more likely to be stuck in a large-sized cluster given a predominantly human-driven traffic system. These insights hold significance for traffic control engineers, as it is easier to design and handle highway elements to counter large localized bottlenecks rather than moderately-sized clusters that may appear at random across a large swathe of highway [116].

At moderate densities, higher ACC penetration may adversely impact the environment and traffic safety

Numerical simulations indicate the formation of several moderately-sized clusters for higher ACC penetration. Such cluster formation may lead to an increase in acceleration and deceleration cycles as vehicles frequently enter and exit several clusters. Consequently, emissions may rise and the propensity for collisions, especially from human

drivers, may increase. However, a detailed study of these effects has not yet been performed [116].

Influential subspaces of connected vehicles can help improve bandwidth utilization and guide policy decision making

Knowledge of the influential subspace of connected vehicles can significantly improve connected vehicles technology. Bandwidth limitations can be overcome by transmitting information to only those vehicles that are currently in their influential subspace. Moreover, future policy decisions on connected vehicles technology, such as setting dynamic speed limits and message hopping requirements, could be guided by knowledge of the influential subspaces [149].

Vehicles entering a cluster have more influence on the self-organized dynamics of cluster formation than vehicles exiting it

A methodology to assess the spatial dependence of agent influence on the self-organized dynamics of large-scale multi-agent systems was developed that leveraged the presence of a low-dimensional manifold in these dynamics. The results indicate that the most influential agent in the system at a given time is usually the vehicle that is about to enter the cluster [150].

7.1.2 *Unsuccessful avenues and some general advice to new researchers in this field*

This subsection is devoted to describing some of the alternative research routes undertaken during the course of this dissertation and the lessons learnt from them. These routes cover various research approaches that did not yield successful results, but some of them hold significant potential and can be used to develop a comprehensive theory of influence and self-organizing systems. These few are also mentioned in the long-term potential future directions in [Section 7.2](#). While some of the issues discussed here may be a reflection of personal characteristics, I nevertheless believe that researchers following up on this research should be aware of them.

Some existing literature on emergence should be taken with a grain of salt

The notion of emergence is *extremely* ill-defined in the literature. While this situation raises several interesting questions – How does one define emergence? What are some potential metrics for emergence? Can emergence be compared across two different systems? Are self-organization and emergence related? – there are very few existing research works to build upon. Further, while several researchers have valiantly attempted to formalize the notion of emergence, and perhaps a larger number have attempted to approach it from a philo-

sophical viewpoint, in my opinion it is better to focus on the notion of self-organization, rather than get stuck in the quagmire of studying emergence. Self-organization itself is an equally challenging topic, but at least the literature documents various scientific attempts to define and measure it in different fields, including in information theory and differential geometry.

Strong mathematical background is critical to pursue research in the field of self-organizing systems

To be forewarned is to be forearmed. It should not be surprising to know that understanding self-organization will not only require knowledge of diverse mathematical concepts, it will also require in-depth knowledge of these concepts. While there isn't any need to be alarmed or disheartened, a new researcher in the field should remember to keep all research avenues open, and be on the constant lookout for any methodology that brings one closer to the answer. During my dissertation, I have had to read texts on differential geometry, statistical mechanics, dynamical systems, information theory, and model order reduction, to name a few. While the usefulness and relationships between these fields may not be immediately relevant, over the years they will hopefully help build connections and yield interesting results. A strong mathematical background or the willingness to learn diverse mathematical tools is essential for tackling problems in the domain of self-organization.

Know the scope of your problem and remain focused

Self-organization is a harsh mistress – it entices you in different directions. A new researcher in this field should realize that a good problem is one that can be solved within a reasonable amount of time. A new researcher should have a good idea of the scope of the problem and remain focused on it. From my personal experience, I have run off on tangents to the work, such as when examining causality and its implications for the phenomenon of self-organization – Are agents the cause of ensemble dynamics, or is the ensemble causing the agents to move in a specific fashion? (see [Figure 5.1](#)) – and this behavior is counterproductive to the timely solution of a problem. That said, occasional bouts of day-dreaming can be helpful to arrive at out-of-the-box questions (and answers)!

7.2 POTENTIAL FUTURE DIRECTIONS

The methodologies and insights contained in this dissertation represent an evolving body of work. As such, they are several open research avenues that can be pursued. Several of the research avenues

presented in this section are short-term in nature, while others would require a longer engagement.

7.2.1 *Short-term future work*

Some of the potential short-term future work includes:

Comparison of results obtained from master equation and statistical mechanics-inspired approaches

The master equation approach presented in [Chapter 3](#) yields a relationship between the ACC penetration rate and the critical density. The numerical simulations performed in [Chapter 4](#) using the statistical mechanics-inspired traffic flow model for mixed species were used to determine the cluster distributions. As potential short-term future work, the data from these simulations could also be used to obtain a relationship between the ACC penetration and critical density, and comparison with the master equation approach could make a more compelling case for these models.

Numerical evaluation of influential subspaces of connected vehicles

The numerical simulation framework in [Chapter 4](#) can be modified to model cooperative cruise controlled vehicles. The simulations can also make use of Newell's simplified car-following model with additional stochastic disturbances in the model dynamics. The simulations can be performed for simple scenarios such as those discussed in [Chapter 5](#), and the numerical results can be compared against the analytical solutions obtained for the event and null horizons.

Influential subspaces in 3-vehicle system with bounded control inputs

The astute reader may have noticed the absence of an event horizon in [Figure 6.7](#). While the analysis in this figure does not directly correspond to the work performed in [Chapter 5](#), there is a general expectation that similar elements will reappear. Thus, the absence of the event horizon in this figure demands further inspection. The next steps in this scenario may be to bound the control inputs on the acceleration and deceleration parameters and observe if an element similar to the event horizon appears. Since the concept of controllability cannot directly handle bounded inputs, additional work related to problem may be long-term in nature (see [Section 7.2.2](#)).

Comparison of alternative measures of controllability in 3-vehicle system

The analysis presented in [Chapter 6](#) utilized a locally linearized model of the 3-vehicle system and evaluated agent influence using Eising's measure of controllability. Alternative measures of controllability, also

presented in the chapter, may be utilized to repeat the analysis and results can be compared across these different measures.

7.2.2 Long-term future work

Some potential long-term future work includes:

Nonlinear model order reduction of 3-vehicle system

The 3-vehicle system analyzed in [Chapter 6](#) helped determine the spatial dependence of agent influence on self-organizing dynamics. However, the presented analysis utilized a locally linearized system to evaluate a measure of system controllability. For developing this methodology into a more comprehensive one for self-organized systems, alternative nonlinear model reduction techniques may be evaluated. These approaches may have to draw from differential geometry to directly obtain the invariant manifold on which the self-organized dynamics reside (e.g. see the works of [Ginoux and Rosseto](#) on invariant manifolds of complex systems [151], or the works of [Sarlette and Sepulchre](#) on consensus optimization on manifolds [152]).

Influential subspaces of connected vehicles in complicated scenarios

The work presented in [Chapter 5](#) simplified the analysis by considering a single lane highway where no passing was allowed, and with only two connected vehicles in the traffic stream. The concept of the influential subspace of a connected vehicle can be expanded to include additional scenarios, such as (a) several connected vehicles on the highway, (b) highways where vehicle passing is allowed, and (c) the presence of on- and off-ramps.

Analytical approach to solve for influential subspaces

The work presented in [Chapter 5](#) makes use of specific control policies in a limited scenario to obtain analytical results for the influential subspaces of connected vehicles. These results are too restrictive, and if the concept of influential subspaces is to succeed, it must be generalized further to be applicable for arbitrary control policies. In this regard, future work could focus on polyhedra-based approaches to determine controllable sets as suggested by [Lasserre](#) and extend the results presented therein to influential subspaces [55]. Alternative approaches, such as the use of mutual information-based Lyapunov functions, may also be potential candidates to achieve this objective.

Additional application domains

The beauty of the concept of the influential subspace is that it is domain-agnostic. Several complex systems exhibit self-organizing be-

havior for which it may be possible to identify event horizons and influential subspaces of ‘smart’ agents. Some applications include control of seizures in the human brain through the use of neural implants, and the control of cascading failures to prevent widespread blackouts. These applications an benefit from an understanding of the influential subspaces of each individual agent that comprises the large-scale multi-agent system.

Measures of self-organization

While self-organized dynamics of traffic systems have been a focus of this study, there remain several unanswered questions as to what constitutes self-organization. When can a system be said to be self-organized? Several researchers, such as [Van Dyke Parunak and Brueckner](#), have proposed entropy-based measures for self-organization, these metrics have not yet been fully developed [153]. Information-theoretic measures such as delayed mutual information may be utilized to develop a measure of self-organization [154]. Future work can also leverage the apparent relationship between controllability and self-organized dynamics as indicated in [Chapter 6](#) to develop a measure of self-organization.

THE ONE-DIMENSIONAL ISING MODEL WITH NEAREST-NEIGHBOR INTERACTIONS

Ernst Ising presented a particle interaction model for ferromagnetism in his Ph.D. thesis in 1925, and this model has since come to be known by his name [31]. In this work, Ising modeled a one-dimensional ferromagnet as an infinitely long chain of ‘magnets’, where each site represented a magnetic dipole moment generated by the atomic spin. If the atomic spins are aligned, the magnetic moments add up, resulting in the magnetic nature of a ferromagnetic material. On the other hand, if the spins are not aligned, such as at high temperatures, the magnetic nature is lost. The phase transition between these two behaviors of a ferromagnetic material occurs at the Curie temperature. The goal of Ising’s thesis was to study if the interaction between neighboring spins was the underlying mechanism for such behavior of ferromagnetic materials.

A.1 MODEL DESCRIPTION

In this model, atomic spins are denoted by σ . The atomic spins can be in one of two states, i.e. $\sigma \in \{-1, +1\}$. The actual values of the spins do not hold any physical significance, except for the fact that they simplify some of the following analysis. Specifically, if two adjacent atomic spins are aligned in the same direction, they could be modeled as either $\{-1, -1\}$ or $\{+1, +1\}$, with no change in the ensuing analysis. Similarly, if two adjacent spins are not aligned, they could either be represented by $\{-1, +1\}$ or $\{+1, -1\}$. Now, the state of the magnet is collectively represented by the atomic spins at each site of the one-dimensional infinitely long chain of magnets as $\sigma = \{\sigma_1, \sigma_2, \dots, \sigma_N\}$, which is known as the system *microstate*. The energy associated with the microstate σ for a one-dimensional Ising model with only nearest-neighbor interactions is given by the Hamiltonian:

$$H(\sigma) = -B \sum_{i=1}^N \sigma_i - \sum_{\langle i,j \rangle} J_{ij} \sigma_i \sigma_j \quad (\text{A.1})$$

where B represents an external field, $\langle i, j \rangle$ represents a nearest-neighbor site pairs, and $J_{ij} = J_{ji}$ denotes the interaction strength between sites i and j . The interaction strength is assumed to be constant, i.e. $J_{ij} = J$. In order to further simplify analysis, the one-dimensional model is assumed to have periodic boundary conditions, so that $\sigma_{N+1} = \sigma_1$. While this assumption does not affect the thermodynamic properties

of the infinitely-long chain, it does allow a symmetric representation of the Hamiltonian as follows:

$$H(\sigma) = -\frac{B}{2} \sum_{i=1}^N (\sigma_i + \sigma_{i+1}) - J \sum_{i=1}^N \sigma_i \sigma_j \quad (\text{A.2})$$

A.2 PARTITION FUNCTION

The partition function plays a very important role in the field of statistical mechanics and can be used to determine the aggregate properties of a system. It derives its name from the fact that it encodes the probability distribution that partitions microstates into ‘bins’ of equal energy. Specifically, the probability of occurrence of a particular microstate σ is given by:

$$P(\sigma) = \frac{1}{Z} e^{-\beta H(\sigma)} \quad (\text{A.3})$$

where Z denotes the partition function and acts as a normalizing constant, $\beta = 1/k_B T$, k_B denotes the Boltzmann constant, and T denotes the temperature. The partition function Z is thus defined as:

$$Z = \sum_{\sigma_1=-1}^{\sigma_1=+1} \sum_{\sigma_2=-1}^{\sigma_2=+1} \dots \sum_{\sigma_N=-1}^{\sigma_N=+1} e^{-\beta H(\sigma)} \quad (\text{A.4})$$

which can be written as:

$$Z = \sum_{\sigma_1=-1}^{\sigma_1=+1} \dots \sum_{\sigma_N=-1}^{\sigma_N=+1} \exp \left\{ \beta \sum_{i=1}^N \left(\frac{B}{2} (\sigma_i + \sigma_{i+1}) + J \sigma_i \sigma_j \right) \right\} \quad (\text{A.5})$$

A.3 TRANSFER MATRIX

In order to evaluate the partition function, Kramers and Wannier suggested the use of transfer matrices [31, pp. 476]. The right-hand side of (A.5) can be expressed as a product of 2×2 matrices as explained below. Consider a situation with only two adjacent sites σ_i and σ_{i+1} . Then, in accordance with (A.2), the Hamiltonian $H(\sigma)$ yields:

$$e^{-\beta H(\sigma)} = \begin{cases} e^{\beta(B+J)}, & \sigma_i = +1, \sigma_{i+1} = +1 \\ e^{\beta(-B+J)}, & \sigma_i = -1, \sigma_{i+1} = -1 \\ e^{-\beta J}, & \text{otherwise} \end{cases} \quad (\text{A.6})$$

Now, consider a vector representation of the spins, such that the spins $+1$ and -1 can be written as $q_1 = [1 \ 0]$ and $q_2 = [0 \ 1]$, respectively. If the transfer matrix P is given by:

$$P = \begin{bmatrix} e^{\beta(B+J)} & e^{-\beta J} \\ e^{-\beta J} & e^{\beta(-B+J)} \end{bmatrix} \quad (\text{A.7})$$

the operation $(\sigma_i P \sigma_{i+1})$ yields the same results as in (A.6), i.e.

$$(\sigma_i P \sigma_{i+1}) = \begin{cases} e^{\beta(B+J)}, & \sigma_i = q_1, \sigma_{i+1} = q_1^T \\ e^{\beta(-B+J)}, & \sigma_i = q_2, \sigma_{i+1} = q_2^T \\ e^{-\beta J}, & \text{otherwise} \end{cases} \quad (\text{A.8})$$

A.4 SOLUTION OF THE PARTITION FUNCTION

Using the transfer matrix representation, the partition function can be re-written as:

$$\begin{aligned} Z &= \sum_{\sigma_1=-1}^{\sigma_1=+1} \cdots \sum_{\sigma_N=-1}^{\sigma_N=+1} (\sigma_1 P \sigma_2) (\sigma_2 P \sigma_3) \cdots (\sigma_N P \sigma_1) \\ &= \sum_{\sigma_1=-1}^{\sigma_1=+1} (\sigma_1 P^N \sigma_1) \\ &= \text{Tr}(P^N) \\ &= \lambda_a^N + \lambda_b^N \end{aligned} \quad (\text{A.9})$$

where λ_a and $\lambda_b (< \lambda_a)$ represent the eigenvalues of P . In the absence of an external field (i.e. $B = 0$), the eigenvalues can be found to be:

$$\lambda_a = 2 \cosh(\beta J) \quad (\text{A.10})$$

$$\lambda_b = 2 \sinh(\beta J) \quad (\text{A.11})$$

which yield a solution of the partition function. With knowledge of the partition function, several other statistics (e.g., free energy and magnetization per spin) can be evaluated along with their trends as a function of inverse temperature β .

American Association of State Highway and Transportation Officials
(AASHTO), 47, 56

complex system, 1

congestion costs, 3, 4

controllability

controllability Gramian, 27

controllable set, 15

local controllability, 113

measures of, 110

cruise control algorithms

constant time headway, 34

driver sensitivity, 47, 56

General Motors' model, 34, 46

intelligent driver model, 34, 112

detailed balance, 74

event horizon, 90, 99, 128

exchange dynamics, 73

far-from-equilibrium systems, 74

graph

adjacency matrix, 23

degree matrix, 22

directed graph, 22

Hénon map, 117

Hamiltonian, 68

influence

agent selection, 21

influential subspace, 20, 86, 89

subspace selection, 2, 14

Ising model, 13

Krylov subspace, 121

starting vector, 121

macrostate, 1, 9

manipulability, 27
master equation, 44
mean-field approximation, 11, 45

networked systems, 21
 consensus dynamics, 21
 graph Laplacian, 22
 topology, 22
null horizon, 89, 99

phantom jams, 41, 60
pinning control, 21, 24

self-organization, 1, 8
 traffic jams, 3, 37
space partition, 66
spin flip dynamics, 73
state space reconstruction, 117
synchronization, 10
 complete, 11
 generalized, 12
 lag, 12
 phase, 11
system microstate, 67

vehicle cluster distribution, 80

BIBLIOGRAPHY

- [1] D L Schrank and T J Tomax. The 2007 Urban Mobility Report. Technical report, Texas Transportation Institute, 2007.
- [2] R. Olfati-Saber, J.A. Fax, and R.M. Murray. Consensus and cooperation in networked multi-agent systems. *Proceedings of the IEEE*, 95(1):215–233, Jan 2007. ISSN 0018-9219. doi: 10.1109/JPROC.2006.887293.
- [3] B. D. Greenshields, J. R. Bibbins, W. S. Channing, and H. H. Miller. A study of traffic capacity. *Highway Research Board Proceedings*, 14:448–477, 1935.
- [4] I. Prigogine and F.C. Andrews. A Boltzmann-like approach for traffic flow. *Operations Research*, 8(6):789–797, 1960.
- [5] Y. Sugiyama, M. Fukui, M. Kikuchi, K. Hasebe, A. Nakayama, K. Nishinari, S. Tadaki, and S. Yukawa. Traffic jams without bottlenecks - experimental evidence for the physical mechanism of the formation of a jam. *New Journal of Physics*, 10, 2008.
- [6] B. S. Kerner and H. Rehborn. Experimental features and characteristics of traffic jams. *Phys. Rev. E*, 53:R1297–R1300, Feb 1996. doi: 10.1103/PhysRevE.53.R1297.
- [7] R. Mahnke, J. Kaupužs, and I. Lubashevsky. *Physics Reports*, volume 408, chapter Probabilistic description of traffic flow, pages 1–130. Mar 2005.
- [8] C. N. Viswanathan, R. W. Longman, and P. W. Likins. A degree of controllability definition - Fundamental concepts and application to modal systems. *Journal of Guidance, Control, and Dynamics*, 7(2):222–230, 1984.
- [9] D. Sornette. *Why Stock Markets Crash: Critical Events in Complex Financial Systems*. Princeton University Press, 2009. ISBN 9781400829552.
- [10] J.A.S. Kelso. *Dynamic Patterns: The Self-organization of Brain and Behavior*. A Bradford book. MIT Press, 1997. ISBN 9780262611312.
- [11] Réka Albert and Albert-László Barabási. Statistical mechanics of complex networks. *Reviews of modern physics*, 74(1):47, 2002.
- [12] H. Haken. *Information and Self-Organization: A Macroscopic Approach to Complex Systems*. Springer Series in Synergetics. Springer, 2006. ISBN 9783540330233.

- [13] K Nagel and M Schreckenberg. A cellular automaton model for freeway traffic. *Journal de Physique I*, 2(12), 1992.
- [14] FHWA. Our nation's highways 2008. Technical report, E.S. DoT, Washington D.C., 2008.
- [15] David Schrank, Bill Eisele, and Tim Lomax. *Proceedings of the 2012 annual urban mobility report. Texas A&M Transportation Institute, Texas, USA*, chapter TTI's 2012 urban mobility report. 2012.
- [16] AC Antoulas, DC Sorensen, and S Gugercin. A survey of model reduction methods for large-scale systems. *Contemporary mathematics*, 280:193–220, 2001.
- [17] Wilhelmus HA Schilders, Henk A Van der Vorst, and Joost Rommes. *Model order reduction: theory, research aspects and applications*, volume 13. Springer, 2008.
- [18] PJ Schweitzer. State aggregation in finite markov chains. *IBM Report RC*, 6200:26635, 1976.
- [19] Zhiyuan Ren and Bruce H Krogh. State aggregation in Markov decision processes. In *Decision and Control, 2002, Proceedings of the 41st IEEE Conference on*, volume 4, pages 3819–3824. IEEE, 2002.
- [20] Xi-Ren Cao, Zhiyuan Ren, Shalabh Bhatnagar, Michael Fu, and Steven Marcus. A time aggregation approach to Markov decision processes. *Automatica*, 38(6):929 – 943, 2002.
- [21] Cosma Rohilla Shalizi and Cristopher Moore. What is a macrostate? Subjective observations and objective dynamics. *arXiv preprint cond-mat/0303625*, 2003.
- [22] P. Adenis, K. Mukherjee, and A. Ray. State splitting and state merging in probabilistic finite state automata. In *American Control Conference (ACC), 2011*, pages 5145–5150, June 2011.
- [23] N. Wiener. *Nonlinear Problems in Random Theory*. The MIT Press, 1958.
- [24] A. T. Winfree. Biological rhythms and the behavior of populations of coupled oscillators. *Journal of Theoretical Biology*, 16: 15–42, 1967.
- [25] Steven H. Strogatz. From kuramoto to crawford: exploring the onset of synchronization in populations of coupled oscillators. *Physica D: Nonlinear Phenomena*, 143(1-4):1–20, 2000. ISSN 01672789. doi: 10.1016/S0167-2789(00)00094-4.

- [26] Y. Kuramoto. *Lecture Notes in Physics*, volume 39, chapter Self-entrainment of a population of coupled non-linear oscillators. Springer, 1975.
- [27] M. G. Rosenblum, A. S. Pikovsky, and J. Kurths. From phase to lag synchronization in coupled chaotic oscillators. *Physical Review Letters*, 78:4193–4196, 1997.
- [28] Nikolai F. Rulkov, Mikhail M. Sushchik, Lev S. Tsimring, and Henry DI Abarbanel. Generalized synchronization of chaos in directionally coupled chaotic systems. *Physical Review E*, 51(2): 980, 1995.
- [29] V. Afraimovich, A. Cordonet, and N. F. Rulkov. Generalized synchronization of chaos in noninvertible maps. *Physical review. E, Statistical, nonlinear, and soft matter physics*, 66(1 Pt 2):016208, Jul 2002.
- [30] I. Z. Kiss, C. G. Rusin, H. Kori, and J. L. Hudson. Engineering complex dynamical structures: sequential patterns and desynchronization. *Science*, 316, 2007.
- [31] R. K. Pathria. *Statistical Mechanics*. Elsevier Science, 3 edition, 2011. ISBN 9780123821898.
- [32] Audun Bakk and Johan S. Høye. One-dimensional ising model applied to protein folding. *Physica A: Statistical Mechanics and its Applications*, 323:504–518, 2003. ISSN 0378-4371.
- [33] Yasser Roudi, Joanna Tyrcha, and John Hertz. Ising model for neural data: Model quality and approximate methods for extracting functional connectivity. *Physical Review E*, 79(5), 2009.
- [34] W-X Zhou and D Sornette. Self-organizing Ising model of financial markets. *The European Physical Journal B - Condensed Matter and Complex Systems*, 55(2):175–181, 2007.
- [35] Ernst Ising. Beitrag zur theorie des ferromagnetismus. *Z. Physik*, 31(1):253–258, 1925. ISSN 00443328. doi: 10.1007/BF02980577. URL http://www.hs-augsburg.de/~harsch/anglica/Chronology/e_saec20.html. English translation by Jane Ising and Tom Cummings.
- [36] Roy Glauber. Time dependent statistics of the Ising model. *Journal of Mathematical Physics*, 4(2), 1963.
- [37] K. G. Wilson. Problems in physics with many scales of length. *Scientific American*, 241:158–179, 1979.
- [38] R. Mahnke and J. Kaupužs. Probabilistic description of traffic flow. *Networks and Spatial Economics*, 1(1-2):103–136, Mar 2001.

- [39] Alexandros Sopsakis. Stochastic noise approach to traffic flow modeling. *Physica A*, 342(3-4), 2004.
- [40] M. Mesbahi and M. Egerstedt. *Graph Theoretic Methods in Multiagent Networks*. Princeton Series in Applied Mathematics. Princeton University Press, 2010. ISBN 9781400835355.
- [41] Rudolf Emil Kalman. Contributions to the theory of optimal control. *Bol. Soc. Mat. Mexicana*, 5(2):102–119, 1960.
- [42] Héctor J. Sussmann and Velimir Jurdjevic. *Journal of Differential Equations*, volume 12, chapter Controllability of nonlinear systems, pages 95–116. Jul 1972.
- [43] Y. Yamamoto. Controllability of nonlinear systems. *J Optim Theory Appl*, 22(1):41–49, May 1977.
- [44] Tingshu Hu, Daniel E. Miller, and Li Qiu. Null controllable region of lti discrete-time systems with input saturation. *Automatica*, 38(11):2009–2013, Nov 2002.
- [45] I. L. Vincent, E.M. Cliff, W. J. Grantham, and W.Y. Peng. *AIAA Journal*, volume 12, chapter Some Aspects of Collision Avoidance, pages 3–4. American Institute of Aeronautics and Astronautics, Jan 1974.
- [46] J. M. Skowronski and T. L. Vincent. volume 36 of *J Optim Theory Appl*, chapter Playability with and without capture, pages 111–128. Kluwer Academic Publishers-Plenum Publishers, Jan 1982.
- [47] J.E. Gayek. A survey of techniques for approximating reachable and controllable sets. In *Decision and Control, 1991., Proceedings of the 30th IEEE Conference on*, volume 2, pages 1724–1729, Dec 1991.
- [48] W. J. Grantham and T. L. Vincent. volume 17 of *J Optim Theory Appl*, chapter A controllability minimum principle, pages 93–114. Kluwer Academic Publishers-Plenum Publishers, Oct 1975. doi: 10.1007/BF00933917.
- [49] Thomas L. Vincent and Zong Y. Wu. *Journal of Guidance, Control, and Dynamics*, volume 13, chapter Estimating projections of the controllable set, pages 572–575. American Institute of Aeronautics and Astronautics, May 1990. doi: 10.2514/3.25372.
- [50] Zong Yeng Wu. *Estimating projected controllable sets for dynamical control systems*. PhD thesis, 1988.
- [51] Walter J. Grantham. volume 40 of *Lecture Notes in Biomathematics*, chapter Estimating Controllability Boundaries for Uncertain Systems, pages 151–162. Springer Berlin Heidelberg, Jan 1981. ISBN 978-3-540-10566-4. doi: 10.1007/978-3-642-46436-2_11.

- [52] W. J. Grantham. *Journal of Dynamic Systems, Measurement, and Control*, volume 103, chapter Estimating reachable sets, pages 420–422. American Society of Mechanical Engineers, 1981.
- [53] Hassan K. Khalil. Prentice Hall, 2002.
- [54] Danny Summers. Lyapunov approximation of reachable sets for uncertain linear systems. *International Journal of Control*, 41: 1235–1243, May 1985.
- [55] J. B. Lasserre. *Journal of optimization theory and applications*, volume 70, chapter Reachable and controllable sets for two-dimensional, linear, discrete-time systems, pages 583–595. Springer, 1991.
- [56] P. d’Alessandro and E. De Santis. *Automatica*. 28(1):227–229, Jan 1992.
- [57] K. B. Lim. Method for optimal actuator and sensor placement for large flexible structures. *Journal of Guidance, Control, and Dynamics*, 15(1):49–57, 1992.
- [58] W. Gawronski. *Journal of Sound and Vibration*, volume 208, chapter Actuator and sensor placement for structural testing and control, pages 101–109. Elsevier, 1997.
- [59] A. Isner and M. Noton. *International Journal of Control*, volume 18, chapter Approximations to optimal control by means of influential subspaces†, pages 77–88. Taylor & Francis, Jul 1973. doi: 10.1080/00207177308932488.
- [60] M. Porfiri and M. di Bernardo. Criteria for global pinning-controllability of complex networks. *Automatica*, 44(12):3100–3106, 2008.
- [61] X. F. Wang and G. Chen. Pinning control of scale-free dynamical networks. *Physica A*, 310:521–531, 2002.
- [62] W. Lu. Adaptive dynamical networks via neighborhood information: Synchronization and pinning control. *Chaos*, 17, 2007.
- [63] L. Y. Xiang, Z. X. Liu, Z. Q. Chen, F. Chen, and Z. Z. Yuan. Pinning control of complex dynamical networks with general topology. *Physica A*, 379:298–306, 2006.
- [64] W. Guo. Lag synchronization of complex networks via pinning control. *Nonlinear Analysis: Real-world applications*, 12, 2011.
- [65] Yang-Yu Liu, Jean-Jacques Slotine, and Albert-Laszlo Barabasi. Controllability of complex networks. *Nature*, 473:167–173, 2011.

- [66] Meng Ji, Abubakr Muhammad, and Magnus Egerstedt. Leader-based multi-agent coordination: Controllability and optimal control. In *American Control Conference*, pages 1358–1363, 2006.
- [67] Andrew Clark, Linda Bushnell, and Radha Poovendran. On leader selection for performance and controllability in multi-agent systems. In *Conference on Decision and Control*, pages 86–93, 2012.
- [68] F. Pasqualetti, S. Zampieri, and F. Bullo. Controllability metrics, limitations and algorithms for complex networks. *Control of Network Systems, IEEE Transactions on*, 1(1):40–52, March 2014.
- [69] Stacy Patterson and Bassam Bamieh. Leader selection for optimal network coherence. In *Decision and Control (CDC), 2010 49th IEEE Conference on*, pages 2692–2697. IEEE, 2010.
- [70] Fu Lin, Makan Fardad, and Mihailo R. Jovanovic. Algorithms for leader selection in large dynamical networks: Noise-corrupted leaders. In *Decision and Control and European Control Conference (CDC-ECC), 2011 50th IEEE Conference on*, pages 2932–2937. IEEE, 2011. ISBN 1612848001.
- [71] Hiroaki Kawashima and Magnus Egerstedt. Leader selection via the manipulability of leader-follower networks. In *American Control Conference (ACC), 2012*, pages 6053–6058. IEEE, 2012.
- [72] Herbert G. Tanner. On the controllability of nearest neighbor interconnections. In *Decision and Control, 2004. CDC. 43rd IEEE Conference on*, volume 3, pages 2467–2472. IEEE, 2004.
- [73] A. Chapman and M. Mesbahi. System theoretic aspects of influenced consensus: Single input case. *Automatic Control, IEEE Transactions on*, 57(6):1505–1511, June 2012.
- [74] K Jerath. Impact of Adaptive Cruise Control on the formation of self-organizing traffic jams on highways. Master’s thesis, The Pennsylvania State University, 2010.
- [75] M. J. Lighthill and G.B. Whitham. On kinematic waves. II. A theory of traffic flow on long crowded roads. *Proceedings of the Royal Society A*, 229(1178):317–345, 1955.
- [76] P. Richards. Shock waves on the highway. *Operations Research*, 4(1), 1956.
- [77] R. E. Chandler, R. Herman, and E. W. Montroll. Traffic dynamics: Studies in car following. *Operations Research*, 6:165–184, 1958.
- [78] D. Helbing. Traffic and related self-driven many-particle systems. *Reviews of Modern Physics*, 73:1067–1141, 2001.

- [79] Carlos Daganzo. *Fundamentals of Transportation and Traffic Operations*. Emerald Group, 1997.
- [80] G. B. Whitham. Exact solutions for a discrete system arising in traffic flow. *Proceedings of the Royal Society of London, Series A*, 428:49–69, 1990.
- [81] H. J. Payne. Freflo: A macroscopic simulation model for freeway traffic. *Transportation Research Record*, pages 68–77, 1979.
- [82] I. Prigogine and R. Herman. *Kinetic Theory of Vehicular Traffic*. Elsevier, New York,, 1971.
- [83] L. A. Pipes. An operational analysis of traffic dynamics. *Journal of Applied Physics*, 24:274–281, 1953.
- [84] D. C. Gazis, R. Herman, and Potts R. B. Car-following theory of steady-state traffic flow. *Operations Research*, 7:499–505, 1959.
- [85] G. F. Newell. Nonlinear effects in the dynamics of car following. *Operations Research*, 9:209–229, 1961.
- [86] A Kesting, M Treiber, M Schonhof, F Kranke, and D Helbing. *Jam-avoiding adaptive cruise control (ACC) and its impact on traffic dynamics*, pages 633–643. Springer, Berlin,, 2005.
- [87] Andrew Ilachinski. *Cellular Automata: A Discrete Universe*. World Scientific, 2001.
- [88] M. Cremer and J. Ludwig. A fast simulation model for traffic flow on the basis of boolean operations. *Mathematics and Computers in Simulation*, 28(4):297 – 303, 1986.
- [89] J Zhou and H Peng. String stability conditions of adaptive cruise control algorithms. In *IFAC Symposium on "Advances in Automotive Control"*, 2004.
- [90] Adolf D May. *Traffic Flow Fundamentals*. Prentice-Hall, Inc., 1990.
- [91] Arne Kesting, Martin Treiber, and Dirk Helbing. Enhanced intelligent driver model to assess the impact of driving strategies on traffic capacity. *Philosophical Transactions of the Royal Society A: Mathematical, Physical and Engineering Sciences*, 368(1928): 4585–4605, 2010.
- [92] Fan Li and Yu Wang. Routing in vehicular ad hoc networks: A survey. *Vehicular Technology Magazine, IEEE*, 2(2):12–22, Jun 2007.
- [93] M. L. Sichitiu and M. Kihl. *Communications Surveys Tutorials, IEEE*, volume 10, chapter Inter-vehicle communication systems: a survey, pages 88–105. Second 2008.

- [94] Ryosuke Nishi, Akiyasu Tomoeda, Kenichiro Shimura, and Katsuhiko Nishinari. Theory of jam-absorption driving. *Transportation Research Part B: Methodological*, 50:116–129, 2013.
- [95] Noah J. Goodall, Brian L. Smith, and Byungkyu (Brian) Park. *Journal of Intelligent Transportation Systems*, chapter Microscopic Estimation of Freeway Vehicle Positions from the Behavior of Connected Vehicles. Taylor & Francis, Mar 2014.
- [96] P. J. Zwaneveld and B. van Arem. *TNO Inro., Delft. Sustainability. Exploring the road ahead for car mobility page*, volume 69, chapter Traffic effects of Automated Vehicle Guidance: A literature survey. 1997.
- [97] B. van Arem, J. H. Hogema, M. J. W. A. Vanderschuren, and C. H. Verheul. An assessment of the impact of autonomous intelligent cruise control. Technical report, 1995.
- [98] P. Varaiya. Smart cars on smart roads: problems of control. *IEEE Transactions on Automatic Control*, 38:195–207, 1993.
- [99] U. Kraaslan, P. Varaiya, and J. Walrand. Two proposals to improve freeway traffic flow. In *Proceedings of American Control Conference*, 1991.
- [100] S. E. Shladover. Potential freeway capacity effects of advanced vehicle control systems. In *Applications of advanced technologies in transportation engineering: proceedings of the second international conference*, 1991.
- [101] B. S. Kerner and P. Konhäuser. Cluster effect in initially homogeneous traffic flow. *Physical Review E*, 48:2335–2338, 1993.
- [102] R. Herman, E. W. Montroll, R. B. Potts, and R. W. Rothery. Traffic dynamics: Analysis of stability in car following. *Operations Research*, 7:86–106, 1958.
- [103] P. Seiler, A. Pant, and K. Hedrick. Disturbance propagation in vehicle strings. *Automatic Control, IEEE Transactions on*, 49(10): 1835–1842, Oct 2004.
- [104] Swaroop Darbha and K R Rajagopal. Intelligent cruise control systems and traffic flow stability. Technical report, California Partners for Advanced Transit and Highways, 1998.
- [105] P. A. Ioannou and C. C. Chien. Autonomous intelligent cruise control. *IEEE Transactions on Vehicular Technology*, 42:657–672, 1993.

- [106] P. Barooah, P.G. Mehta, and J.P. Hespanha. Mistuning-based control design to improve closed-loop stability margin of vehicular platoons. *Automatic Control, IEEE Transactions on*, 54(9): 2100–2113, Sept 2009.
- [107] Kai Nagel. Particle hopping models and traffic flow theory. *Physical Review E*, 53(5), 1996.
- [108] Reinhart Kühne, Reinhard Mahnke, Ihor Lubashevsky, and Jevgenijs Kaupužs. Probabilistic description of traffic breakdowns. *Physical review. E, Statistical, nonlinear, and soft matter physics*, 65 (6 Pt 2), Jun 2002.
- [109] R. Mahnke and N. Pieret. Stochastic master-equation approach to aggregation in freeway traffic. *Phys. Rev. E*, 56:2666–2671, Sep 1997.
- [110] R. Akcelik and D. C. Biggs. Acceleration profile models for vehicles in road traffic. *Transportation Science*, 21(1):36–54, 1987.
- [111] Gary Long. Acceleration characteristics of starting vehicles. *Journal of the Transportation Research Board*, 1737:58–70, 2000.
- [112] Masako Bando, Katsuya Hasebe, Ken Nakanishi, and Akihiro Nakayam. Analysis of Optimal Velocity model with explicit delay. *Physical Review E*, 58(5), 1998.
- [113] Timur Alperovich and Alexandros Sopsakis. Stochastic description of traffic flow. *Journal of Statistical Physics*, 133(6), 2008.
- [114] K Jerath and S N Brennan. Analytical prediction of self-organized traffic jams as a function of increasing ACC penetration. *IEEE Trans. on Intelligent Transportation Systems*, 13(4), 2012.
- [115] Hideyuki Suzuki, J Imura, and Kazuyuki Aihara. Chaotic Ising-like dynamics in traffic signals. *Scientific Reports*, 3, 2013.
- [116] Kshitij Jerath, Asok Ray, Sean N. Brennan, and Vikash V. Gayah. Statistical mechanics-inspired framework for studying the effects of mixed traffic flows on highway congestion. In *Proceedings of the American Control Conference*, pages 5402–5407, June 2014.
- [117] Anatoly Kolomeisky, Gunter Schutz, Eugene Kolomeisky, and Joseph Staley. Phase diagram of one-dimensional driven lattice gases with open boundaries. *Journal of Physics A*, 31(33), 1998.
- [118] E. Bayong, H. T. Diep, and Viktor Dotsenko. Potts model with long-range interactions in one dimension. *Physical review letters*, 83(1):14, 1999.

- [119] B. Eisenblätter, L. Santen, A. Schadschneider, and M. Schreckenberg. Jamming transition in a cellular automaton model for traffic flow. *Phys. Rev. E*, 57:1309–1314, Feb 1998. doi: 10.1103/PhysRevE.57.1309.
- [120] Ihab El-Shawarby, Hesham Rakha, Vaughan W. Inman, and Gregory W. Davis. Evaluation of driver deceleration behavior at signalized intersections. *Journal of the Transportation Research Board*, 2018:29–35, 2007.
- [121] P. L. Krapivsky, S. Redner, and E. Ben-Naim. *A Kinetic View of Statistical Physics*. Cambridge University Press, 2010. ISBN 9781139493345.
- [122] Siddhartha Chib and Edward Greenberg. Understanding the Metropolis-Hastings algorithm. *The American Statistician*, 49(4): 327–335, 1995.
- [123] Hao Wu, Richard Fujimoto, and George Riley. Analytical models for information propagation in vehicle-to-vehicle networks. In *Proceedings of the IEEE 60th Vehicular Technology Conference*, volume 6, pages 4548–4552, 2004.
- [124] Thomas DC Little and Ashish Agarwal. An information propagation scheme for VANETs. In *Proceedings of IEEE Intelligent Transportation Systems*, pages 155–160, 2005.
- [125] Martin Schönhof, Arne Kesting, Martin Treiber, and Dirk Helbing. Coupled vehicle and information flows: Message transport on a dynamic vehicle network. *Physica A: Statistical Mechanics and its Applications*, 363(1):73–81, 2006.
- [126] H. Hartenstein and K. P. Laberteaux. A tutorial survey on vehicular ad hoc networks. *IEEE Communications Magazine*, 46(6): 164–171, 2008.
- [127] M. Torrent-Moreno. *Inter-Vehicle Communications : Achieving Safety in a Distributed Wireless Environment : Challenges, Systems and Protocols*. PhD thesis, University of Karlsruhe, 2007.
- [128] S Shladover, C Nowakowski, and D Cody. *Effects of cooperative adaptive cruise control on traffic flow: testing drivers' choices of following distances*. California PATH Program, Institute of Transportation Studies, University of California at Berkeley, 2009.
- [129] Julien Monteil, Romain Billot, Frédéric Armetta, Salima Hassas, and Nour-Eddin El Faouzi. Cooperative highway traffic: multi-agent modeling and robustness assessment to local perturbations. In *The 92nd Annual Meeting of the Transportation Research Board, reviewed by TRB's Traffic Flow Theory and Characteristics Committee (AHB45)*, pages 1–19, 2013.

- [130] Yu Liu, Francois Dion, and Subir Biswas. Dedicated short-range wireless communications for intelligent transportation system applications: State of the art. *Transportation Research Record: Journal of the Transportation Research Board*, 1910(1):29–37, 2005.
- [131] Detlev Boison. Adenosine kinase, epilepsy and stroke: mechanisms and therapies. *Trends in pharmacological sciences*, 27(12): 652–658, Dec 2006.
- [132] Rikus Eising. Between controllable and uncontrollable. *Systems & Control Letters*, 4(5):263 – 264, 1984.
- [133] Daniel L. Boley and Wu-Sheng Lu. Measuring how far a controllable system is from an uncontrollable one. *Automatic Control, IEEE Transactions on*, 31(3):249–251, Mar 1986.
- [134] D. K. Lindner, J. Babendreier, and A. M. A. Hamdan. Measures of controllability and observability and residues. *IEEE Transactions on Automatic Control*, 34(6):648–650, 1989.
- [135] A. M. A. Hamdan and A. M. Elabdalla. Geometric measures of modal controllability and observability of power system models. *Electric Power Systems Research*, 15(2):147 – 155, 1988.
- [136] Annissa Heniche and Innocent Kamwa. Using measures of controllability and observability for input and output selection. In *International Conference on Control Applications*, volume 2, pages 1248–1251, 2002.
- [137] Youdan Kim and John L. Junkins. Measure of controllability for actuator placement. *Journal of Guidance, Control, and Dynamics*, 14(5):895–902, 1991.
- [138] Louis M. Pecora and Thomas L. Carroll. Master stability functions for synchronized coupled systems. *Physical Review Letters*, 80(10):2109–2112, 1998.
- [139] Francesco Sorrentino, Mario di Bernardo, Franco Garofalo, and Guanrong Chen. Controllability of complex networks via pinning. *Phys. Rev. E*, 75:046103, Apr 2007.
- [140] Ralph Byers. Detecting nearly uncontrollable pairs. In *Numerical Methods Proceedings of the International Symposium MTNS-89, volume III*, pages 447–457. Springer-Verlag, 1990.
- [141] C. Beck and F. Schögl. *Thermodynamics of Chaotic Systems: An Introduction*. Cambridge Nonlinear Science Series. Cambridge University Press, 1995. ISBN 9780521484510.

- [142] Matthew B. Kennel, Reggie Brown, and Henry DI Abarbanel. Determining embedding dimension for phase-space reconstruction using a geometrical construction. *Physical Review A*, 45(6): 3403, 1992.
- [143] Floris Takens. *Dynamical systems and turbulence, Warwick 1980*, volume 898, chapter Detecting strange attractors in turbulence, pages 366–381. Springer, 1981.
- [144] Andrew M Fraser and Harry L Swinney. Independent coordinates for strange attractors from mutual information. *Physical review A*, 33(2):1134, 1986.
- [145] Liangyue Cao. Practical method for determining the minimum embedding dimension of a scalar time series. *Physica D: Nonlinear Phenomena*, 110(1–2):43–50, Dec 1997.
- [146] AC Antoulas, DC Sorensen, and S Gugercin. A survey of model reduction methods for large-scale systems. *Contemporary mathematics*, 280:193–220, 2001.
- [147] Boris Lohmann and Behnam Salimbahrami. Introduction to krylov subspace methods in model order reduction. *Methods and Applications in Automation*, pages 1–13, 2000.
- [148] D. S. Watkins. *The Matrix Eigenvalue Problem: GR and Krylov Subspace Methods*, chapter Krylov Subspace Methods. Society for Industrial and Applied Mathematics, 2007.
- [149] Kshitij Jerath, Vikash V. Gayah, and Sean Brennan. Event horizons and influential subspaces of connected vehicles. *Submitted*.
- [150] Kshitij Jerath and Sean Brennan. Identification of locally influential agents in self-organizing multi-agent systems. *Submitted*.
- [151] J-M. Ginoux and B. Rosseto. Invariant manifolds of complex systems. In C. Bertelle, G. H. E. Duchamp, and H. Kadri-Dahmani, editors, *Complex Systems and Self-organization Modelling, Understanding Complex Systems*, pages 41–49. Springer Berlin Heidelberg, 2009.
- [152] Alain Sarlette and Rodolphe Sepulchre. Consensus optimization on manifolds. *SIAM Journal on Control and Optimization*, 48(1):56–76, 2009.
- [153] H Van Dyke Parunak and Sven Brueckner. Entropy and self-organization in multi-agent systems. In *Proceedings of the fifth international conference on Autonomous agents*, pages 124–130. ACM, 2001.

- [154] RT Wicks, Sandra C Chapman, and RO Dendy. Mutual information as a tool for identifying phase transitions in dynamical complex systems with limited data. *Physical Review E*, 75(5): 051125, 2007.

VITA

KSHITIJ JERATH

EDUCATION

- December 2014* Ph.D. (Mechanical Engineering), The Pennsylvania State University
December 2014 M.S. (Electrical Engineering), The Pennsylvania State University
May 2010 M.S. (Mechanical Engineering), The Pennsylvania State University
June 2006 B.Tech. (Mechanical and Automation Engineering), Guru Gobind Singh
Indraprastha University

WORK EXPERIENCE

- 2013-2014* Instructor, Penn State
2011-2013 Graduate Teaching Assistant, Penn State
2007-2011 Graduate Research Assistant, Department of Mechanical and Nuclear
Engineering, Penn State
2006-2007 Research Associate, Intellectual Property, Evaluateserve.com

GRADUATE RESEARCH EXPERIENCE

- 2008-2014* Effects of adaptive cruise control and connected vehicles on traffic
jam dynamics
2012 Human detection in complex construction environments using LIDAR
2009-2011 GPS-free terrain-based vehicle tracking using low-cost sensors
2007-2009 Reliability analysis of in-service transit buses

ACTIVITIES AND HONORS

- 2014* Best presentation in session at the American Control Conference 2014
2014 Selected for Kulakowski Travel Award by MNE department at Penn
State
2013 *Media article:* Research mentioned in Society of Industrial and Ap-
plied Mathematics News, *Smells like a traffic jam*
2013 Awarded Graduate Teaching Fellowship by Department of Mecha-
nical and Nuclear Engineering at The Pennsylvania State University
2012 Best presentation in session at the American Control Conference 2012
2012 Awarded second place in Student Essay Competition organized by In-
telligent Transportation Society of America for essay titled *Cooperative
intelligent vehicles: are we there yet?*
2007-2009 Member, Penn State Robotics Club and IGVC team